Reduction of Chlorinated Aliphatic and Nitro Aromatic Compounds at the Fe^0-Oxide-Water Interface

Michelle Marie Scherer
B.S., University of Virginia, 1989
M.S., University of Connecticut, 1994

A thesis presented to the faculty of the
Oregon Graduate Institute of Science and Technology
in partial fulfillment of the
requirements for the degree
Doctor of Philosphy
in
Environmental Science and Engineering

June 1998

This dissertation "Reduction of Chlorinated Aliphatic and Nitro Aromatic Compounds at the Fe^0-Oxide-Water Interface" by Michelle M. Scherer has been examined and approved by the following Examination Committee:

Paul G. Tratnyek, Disseration Advisor
Associate Professor

John C. Westall, Dissertation Co-Advisor
Professor

William Fish
Associate Professor

Margaret Ziomek-Moroz
Associate Professor

ACKNOWLEDGEMENTS

As I was finishing up my Master's degree at the University of Connecticut, I commented to my advisor, Nik Nikolaidis, that although I had learned a lot during my tenure at UCONN, I felt there was so much more I needed to understand. I still remember his reply, "Meechelle (sic), it only gets worse." Well, five years later, as I am finishing up my Ph.D., I realize just how wise those words were.

For guiding me through these vast new worlds of science and academics, I want to thank my advisor and close friend, Paul Tratnyek. His enthusiasm for pursuing unexplored territorities (in both science and life) has been a wonderful source of inspiration. I hope the journey continues for many years to come.

I would like to thank John Westall for introducing me to the world of electrochemistry (ever so patiently!). I will always remember our day long "jam" sessions with great fondness.

OGI would not have been the same without the companionship and friendship provided by my many lunch pals throughout the years. My warmest thanks to Cheryl Martin, Jane Allen, Diane Grady, Barb Balko, Wendy Sommerfield, Anna Farrenknopf, Phil Pearson, Jeff Darland, and Brian Mader.

A prerequisite for surviving graduate school is a close group of friends who you can vent to on a regular basis. For me, this group took the form of a Quilting Bee. Yes, this is the 90's, and it is probably one of the few quilting bee's in the world that required a M.S. or higher to join. For the many wonderful evenings spent quilting, venting, dog-sitting, baby-sitting, I thank Cheryl Martin, Leah Matheson, and Barb Balko.

My many thanks to Cheryl, Rob and Adrian Martin for being the next best thing to family here in Oregon.

I would like to thank my family for their unwavering confidence and support throughout the years. Finally, I thank Craig, for his love, and unique ability to make me laugh throughout it all.

DEDICATION

To my parents, Bill and Lila-Ann Scherer and my husband, Craig Martin.

TABLE OF CONTENTS

LIST OF TABLES

LIST OF FIGURES

Abstract

Reduction of Chlorinated Aliphatic and Nitro Aromatic Compounds
at the Fe^0-Oxide-Water Interface

Michelle M. Scherer

Oregon Graduate Institute of Science & Technology, 1998
Supervising Professor: Paul G. Tratnyek

The widespread use of chlorinated aliphatic and nitro aromatic compounds has made them among the most frequently encountered environmental contaminants. A passive, cost effective alternative for in situ treatment of these organic contaminants is the use of zero-valent iron (Fe^0) as a reductant in permeable reactive barriers (PRBs). The resounding success of Fe^0 PRBs has sparked intense interest in the chemistry of the Fe^0-water interface.

Reactivity at the Fe^0-water interface, however, is complicated by the accumulation of corrosion products due to the dissolution of Fe^0 in the presence of water and other oxidants. To evaluate the role of the oxide film, three conceptual models of the oxide are presented and intepreted in terms of their implications for Fe^0 PRBs, including the oxide as a passive film, a semiconductor, and a coordinating surface.

An oxide-free Fe^0 rotating disk electrode (RDE) was used to quantify the effect of mass transport and surface reaction on the kinetics of reduction by Fe^0. Experiments with the Fe^0 RDE show that rate of carbon tetrachloride (CCl_4) reduction is dominated by reaction at the Fe^0 surface, whereas the rate of nitrobenzene ($ArNO_2$) reduction is influenced by both surface reaction *and* mass transport. The kinetic limitation imposed by the rate of surface reaction observed in CCl_4 reduction by Fe^0 appears to extend to other chlorinated aliphatic compounds. Correlation analysis with surface area normalized rate constants (k) for chlorinated aliphatic compounds reveals satisfactory correlations with a variety of measures of electron affinity. Linear free energy relationships (LFERs) are developed based on estimated one-electron reduction potentials (E_1), and lowest

unoccupied molecular orbital (LUMO) energies calculated from semi-empirical and ab initio methods.

To determine whether surface-active substances could influence the the reduction of contaminants by Fe^0, a series of batch experiments with seven natural organic matter (NOM) samples and eight anthropogenic surfactants was undertaken. For the range of conditions studied, there was no observable influence on the rate of $ArNO_2$ reduction and only a slight inhibition of rate was observed for the reduction of CCl_4 in the presence of high concentrations of NOM.

CHAPTER 1

Overview

1.1 Introduction

The widespread use of chlorinated aliphatic and nitro aromatic compounds has made them among the most frequently encountered environmental contaminants (1). A passive, cost effective alternative for in situ treatment of these organic contaminants is the use of zero-valent iron (Fe^0) as a reductant in permeable reactive barriers (PRBs) (2). The resounding success of Fe^0 PRBs has sparked intense interest in the chemistry of the Fe^0-water interface within the environmental science and engineering community.

Reactivity at the Fe^0-water interface, however, is complicated by the accumulation of corrosion products due to the dissolution of Fe^0 in the presence of water and other oxidants. The first part of this dissertation (Chapter 2), examines the role of oxides in reduction reactions at the metal-water interface. The goal was to integrate metal-water interface models used in corrosion science, physical chemistry, and geochemistry to understand the reduction of organic contaminants by Fe^0. Specifically, three conceptual models of the oxide are presented and interpreted in terms of their implications for Fe^0 PRBs: the oxide as a passive film, a semiconductor, and a coordinating surface.

As a passive film, oxides may inhibit reduction of organic contaminants by serving as a physical barrier to electron transfer (ET) between the underlying metal and organic contaminant. Sustained reduction requires localized defects in the passive film (e.g., pits), or some mechanism for transferring electrons through the oxide. Although there has been much speculation on the "passivation" of Fe^0 PRBs, a systematic study of the role of passivation and localized corrosion (e.g., pitting) in the reduction of organic contaminants by Fe^0 remains to be done. In the semiconductor model, reduction of the organic contaminant may occur by ET from the oxide conduction band to the organic contaminant. The effect of light on carbon tetrachloride (CCl_4) reduction by Fe^0, however, suggests that other ET mechanisms (e.g., resonance tunneling) may be more important, because of the high population of localized states in oxides formed under environmental conditions (3). As

a coordinating surface, Fe(II) sites at the surface of the oxide are responsible for reduction of the organic contaminant. Although there is some evidence of competition for surface sites by common environmental ligands, it is still unclear how important this surface site limitation is in Fe^0 PRBs.

The second part of this dissertation (Chapters 3 and 4), addresses the kinetics of reduction of organic contaminants by Fe^0 in the absence of an oxide layer. The major goal of these studies is to resolve the rate determining step in the reduction of CCl_4 and $ArNO_2$ by Fe^0. The oxide layer was eliminated because it introduces complex processes associated with the porous structure of the oxide that are difficult to quantify. In the absence of an oxide layer, the overall kinetics of heterogeneous reactions can be divided unambiguously into mass transport and surface reaction. Mass transport involves diffusion of the contaminant through the stagnant water layer to the Fe^0 surface, and surface reaction includes both complexation (or adsorption) and electron transfer.

To quantify the effect of mass transport and surface reaction on the kinetics of reduction by Fe^0, we used a polished Fe^0 rotating disk electrode (RDE) in an electrochemical cell. In Chapter 3, experiments with the Fe^0 RDE clearly show that the rate of CCl_4 reduction is not influenced by mass transport to the surface. Instead, the kinetics are dominated by reaction at the Fe^0 surface. The surface reaction step also appears to control the kinetics of other chlorinated aliphatic compounds as well based on the large range of reactivities (over four orders of magnitude (4)) displayed for only a small variation (less than one order of magnitude) in their diffusion coefficients. Linear sweep voltammograms are used to develop a kinetic model to describe the individual surface reactions controlling the rate of CCl_4 reduction by Fe^0. Results of the model suggest that applying a reducing potential to Fe^0 PRBs to enhance the rate of reduction may not be efficient because of the instability of water at these potentials (5).

The investigation of $ArNO_2$ reduction by Fe^0 (Chapter 4) was initiated because, unlike chlorinated aliphatic compounds, reported reduction rates for nitro aromatic compounds were unaffected by chemical structure (6), suggesting a greater influence of mass transport. Experiments with the Fe^0 RDE clearly show that the kinetics of $ArNO_2$ reduction by Fe^0 is influenced by mass transport. The effect, however, is not strong enough to conclude that mass transport dominates the overall kinetics, but rather that both mass transport *and* surface reaction (i.e., mixed-control) influence the overall kinetics. The role of the surface reaction rate constant (k_{ct}) and mass transport rate constant (k_{mt}) in the mixed-control kinetics is evaluated for $ArNO_2$ and CCl_4 reduction by Fe^0.

The third part of this dissertation (Chapter 5), builds on the strong influence of surface reaction on CCl_4 reaction kinetics found in Chapter 3 to investigate the relationship between reduction rates and redox properties of the individual compounds. Correlation analysis with the surface area normalized rate constants (k) compiled in Johnson et. al. (4) reveals satisfactory correlations with a variety of measures of electron affinity. Linear free energy relationships (LFERs) are developed based on estimated one-electron reduction potentials (E_1), and lowest unoccupied molecular orbital (LUMO) energies calculated from semi-empirical and ab initio methods. Solvation effects are modeled with COSMO (by imposing a dielectric medium) and incorporated into semi-empirical estimates of E_{LUMO}, but this did not improve the correlation. Predicted values of k can be used with fate and transport models to estimate the appropriate barrier width for Fe^0 PRBs (7). Trends in the k values predicted with the E_{LUMO} and E_1 LFERs provide several insights into the mechanistic factors influencing the reduction rates. For example, as expected, the rate of reduction increases as the number of chlorines on the compound increases within each congener family. However, the influence of the number of chlorines seems to be substantial even among different congener families (i.e., all di-chlorinated aliphatic compounds appear to have a $k \approx 10^{-4}$ L m^{-2} hr^{-1}, regardless of whether they are methanes, ethanes, or ethenes).

The integral role of the metal-oxide-water interface in the reduction of contaminants by Fe^0 (Chapter 2), suggests that the presence of surface-active substances could influence the effectiveness of Fe^0 PRBs. To this end, the final part of this dissertation (Chapter 6), focuses on the role of surface-active substances in the reduction of contaminants by Fe^0. Three pathways in which surface-active substances could influence the rate of contaminant reduction by Fe^0 are described: (i) solubilization of the contaminant into hydrophobic aggregates formed by the surfactants, (ii) adsorption of the contaminant to a surfactant film at the oxide-water interface, and (iii) reduction of the contaminant by electron transfer that is mediated by surfactants with reactive functional groups. To determine whether these (or other) pathways influence the reduction of contaminants by Fe^0, a series of batch experiments with seven natural organic matter samples and eight anthropogenic surfactants was undertaken. For the range of conditions studied, there was no observable influence on the rate of $ArNO_2$ reduction and only a slight inhibition of rate was observed for the reduction of CCl_4 in the presence of high concentrations of natural organic matter.

1.2 Summary of Contributions

The kinetics of organic contaminant reduction in Fe^0 systems are important because they are integral to: (i) designing full-scale treatment operations, (ii) developing enhancement techniques, and (iii) predicting the reactivity of untested compounds. This dissertation has made the following contributions toward improving our understanding of the kinetics to aid in the design, development and prediction of future Fe^0 applications:

(i) A framework for understanding the role of oxides in reduction reactions at the metal-water interface has been developed. The passive film, semiconductor, and surface complexation models presented in Chapter 2 provide an improved basis for future research initiatives. Specifically, a framework is provided to integrate models from specialized disciplines to achieve a more comprehensive generalized picture of the oxide-water interface.

(ii) The kinetic models derived in this dissertation have shown that the rate of reduction of chlorinated aliphatic compounds by Fe^0 is controlled by surface reaction rather than mass transport to the surface. Based on this finding, future work should focus on enhancing the rate of surface reaction (e.g., catalysts or dopants that increase the rate of electron transfer) in order to improve the performance of Fe^0 technologies. Proposed enhancement scenarios can be evaluated using the electrochemical kinetic model derived in Chapter 3.

(iii) Linear free energy relationships (LFERs) were developed for the dechlorination of chlorinated aliphatic compounds by Fe^0. Rate constants derived from a wide range of experimental conditions applicable to Fe^0 remediation were used to develop a statistically robust predictive tool *and* provide a better understanding of the dechlorination process (Chapter 5). The goal was to develop an LFER that is consistent with the combination of statistical and mechanistic criteria that reflect the mixed purposes of environmental scientists and engineers (8). The LFERs based on estimated one-electron reduction potentials (E_1) and LUMO energies (E_{LUMO}) provide tools for estimating the reactivity of untested chlorinated aliphatic compounds (e.g., most chloropropanes).

1.3 Literature Cited

(1) Pankow, J. F.; Feenstra, S.; Cherry, J. A.; Ryan, M. C. *Dense Chlorinated Solvents in Groundwater Systems: Principles Affecting Fate, Transport, and Remediation*; Pankow, J. F., Ed; Waterloo Press, Portland, OR. 1994.

(2) O'Hannesin, S. F.; Gillham, R. W. Long-term performance of an in situ "iron wall" for remediation of VOCs. *Ground Water,* 1998, *36*, 164-170.

(3) Balko, B. A.; Tratnyek, P. G. Photoeffects on the reduction of carbon tetrachloride by zero-valent iron. *J. Phys. Chem.,* 1998, *B, 102*, 1459-1465.

(4) Johnson, T. L.; Scherer, M. M.; Tratnyek, P. G. Kinetics of halogenated organic compound degradation by iron metal. *Environ. Sci. Technol.,* 1996, *30*, 2634-2640.

(5) Scherer, M. M.; Westall, J. C.; Tratnyek, P. G. An electrochemical interpretation of carbon tetrachloride reduction at an oxide-free iron electrode*; 214th National Meeting,* Las Vegas, NV, American Chemical Society, 1997; Vol. 37, No. 2, pp. 247-248.

(6) Agrawal, A.; Tratnyek, P. G. Reduction of nitro aromatic compounds by zero-valent iron metal. *Environ. Sci. Technol.,* 1996, *30*, 153-160.

(7) Tratnyek, P. G.; Johnson, T. L.; Scherer, M. M.; Eykholt, G. R. Remediating groundwater with zero-valent metals: Kinetic considerations in barrier design. *Ground Water Monit. Rem.,* 1997, 108-114.

(8) Tratnyek, P. G. Correlation analysis of the environmental reactivity of organic substances. In *Perspectives in Environmental Chemistry*; Macalady, D. L., Ed; Oxford: New York, 1998; pp. 167-194.

CHAPTER 2

The Role of Oxides in Reduction Reactions at the Metal-Water Interface[1]

2.1 Abstract

The oxide layer that lies at the iron-water interface under environmental conditions can influence the reduction of solutes by acting as a passive film, semiconductor, or coordinating surface. As a passive film, oxides may inhibit reaction by providing a physical barrier between the underlying metal and dissolved oxidants. Sustained reduction of solutes requires localized defects in the passive film (e.g., pits), or some mechanism for transferring electrons through the oxide. In the semiconductor model, conduction band electrons from the oxide may contribute to solute reduction, but electron hopping (resonance tunneling) appears to be more important due to the high population of localized states in oxides formed under environmental conditions. Ultimately, electron transfer to the solute must occur via a precursor complex at the oxide-water interface. For dehalogenation of chlorinated aliphatic compounds on an iron oxide surface, a surface complexation model suggests that the outer-sphere precursor complex is weak and partially displaced by common environmental ligands.

2.2 Introduction

Zero-valent metals such as iron, tin, and zinc, are moderately strong reducing agents that react with a variety of oxidants, including halogenated alkanes and alkenes, nitro aromatic compounds, nitrate, and chromate. Although these reactions have been known for a long time, the recent application of granular iron metal (Fe^0) to remediation of contaminated groundwater has sparked new interest in their chemistry (1, 2). The majority of new work in this area concerns reduction of chlorinated aliphatic compounds, so we

[1] Scherer, M.M., B.A. Balko, and P.G. Tratnyek. 1998. The role of oxides in reduction reactions at the mineral-water interface. In: *Mineral-Water Interfacial Reactions: Kinetics and Mechanisms*, D.L. Sparks and T.J. Grundl, Eds. ACS Symposium Series #715.

haved focused our analysis on this class of reactions. The analysis, however, should be broadly applicable to contaminant reactions in heterogeneous environmental systems.

Under environmental conditions, the Fe^0-H_2O interface has a surface layer of corrosion products that develops due to the thermodynamic instability of Fe^0 in the presence of water. Long-term batch and column studies have shown that this layer evolves with time into a complex mixture of amorphous iron oxides, iron oxide salts, and other mineral precipitates (2-5). Because this material lies at the metal-water interface, it must, in some manner, mediate the reduction of contaminants by the underlying metal. Understanding the mechanism by which metals reduce contaminants in the presence of a substantial layer of oxides is one of the critical, remaining challenges for researchers in this field. The goal of the following analysis is to develop a conceptual framework for this problem by reevaluating recent data in terms of established models for the structure and reactivity of metal oxides.

2.3 Background

2.3.1 Chemical Background

Reduction reactions in Fe^0-H_2O systems are heterogeneous reactions driven by the oxidation of Fe^0 (equation 1) or the oxidation of surface-bound Fe^{2+} ($Fe^{2+}_{(sur)}$) (equation 2). In the absence of oxygen, these oxidations are coupled with the reduction of interfacial H_2O (6-8):

$$Fe^0 \rightleftharpoons Fe^{2+} + 2\,e^- \quad (1)$$

$$Fe^{2+}_{(sur)} \rightleftharpoons Fe^{3+}_{(sur)} + e^- \quad (2)$$

$$2\,H_2O + 2\,e^- \rightleftharpoons H_2(g) + 2\,OH^- \quad (3)$$

In principle, Fe^0, $Fe^{2+}_{(sur)}$, and H_2 can contribute to the reduction of contaminants (6). However, for chlorinated aliphatic compounds (RX), several lines of evidence suggest that most of the observed reduction is due to reaction with Fe^0 or $Fe^{2+}_{(sur)}$, and little, if any, involves H_2 (or H• or H^-) at near neutral pH values (9, 10). The predominant degradation pathway for RX appears to be reductive dechlorination,

$$RX + H^+ + 2\,e^- \rightarrow RH + X^- \quad (4)$$

although variable amounts of reductive elimination have been reported (11, 12). Both pathways presumably involve heterogeneous electron transfer (ET) from the iron metal or iron oxide to RX. The ET mechanism requires formation of a precursor complex, which appears to be weak and outer sphere for typical organic contaminants (13).

In the absence of an oxide layer, it appears that reduction of RX involves primarily ET from Fe^0 (i.e., equations 1 and 4). An oxide free iron metal surface can be achieved in electrochemically-controlled laboratory systems (9), and may apply where localized corrosion occurs at defects in the oxide surface layer (see section on The Oxide as a Physical Barrier). Under environmental conditions, however, the layer of iron oxides that covers the Fe^0 surface will contain $Fe^{2+}_{(sur)}$. Therefore, the observed reduction of RX, may reflect ET from $Fe^{2+}_{(sur)}$ as well as Fe^0 (equations 1, 2, and 4). For the purposes of the following discussion, $Fe^{2+}_{(sur)}$ may be adsorbed or structural iron (14), as long as it is available for reaction at the oxide-water interface.

2.3.2 Mass Transport to the Interface

Heterogeneous reactions can be broken down into mass transport and surface reaction steps. In the case portrayed in Figure 2.1a, mass transport involves diffusion of dissolved RX through the stagnant water layer to the surface, and surface reaction involves precursor complex formation and electron transfer. Controlled experiments conducted with a rotating disk electrode clearly show that mass transport has a negligible effect on the overall reduction rate of carbon tetrachloride (CCl_4) on oxide-free Fe^0 (9). Over the range of conditions of interest in environmental applications, however, both steps could influence the reaction rate, so it is not surprising that some evidence for mass transport effects has been reported (summarized in 9). The surface reaction step appears to be the dominant factor for chlorinated aliphatics, however, because reported reduction rates vary widely (over four orders of magnitude) with chemical structure (15), while there is only a small (less than one order of magnitude) variation in their diffusion coefficients (9).

2.4 The Oxide-Water Interface

In the presence of an oxide layer, there are several mechanisms by which electrons may be transferred from the underlying Fe^0 or $Fe^{2+}_{(sur)}$ to the adsorbed RX. The major mechanisms of ET are represented by three conceptual models in which the oxide layer serves as (i) an inert physical barrier, where electrons must come directly from the metal through defects, such as pits or grain boundaries in the oxide layer (Figure 2.1b); (ii) a

semiconductor, where electrons are transported through the oxide layer via the oxide conduction band, impurity bands, or localized states (Figure 2.1c); and (iii) a surface consisting of a finite number of coordination sites, where reduction may occur by metal-to-ligand charge transfer (Figure 2.1d). These models are not necessarily exclusive of one another; in fact, it is likely that the observed dehalogenation of RX by Fe^0 is affected by the oxide layer acting in all three ways. However, it is necessary to have a conceptual framework that clearly distinguishes between each mode of ET before their relative importance can be assessed from experimental data.

2.4.1 Composition of the Oxide

All three modes of reactivity for oxides on Fe^0 (Figure 2.1) are influenced by the composition of the oxide layer. The composition of this layer can be complex and variable, but spectroscopic analysis of electrochemically generated oxide films (passive films) have generally confirmed the two-layer model originally proposed by Nagayama and Cohen (16), in which the film consists of an inner layer of magnetite (Fe_3O_4) and an outer layer of maghemite (γ-Fe_2O_3) (17, 18). Other models that have been postulated include: (i) less discrete layers of amorphous oxides (similar in structure to $Fe(OH)_2$, Fe_3O_4, and γ-Fe_2O_3) (19, 20); (ii) one layer of a mixed-valent iron oxide in which the proportion of Fe^{2+} decreases exponentially from the metal-oxide contact to the oxide-water interface (21); or (iii) a layer consisting of a spinel structure similiar to Fe_3O_4 and γ-Fe_2O_3 with random cation vacancies and interstitials (22). The amorphous, non-crystalline character of these materials has been attributed to the presence of coordinated water molecules (23, 24).

The oxide layer that forms on the iron used in remediation applications, however, may differ from models developed to describe passive films because the iron used is an impure, recycled material that is manufactured primarily for use as a conditioner in building materials. Spectroscopic analyses of these materials show that they consist of a complex mixture of crystalline phases (25-27). Recently, Raman spectra obtained on iron particles from Master Builder Inc. (Cleveland, OH) and Peerless Metal Powder & Abrasives (Detroit, MI) revealed maghemite, magnetite, and hematite (α-Fe_2O_3) on samples analyzed as received (27).

With exposure to aqueous solutions, the original air-dried oxides on iron metal rehydrate and new phases may be formed by diagenesis or precipitation. For example, scanning electron microscopy (SEM) with energy dispersive X-ray spectroscopy (EDS) on iron particles (Aldrich) exposed to carbonate buffer (15 mM) and nitrobenzene for several days revealed the formation of siderite ($FeCO_3$) (28). Siderite was also identified in a

column of iron filings (VWR Scientific) exposed to carbonate buffered water and trichloroethene (5). Peerless iron that had been exposed to groundwater from the Borden aquifer for several weeks showed disappearance of maghemite, an abundance of magnetite, and the formation of a new phase identified by Raman spectroscopy as green rust (27). Green rusts are mixed-valent iron oxyhydroxide salts whose interlayers contain anions such as chloride, sulfate, and carbonate (29-31). Green rusts have been identified in natural soil like environments (32), and are commonly found as aqueous corrosion products of iron (33). More relevant is the greenish-blue precipitate observed on iron particle surfaces in a column exposed to high concentrations of CCl_4 in our laboratory (3). SEM on grains removed from this column revealed hexagonal crystals (Figure 2.2) that are consistent with those of green rust (33).

Thus, it appears likely that the oxide layer on Fe^0 evolves from a predominantly Fe(III) phase under air-formed conditions to a mixed-valent or pure Fe(II) phase under the highly-reducing conditions found in groundwater remediation applications. Therefore, the oxide formed on Fe^0 during long-term dechlorination experiments is probably best modeled as a mixed-valent or pure Fe(II) phase such as magnetite, siderite, or green rust, rather than a pure Fe(III) phase such as maghemite, hematite, or goethite. Additional solid phases, due to precipitation of sulfides and carbonates, may be important under some environmental conditions, but their role in the reduction of contaminants by Fe^0 is not addressed in the following discussion.

2.4.2 The Oxide as a Physical Barrier

The oxide surface layer can be interpreted as a physical barrier to mass transport (similar to the role of an oxide film on a passivated electrode) that inhibits ET from the iron metal to RX (4). If the oxide layer is a non-conductive physical barrier, then ET may occur from the metal to the dissolved substrate through defects such as pits or grain boundaries. Pitting and crevice (grain) corrosion are localized forms of corrosion, where rupture of the oxide layer introduces new paths for diffusion (i.e., pore diffusion) and new "catalytic" dissolution pathways (34, 35).

Pitting is typically initiated where an aggressive anion, such as chloride, stimulates dissolution at a defect or inclusion in the surface of the oxide (36, 37). Once pit growth is established, it usually continues until the oxide film is perforated, exposing bare metal (Figure 2.1b). The new, longer diffusion path to the bottom of the pit restricts transport of aqueous oxidants (e.g., O_2 or RX) from the bulk solution, which creates a concentration gradient in the pit that is known as a differential aeration cell (in reference to pitting

corrosion in the presence oxygen) (38, 39). Alone, the oxidant concentration gradient that develops across the pit is not enough to sustain a significantly increased corrosion rate, but two additional effects are involved. First, a pH gradient develops as hydrolysis of Fe^{2+} at the bottom of the pit releases hydrogen ions which make the bottom of the pit more acidic (37). Acidic conditions at the bottom of the pit prevent an oxide layer from reforming. Second, at the mouth of the pit, relatively alkaline conditions and Fe^{2+} diffusing from below favor repassivation along the edges of the pit (38).

Although the microscopic mechanism of pit initiation and oxide breakdown is still not fully understood (40, 41), the macroscopic behavior of enhanced local dissolution and diffusion of dissolved metal ions can be described with current-potential (i-E) curves as shown in Figure 2.3. The solution conditions in a pit create two distinct electrochemical cells. At the bottom of the pit, the oxidation half-reaction is acidic dissolution of Fe^0 (equation 1), which is balanced primarily by reduction of water to hydrogen gas (equation 3). The second cell is at the mouth of the pit, where the half-reactions are dissolution at a passivated iron metal surface (alkaline conditions) and reduction of water or stronger oxidants such as O_2 or RX.

If the pitting mechanism is involved in the reduction of RX by Fe^0, then (in the absence of O_2 and presence of RX) the major reduction half-reaction at the mouth of the pit will be dehalogenation of RX (equation 4) (9). At equilibrium, anodic and cathodic reactions must be balanced in each cell, and these conditions determine the net corrosion rate in each case. Figure 2.3 illustrates this principle for conditions at the bottom of a pit (labeled B) and for the mouth of a pit (labeled M) using i-E curves. The acceleration of corrosion associated with pitting results because the proximity of the two cells creates a coupled cell where acidic iron dissolution at the bottom of the pit and reduction of a strong oxidant at the mouth of the pit become the controlling anodic and cathodic processes. If pitting contributes to reduction of RX by Fe^0, the dehalogenation rate will equal the net corrosion rate of the short-circuited cell (labeled Pit in Figure 2.3).

Since pitting corrosion is greatly accelerated by aggresive anions such as chloride (42, 43), and chloride is a product of dechlorination (equation 4), it is possible that dechlorination might favor further dechlorination if enough chloride accumulates to provide auto-catalysis. At least two studies have found effects consistent with the possibility of an auto-catalytic link between dechlorination and pitting corrosion: Heland *et al.* reported a 60% increase in CCl_4 reduction rates by Fe^0 with increased contact time in batch systems (44), and Johnson *et al.* showed that large concentrations of added chloride (up to 60 mM) increased the rate of CCl_4 degradation as much as four-fold (13). However, the gradual

increase in rate with time that would be expected from a strongly auto-catalytic process has rarely been observed, and most groups have reported consistently first-order degradation kinetics (5, 45), or gradually decreasing rates with time (i.e., tailing) (2, 46-48).

Although there is little evidence for auto-catalysis in dechlorination by Fe^0, it is still possible that localized corrosion contributes to the remediation of contaminants in environmental applications. Various investigators have postulated that localized corrosion contributes through increased surface area (44) and creation of corrosion cell domains (49-51). The corrosion cell model works on the same principle as the electrochemical model described above (Figure 2.3), but invokes additional effects such as the reduction of protons as the major cathodic reaction, and the creation of an electrical double layer between the anode and cathode that permits transport due to electrical migration as well as diffusion. Although many aspects of these models are plausible, there are not yet any data that specifically support them, and a study that systematically addresses the role of localized corrosion in remediation applications of Fe^0 remains to be done.

2.4.3 The Oxide as a Semiconductor

In addition to direct reduction of RX via pits or other defects in the oxide layer, it is possible that reduction occurs indirectly, by transport of charge through the oxide from Fe^0 to RX. Possible charge carriers within the oxide include: (i) anion and cation vacancies (lattice sites where ions are absent), (ii) anion and cation interstitials (sites where ions are imbedded between lattice sites), and (iii) electrons and holes (52). In this section, we will focus on electrons as the charge carriers and examine the transport of electrons through the oxide layer, treating the oxide as a semiconductor.

Most iron oxides are semiconductors (Table 2.1). Specifically, this means that they exhibit a bandgap (E_{BG}) where no energy levels are found, between the conduction band (energy levels unoccupied by electrons) and the valence band (energy levels occupied by electrons) (53-55). The oxide layer that forms on Fe^0 can also be considered a semiconductor. For example, passive films composed of magnetite, maghemite, and other mixed-valent *(hydr)oxides (see section on Composition of the Oxide)* have been modeled as semiconducting Fe_2O_3 that is doped with Fe(II) (56).

Long term exposure of granular Fe^0 to the highly-reducing conditions found in groundwater remediation applications, however, is likely to produce oxides that are mixed-valent. These oxides will exhibit metallic conductivity, because mixed oxidation states impart mobility of electrons between atoms (53). For example, magnetite is mixed-valent, has a very small band gap (Table 2.1), and exhibits conductivity that is typical of a metal.

The same should be true for the green rusts. (Green rusts, however, do not have well-defined crystal structures (57), so their electronic structure does not appear to have been investigated.) Green rusts are of particular interest because of recent reports that they form on Fe^0 under environmental conditions (3, 27).

The details of ET involving semiconductors are determined by their electron energy levels. Important energy levels include: (i) the upper edge of the valence band (E_{VB}); (ii) the lower edge of the conduction band (E_{CB}); and (iii) the Fermi energy (E_F), which is the electrochemical potential of electrons in the bulk semiconductor. Table 2.1 contains a compilation of these energies for the iron oxides. Passive films on Fe^0 have a bandgap of ~1.9 eV and a flatband potential of -0.3 to 0.0 V (vs. NHE at pH 7) (58-61). (The flatband potential is equivalent to the Fermi energy before ET in or out of the semiconductor produces a space charge region (55). Figure 2.1c summarizes these energy levels in a band diagram for a single crystal semiconductor that has been adapted for the Fe^0-oxide-water system (62).

A fully-accurate band diagram for oxides present on grains of Fe^0 used in remediation applications, however, would be more complicated than the version portrayed in Figure 2.1c, because the oxide layer that forms on granular Fe^0 lacks long-range order. Passive films on Fe^0 are typically only a few monolayers thick, so long-range order normal to the surface cannot develop. Thicker oxide layers tend to be amorphous because a more coherent film would be strained and break up (55, 63-66). While thick oxide layers will have bands equivalent to the conduction and valence bands found in single crystal semiconductors (shown in Figure 2.1c), additional bands, which result from a large density of impurities or ions in a different oxidation state, may also be present (55, 67). In addition, there will be a much greater density of localized states (energy levels that exist in the bandgap) than is found in single crystal semiconductors. These localized states result from the lack of identical lattice sites throughout the oxide (55, 63, 65-67). Impurity bands and localized states are important because they can serve as electron donors in ET (60, 68), and because they are likely to be abundant in the oxide layers that develop during remediation applications of Fe^0.

The band diagram in Figure 2.1c is also simplified with respect to electric field effects. The differences in energy levels of E_F(metal), E_F(oxide), and E^0(RX/R•) will produce electric fields in the oxide layer, and these fields can affect ET. For example, at equilibrium, there will be a potential barrier for injecting electrons from Fe^0 to the conduction band of the iron oxide, because E_F(oxide) is more negative than E_F(metal) (69). Similarly, because E_F(oxide) can be more negative than E^0(RX/R•), the oxide layer may be

in depletion: that is, there may be a space charge region in the oxide layer that acts as a barrier to electron transport from the conduction band to RX. It should be noted that this barrier develops as equilibrium is established between the semiconductor and RX because ET occurs from the semiconductor to RX until E_F(oxide) = E^0(RX) (54). This barrier may not be fully established, however, because the rate at which equilibration occurs depends on the rate of ET between the oxide and redox couples in solution (54), and this appears to be fairly slow for iron-oxide-RX systems (9, 15).

Although the semiconductor band model shown in Figure 2.1c is a simplification of the iron-oxide-solution system, it does help reveal some of the factors controlling reduction of chlorinated aliphatic compounds by passivated iron. For ET from Fe^0 through the oxide layer to RX to be thermodynamically favorable, the energy of electrons in the metal and/or the oxide must be more negative than E^0(redox). In addition, the likelihood of ET from the semiconductor to the electrolyte is greater if there is good overlap between electron energy levels in the metal or semiconductor and the unoccupied electron energy levels of the redox couple in solution (55, 67).

If ET through the oxide originates from the metal, then E_F(metal) will determine the driving force for reaction. For the reduction of CCl_4 by passivated iron, E_F(metal) is more negative than $E^0(CCl_4/{\bullet}CCl_3)$ (62) so electrons could originate from Fe^0. ET through the oxide may occur by tunneling (direct or resonance) (55, 65, 70, 71). Direct tunneling of electrons from the underlying Fe^0 through the oxide layer is only possible for thin films of oxide (~10 Å). Resonance tunneling, in which the electrons tunnel or "hop" between localized states in the oxide (55, 65, 66, 70, 71), is more probable for the oxide layer that forms on grains of Fe^0 in remediation applications.

If, however, ET from the oxide layer is not influence by the underlying Fe^0, the driving force will be determined by E_{CB} of the oxide, E_F(oxide), or the energies of localized states or impurity bands. For the reduction of CCl_4 by passivated iron, E_{CB} and E_F(oxide) are both more negative than $E^0(CCl_4/{\bullet}CCl_3)$ (62). The energy levels of localized states and impurity bands are unknown, but presumably there will be a significant number of localized states with energies sufficiently negative to drive reduction of most chlorinated aliphatic compounds. Thus, the electrons involved in ET to RX could originate from the conduction band or localized states in the oxide. If a space charge barrier exists (which we believe to be the case for passivated iron in the presence of aqueous CCl_4), conduction band electrons will have to tunnel through the barrier either directly or via localized states (55, 63, 66, 68, 72). There is evidence that ET to dissolved ferrous cyanide can occur via tunneling from the conduction band through the space charge region of a passivated iron

electrode (73, 74). However, our studies have shown that ET from granular Fe^0 to aqueous CCl_4 does not occur via the oxide conduction band (62). Thus, in groundwater remediation applications, where there are likely to be high concentrations of Fe(II) ions in the oxide layer, ET is more likely to occur via resonance tunneling from the metal.

2.4.4 The Oxide as a Coordinating Surface

In addition to direct ET from zero-valent metal to the adsorbed contaminant (Figures 2.1a-b) or indirect ET through the oxide film (Figure 2.1c), there are two possibilities for reduction of RX at the surface of the oxide film (Figure 2.1d): (i) electrons may be donated from surface-bound Fe(II) sites created by adsorption of Fe^{2+} from solution (75), or (ii) electrons may originate from the underlying metal, creating Fe(II) sites within the oxide lattice ("structural" Fe(II) (76)), which eventually result in surface sites that reduce RX. Reactive surface Fe(II) sites have been postulated in a recent study of the reduction of nitro aromatic compounds in suspensions of Fe(III) minerals in the presence of dissolved Fe(II) (75). Reduction via ET from surface reactive sites is further supported by additional studies showing the reduction of chlorinated aliphatics (7, 77-81) and inorganic groundwater contaminants in the presence of iron oxides (alone, no Fe^0) (82, 83).

In the presence of a finite number of sites, the rate of dehalogenation should increase with increasing concentration of RX until there are no more vacant surface sites, producing the hyperbolic profile often attributed to site saturation effects in heterogeneous systems (84). Site saturation behavior has been observed for the reduction of CCl_4 by Fe^0 (13, 15, 85), and the reduction of tetrachloroethene by zinc metal in laboratory batch experiments (12). It has also been suggested that the effects of initial contaminant concentration and competing adsorbates (such as chromate or EDTA) on the kinetics of reduction of chlorinated aliphatic compounds might reflect competition for surface coordination sites (12, 13).

Adsorbate competition for a limited number of sites may be modeled with surface complexation models (SCMs). The SCMs extend equilibrium solution chemistry to include surface chemical species. Fundamentally, these models are based on two main assumptions: (i) adsorption occurs at coordinating sites with specific functional groups, and (ii) equilibrium can be described using mass law equations with an electrostatic correction derived from electric double layer theory (86-88). The mass law equations and a mole balance on the total number of sites yield a set of simultaneous equations that can be solved numerically. In the following analysis, we derive a simplified SCM (with no electrostatics) that describes the site saturation behavior observed in Fe^0 systems.

Additional applications of the SCM to remediation by Fe^0 include: (i) evaluation of the role of adsorption of Fe^{2+} to the iron oxide surface, and (ii) understanding the effect of site competition from co-contaminants and naturally occurring ligands.

SCMs have been used to study metal oxide dissolution where the dissolution rate is proportional to the number of sites occupied by ligands that promote dissolution (89-92). The oxide surface is modeled assuming a finite number of surface functional groups exist that act as possible dissolution sites. The following derivation is based on a similiar hypothesis: that the dehalogenation rate is proportional to the number of sites occupied by the chlorinated aliphatic compound.

As discussed earlier, it is reasonable to assume the surface is a mixed Fe(II)/Fe(III) oxide, sometimes approaching a pure Fe(II) oxide under highly reducing conditions (Figure 2.1d). The model involves adsorption (or association) of the dissolved species with the surface and subsequent ET to form products:

$$\equiv FeOH^0 + RX \underset{k_2}{\overset{k_1}{\rightleftharpoons}} \equiv FeOH\text{-}RX \overset{k_{RX}}{\rightarrow} \text{Products} \qquad (5)$$

The rate equation, with the assumption of a steady-state population of the precusor complex ≡FeOH-RX, is:

$$-\frac{d[RX]}{dt} = -k_{RX}\rho_a[\equiv FeOH\text{-}RX] \qquad (6)$$

where ρ_a is the surface area concentration of the solid ($m^2\ L^{-1}$), which relates surface concentrations (mol m^{-2}) to aqueous concentrations (mol L^{-1}). The rate equation can be modified to include additional terms that represent adsorption to non-reactive sites (93, 94), or solubility enhancements in the presence of surfactants (95) and dissolved organic matter, as the significance of these processes becomes better understood. The concentration of the precusor complex can be found by substituting the mass law equations (from Table 2.2) into a mole balance equation for the total number of surface sites, $[\equiv Fe_{TOT}]$:

$$[\equiv Fe_{TOT}] = [\equiv FeOH^0] + [\equiv FeL] + [\equiv FeOH\text{-}RX] \qquad (7)$$

As written, equation 7 does not include adsorption of aqueous metals (such as Fe^{2+}), formation of ternary complexes, or formation of binuclear complexes. These terms have

been neglected only because there is not yet a three-dimensional data set collected as a function of pH, ionic strength, and ligand concentration with which to evaluate the importance of such a large number of complexes and adsorptive sinks. When the data become available, the model can be revised to include the sum of all plausible metal-centered complexes.

Substitution of the mass law equations from Table 2.2 into equation 7 gives a general competition model describing the rate of dehalogenation by iron in the presence of a competing ligand:

$$-\frac{d[\mathrm{RX}]}{dt} = \frac{k_{RX}K_{RX}[\equiv \mathrm{Fe_{TOT}}][\mathrm{RX}]}{1 + K_{RX}[\mathrm{RX}] + K_L[\mathrm{HL}]} \tag{8}$$

In the absence of any competition (e.g., a single RX with no ligands present), equation 8 simplifies to:

$$-\frac{d[\mathrm{RX}]}{dt} = \frac{k_{RX}K_{RX}[\equiv \mathrm{Fe_{TOT}}][\mathrm{RX}]}{1 + K_{RX}[\mathrm{RX}]} \tag{9}$$

Equation 9 is a hyperbolic relationship, similar to the Michaelis-Menton equation derived for enzyme kinetics (96), the Langmuir equation as applied to adsorption on soils (97), and an adaptation of these models for dechlorination by Fe^0 that we published previously (13). As such, all four models are capable of describing site saturation phenomena commonly found in heterogenous systems; however, only the new model (equations 8 and 9) explicitly distinguishes thermodynamically-related parameters from the kinetic constants.

The non-competitive SCM (equation 9) can estimate the equilibrium association of RX with the surface (K_{RX}), and the surface rate constant (k_{RX}), by fitting previously published site saturation data for systems containing Fe^0 (Figure 2.4). To do this, we estimated the total number of sites using

$$[\equiv \mathrm{Fe_{TOT}}] = \rho_a N_s / A \tag{10}$$

where N_s is the number of sites per unit area and A is Avogadro's number. Experimental values of N_s for common iron oxides range from 2 -16 sites nm^{-2} (98), with an average

calculated surface density of 5 sites nm^{-2} (87). Using reported Fe^0 surface area concentrations (ρ_a, typically measured using BET adsorption techniques) and an estimated value of N_s of 5 sites nm^{-2}, the total number of sites was estimated for two different Fe^0 systems (Table 2.3). K_{RX} and k_{RX} were then determined as adjustable parameters by nonlinear least-squares parameter adjustment with equation 9. The arrows in Figure 2.4 provide graphical interpretation of K_{RX} and k_{RX} by indicating the maximum rate of dechlorination (equivalent to V_{max} in the Michaelis-Menton formulation (13)) and the conditional equilibrium constant for the association of RX with the surface (equivalent to the reciprocal of $K_{1/2}$, which is the concentration of RX at $V_{max}/2$ in the Michaelis-Menton formulation (13)).

Even though the two systems contain different types of Fe^0, the estimated values of K_{RX} are the same within five percent (Table 2.3). Since CCl_4 is most likely adsorbed to the surface by a weak hydrophobic interaction (13), partitioning of CCl_4 to the surface should be independent of iron type. On the other hand, values for the surface reaction rate constant (k_{RX}) differ by a factor of ten. This can be attributed to differences in intrinsic reactivity of the sites on each metal. Similar results and conclusions were obtained previously from the same data using a less explicit model (13).

The competitive SCM (equation 8) can be used to model the rate of dehalogenation in the presence of competing ligands. Given the weak interaction of RX with the surface, complex formation by strong ligands will block sites, thereby decreasing the rate of dehalogenation. This effect has been observed for the reduction of CCl_4 in the presence of acetate, ascorbate, and catechol (13). However, as shown in Figure 2.5, the observed inhibition is less than that which is predicted from the competitive SCM (equation 8) with the values in Table 2.3. The implication of this result is that dehalogenation rates approach a plateau at 50-70% of non-competitive rates, rather than declining rapidly toward zero as predicted by the model. For this to be the case, there must be two (or more) mechanisms of reaction, at least one of which is unaffected by ligand competition. There is not yet enough data on the effect of ligands to be certain of this interpretation, but several mechanisms that might not be sensitive to ligand competition can be suggested based on what has already been discussed. One possibility is formation of ternary complexes (FeOFeL) or metal bound complexes ($FeOFe^+$) that permit or even facilitate ET through bridging ligands. An example of the latter was observed in the catalytic dissolution of hematite in the presence of Fe(II) and oxalate (99). Other possibilities include pitting of the surface oxide layer or tunneling across the oxide-water interface (see section on The Oxide as a Semiconductor).

2.5 Implications for Environmental and Engineering Applications

The treatment of environmental contaminants with zero-valent metals is still a new field, but one that has fundamental features in common with a variety of other chemical technologies. These include environmental applications such as (i) "redox manipulation" to form in-situ treatment walls of structural ferrous iron (100), (ii) high pressure grinding (ball milling) to degrade chlorinated benzenes (101), (iii) high temperature oxidation on metal oxides (102), and (iv) oxidation by photocatalysis using semiconducting oxides (103), as well as non-environmental applications like (v) chemical synthesis with dissolving metals (104) and Grignard reagents (105), (vi) controlling material damage by corrosion of metals and metal oxides (38), and (vii) high pressure lubrication with chlorinated hydrocarbons (106). Although our primary concern in this paper has been with contaminant degradation by Fe^0, we have tried to perserve generality in our perspective throughout.

In an effort to reach a comprehensive general picture of the mechanism of contaminant degradation in metal-oxide-water systems, we have tried to balance our treatment of the oxide to reflect its various roles as a physical barrier, a semiconductor, and a coordinating surface. Each model provides its own useful insights into the treatability of contaminants with zero-valent metals. For example: (i) the physical barrier posed by the oxide layer may be overcome by reversing the strategies used by corrosion engineers to protect metals from corrosion, (ii) the semiconducting properties of the oxide layer may respond to manipulations that are equivalent to doping, and (iii) the coordination properties of the surface may be altered in predictable ways by various types of ligands and surfactants. To develop these ideas further, it will help to clearly distinguish the processes involved in each model (as we have tried to do in Figs. 2.1b-d).

Distinguishing the passive film, semiconductor, and coordinating surface models does not make them exclusive, however, and additional insights are to be gained by examining their common elements. For example, (de)passivation involves changes in the oxide layer that can be caused by surface complexation (92), photoinduced electrochemical reactions on passive films can be attributed to semiconducting properties of the film (64), and doping of a semiconductor may be initiated by ligand attachment (i.e., surface complexation) (107). One consequence of the former, is that surface complexation by corrosion inhibitors can inhibit the degradation of chlorinated solvents on aluminum (108). A consequence of the latter, is that defects in coordination structure of semiconducting

oxides can enhance photoreactivity (109). With respect to the remediation of RX by Fe^0, there are many elements common to all three models discussed in this review.

The benefits of unifying specialized models of the oxide-water interface into a more comprehensive general picture have been argued previously for geochemistry and corrosion science (34, 92, 110). Organic substances play a small role in these fields, mainly as ligands whose fate is not of primary interest. Perhaps the impact of future research in remediation with zero-valent metals will be the development of the largely unexplored disciplinary-interface between organic chemistry (contaminant degradation) and corrosion science (passive films as physical barriers), solid state physics (semiconducting oxides), and geochemistry (surface complexation at the mineral-water interface).

2.6 List of Symbols

ρ_a Surface area concentration ($m^2\ L^{-1}$)

k_1 Forward association rate constant ($L\ mol^{-1}\ s^{-1}$)

k_2 Backward association rate constant (s^{-1})

k_{RX} Rate constant for reduction of RX at the surface (s^{-1})

K_{RX} Conditional equilibrium constant for association of RX with surface ($L\ mol^{-1}$)

N_s Number of sites per unit area ($mol\ m^{-2}$)

A Avogadro's number (6.02×10^{23} sites mol^{-1})

E_F Fermi energy (eV)

E_{CB} Conduction band energy (eV)

E_{VB} Valence band energy (eV)

E_{BG} Band gap energy (eV)

2.7 Acknowledgments

Acknowledgement is made to the donors of The Petroleum Research Fund, administered by the ACS, for the primary support of this research through Type AC award number 29995-AC5 and two supplemental awards. Additional support was provided by the University Consortium Solvents-In-Groundwater Research Programme, and the Murdock Trust. In addition, the authors gratefully acknowledge J. Westall (Oregon State University) and B. Fish (Oregon Graduate Institute) for their insightful comments on this manuscript, and T. Johnson (Oregon Graduate Institute) for use of Figure 2.2.

2.8 Literature Cited

(1) Tratnyek, P. G. Putting corrosion to use: Remediation of contaminated groundwater with zero-valent metals. *Chem. Ind. (London)* 1996, 499-503.

(2) Gillham, R. W.; O'Hannesin, S. F. Enhanced degradation of halogenated aliphatics by zero-valent iron. *Ground Water,* 1994, *32*, 958-967.

(3) Johnson, T. L.; Tratnyek, P. G. A column study of carbon tetrachloride dehalogenation by iron metal; *Proceedings of the 33rd Hanford Symposium on Health & the Environment. In-Situ Remediation: Scientific Basis for Current and Future Technologies,* Pasco, WA, Battelle Pacific Northwest Laboratories, 1994; Vol. 2, pp. 931-947.

(4) Agrawal, A.; Tratnyek, P. G. Reduction of nitro aromatic compounds by zero-valent iron metal. *Environ. Sci. Technol.* 1996, *30*, 153-160.

(5) Mackenzie, P. D.; Baghel, S. S.; Eykholt, G. R.; Horney, D. P.; Salvo, J. J.; Sivavec, T. M. Pilot-scale demonstration of reductive dechlorination of chlorinated ethenes by iron metal; *209th National Meeting,* Anaheim, CA, American Chemical Society, 1995; Vol. 35, No. 1, pp. 796-799.

(6) Matheson, L. J.; Tratnyek, P. G. Reductive dehalogenation of chlorinated methanes by iron metal. *Environ. Sci. Technol.,* 1994, *28*, 2045-2053.

(7) Sivavec, T. M.; Horney, D. P. Reduction of chlorinated solvents by Fe(II) minerals; 213th National Meeting, San Francisco, CA, American Chemical Society, 1997; Vol. 37, No. 1, pp. 115-117.

(8) Sivavec, T. M.; Horney, D. P. Reductive dechlorination of chlorinated ethenes by iron metal; *209th National Meeting,* Anaheim, CA, American Chemical Society, 1995; Vol. 35, No. 1, pp. 695-698.

(9) Scherer, M. M.; Westall, J. C.; Ziomek-Moroz, M.; Tratnyek, P. G. Kinetics of carbon tetrachloride reduction at an oxide-free iron electrode. *Environ. Sci. Technol.* 1997, *31*, 2385-2391.

(10) Johnson, T. L.; Tratnyek, P. G. Dechlorination of carbon tetrachloride by iron metal: The role of competing corrosion reactions; *209th National Meeting,* Anaheim, CA, American Chemical Society, 1995; Vol. 35, No. 1, pp. 699-701.

(11) Roberts, A. L.; Totten, L. A.; Arnold, W. A.; Burris, D. R.; Campbell, T. J. Reductive elimination of chlorinated ethylenes by zero-valent metals. *Environ. Sci. Technol.* 1996, *30*, 2654-2659.

(12) Arnold, W. A.; Roberts, A. L. Development of a quantitative model for chlorinated ethylene reduction by zero-valent metals; *213th National Meeting,* San Francisco, CA, American Chemical Society, 1997; Vol. 37, No. 1, pp. 76-77.

(13) Johnson, T. L.; Fish, W.; Gorby, Y. A.; Tratnyek, P. G. Degradation of carbon tetrachloride by iron metal: Complexation effects on the oxide surface. *J. Contam. Hydrol.* 1998, *29*, 377-396.

(14) Haderlein, S. B.; Pecher, K. Pollutant reduction in heterogeneous Fe(II)/Fe(III) systems. In *Kinetics and Mechanism of Reactions at the Mineral/Water Interface*; Grundl, T.; Sparks, D., Eds; American Chemical Society: 1998.

(15) Johnson, T. L.; Scherer, M. M.; Tratnyek, P. G. Kinetics of halogenated organic compound degradation by iron metal. *Environ. Sci. Technol.,* 1996, *30*, 2634-2640.

(16) Nagayama, M.; Cohen, M. The anodic oxidation of iron in neutral solution: 1. The nature and composition of the passive film. *J. Electrochem. Soc.,* 1962, *109*, 781-790.

(17) Davenport, A. J.; Bardwell, J. A.; Vitus, C. M. In situ XANES study of galvanostatic reduction of the passive film on iron. *J. Electrochem. Soc.,* 1995, *142*, 721-724.

(18) Davenport, A. J.; Sansone, M. High resolution in situ XANES investigation of the nature of the passive film on iron in a pH 8.4 borate buffer. *J. Electrochem. Soc.,* 1995, *142*, 725-730.

(19) Oblonsky, L. J.; Devine, T. M. A surface enhanced Raman spectroscopic study of the passive films formed in borate buffer on iron, nickel, chromium and stainless steel. *Corr. Sci.* 1995, *37*, 17-41.

(20) Gui, J.; Devine, T. M. In situ vibrational spectra of the passive film on iron in buffered borate solution. *Corr. Sci.,* 1991, *32*, 1105-1124.

(21) Cahan, B. D.; Chen, C.-T. The nature of the passive film on iron. III. The chemi-conductor model and further supporting evidence. *J. Electrochem. Soc.* 1982, *129*, 921-925.

(22) Toney, M. F.; Davenport, A. J.; Oblonsky, L. J.; Ryan, M. P.; Vitus, C. M. Atomic structure of the passive oxide film formed on iron. *Phys. Rev. Let.,* 1997, *79*, 4282-4285.

(23) O'Grady, W. E. Mössbauer study of the passive oxide film on iron. *J. Electrochem. Soc.,* 1980, *127*, 555-563.

(24) Bockris, J. O. M. Spectroscopic observations on the nature of passivity. *Corr. Sci.,* 1989, *29*, 291-312.

(25) Sivavec, T. M.; Horney, D. P.; Baghel, S. S. Reductive dechlorination of chlorinated ethenes by iron metal and iron sulfide minerals; *Emerging Technologies in Hazardous Waste Management VII, Extended Abstracts for the Special Symposium,* Atlanta, GA, Industrial & Engineering Chemistry Division, American Chemical Society, 1995; Vol. pp. 42-45.

(26) Pratt, A. R.; Blowes, D. W.; Ptacek, C. J. Products of chromate reduction on proposed subsurface remediation material. *Environ. Sci. Technol.,* 1997, *31*, 2492.

(27) Odziemkowski, M. S.; Gillham, R. W. Surface redox reactions on commerical grade granular iron (steel) and their influence on the reductive dechlorination of solvent. Micro Raman spectroscopy studies*; 213th National Meeting,* San Francisco, CA, American Chemical Society, 1997; Vol. 37, No. 1, pp. 177-180.

(28) Agrawal, A.; Tratnyek, P. G.; Stoffyn-Egli, P.; Liang, L. Processes affecting nitro reduction by iron metal: Mineralogical consequences of precipitation in aqueous carbonate environments; *209th National Meeting,* Anaheim, CA, American Chemical Society, 1995; Vol. 35, No. 1, pp. 720-723.

(29) Taylor, R. M. Formation and properties of Fe(II)Fe(III) hydroxy-carbonate and its possible significance in soil formation. *Clay Miner.,* 1980, *15*, 369-382.

(30) Schwertmann, U.; Cornell, R. M. *Iron Oxides in the Laboratory*; VCH: Weinheim, 1991.

(31) Hansen, H. C. B.; Borggaard, O. K.; Sørensen, J. Evaluation of the free energy of formation of Fe(II)-Fe(III)hydroxide-sulphate (green rust) and its reduction of nitrite. *Geochim. Cosmochim. Acta,* 1994, *58*, 2599-2608.

(32) Koch, C. B.; Moerup, S. Identification of green rust in an ochre sludge. *Clay Miner.,* 1991, *26*, 577-82.

(33) Kassim, J.; Baird, T.; Fryer, J. R. Electron microscope studies of iron corrosion products in water at room temperature. *Corr. Sci.,* 1982, *22*, 147-158.

(34) Sato, N. Toward a more fundamental understanding of corrosion processes. *Corrosion,* 1989, *45*, 354-368.

(35) Sukamto, J. P. H.; Smyrl, W. H.; Casillas, N.; Al-Odan, M.; James, P.; Jin, W.; Douglas, L. Microvisualization of corrosion. *Mat. Sci. Eng.,* 1995, *A198*, 196.

(36) Sato, N. Anodic breakdown of passive films on metals. *J. Electrochem. Soc.,* 1982, *129*, 255-260.

(37) Sato, N. The stability of pitting dissolution of metals in aqueous solution. *J. Electrochem. Soc.,* 1982, *129*, 260-264.

(38) Jones, D. A. *Principles and Prevention of Corrosion*; Macmillan: New York, 1992.

(39) Roe, F. L.; A., L.; Funk, T. Simulating microbiologically influenced corrosion by depositing extracellular biopolymers on mild steel surfaces. *Corr. Sci.,* 1996, *52*, 744-752.

(40) Pou, T. E.; Murphy, O. J.; Young, V.; Bockris, J. O. M. Passive films on iron: The mechanism of breakdown in chloride containing solutions. *J. Electrochem. Soc.,* 1984, *131*, 1243-1251.

(41) Asanuma, M.; Aogaki, R. Nonequilibrium fluctuation theory on pitting dissolution. II. Determination of surface coverage of nickel passive film. *J. Chem. Phys.*, 1997, *106*, 9938-9943.

(42) Abdel, M. S.; Wahdan, M. H. Anodic behaviour of mild steel in deaerated carboxylic acid solutions containing NO_2^-, Cl^-, and NO_3^- ions. *Br. Corrosion J.*, 1981, *16*, 205-211.

(43) Bardwell, J. A.; Fraser, J. W.; MacDougall, B.; Graham, M. M. Influence of the anodic oxide film on pitting of iron. *J. Electrochem. Soc.*, 1992, *139*, 366-370.

(44) Helland, B. R.; Alvarez, P. J. J.; Schnoor, J. L. Reductive dechlorination of carbon tetrachloride with elemental iron. *J. Haz. Mat.*, 1995, *41*, 205-216.

(45) Orth, S., W.; Gillham, R. W. Dechlorination of trichlorethene in aqueous solution using Fe(0). *Environ. Sci. Technol.*, 1996, *30*, 66-71.

(46) Lipczynska-Kochany, E.; Harms, S.; Milburn, R.; Sprah, G.; Nadarajah, N. Degradation of carbon tetrachloride in the presence of iron and sulphur containing compounds. *Chemosphere,* 1994, *29*, 1477-1489.

(47) Schreier, C. G.; Reinhard, M. Transformation of chlorinated organic compounds by iron and manganese powders in buffered water and in landfill leachate. *Chemosphere,* 1994, *29*, 1743-1753.

(48) Campbell, T. J.; Burris, D. R.; Roberts, A. L.; Wells, J. R. Trichloroethylene and tetrachloroethylene reduction in a metallic iron-water-vapor batch system. *Environ. Toxicol. Chem.*, 1997, *16*, 625-630.

(49) Powell, R. M.; Puls, R. W.; Hightower, S. K.; Sabatini, D. A. Coupled iron corrosion and chromate reduction: Mechanisms for subsurface remediation. *Environ. Sci. Technol.*, 1995, *29*, 1913-1922.

(50) Powell, R. M.; Puls, R. W. Proton generation by dissolution of intrinsic or augmented aluminosilicate minerals for in situ contaminant remediation by zero-valence-state iron. *Environ. Sci. Technol.*, 1997, *31*, 2244-2251.

(51) Khudenko, B. M. Feasibility evaluation of a novel method for destruction of organics. *Wat. Sci. Technol.*, 1991, *23*, 1873-1881.

(52) Battaglia, V.; Newman, J. Modeling of a growing oxide film: The iron/iron oxide system. *J. Electrochem. Soc.*, 1995, *142*, 1423-1430.

(53) Cox, P. A. *Transition Metal Oxides: An Introduction to their Electronic Structure and Properties*; Oxford: New York, 1997.

(54) Finklea, H. O. Semiconductor electrode concepts and terminology. In *Semiconductor Electrodes*; Finklea, H. O., Ed; Elsevier: Amsterdam, 1988; pp. 1-42.

(55) Morrison, S. R. *Electrochemistry at Semiconductor and Oxidized Metal Electrodes*; Plenum: New York, 1980.

(56) Schmuki, P.; Büchler, M.; Virtanen, S.; Böhni, H.; Muller, R.; Gauckler, L. J. Bulk metal oxides as a model for the electronic properties of passive films. *J. Electrochem. Soc.*, 1995, *142*, 3336-3342.

(57) Leland, J. K.; Bard, A. J. Photochemistry of colloidal semiconducting iron oxide polymorphs. *J. Phys. Chem.*, 1987, *91*, 5076-5083.

(58) Schmuki, P.; Böhni, H. Illumination effects on the stability of the passive film on iron. *Electrochim. Acta,* 1995, *40*, 775-783.

(59) Abrantes, L. M.; Peter, L. M. Transient photocurrents at passive iron electrodes. *J. Electroanal. Chem.*, 1983, *150*, 593-601.

(60) Stimming, U.; Schultze, J. S. The capacity of passivated iron electrodes and the band structure of the passive film. *Ber. Bunsenges. Phys. Chem.*, 1976, *80*, 1297-1302.

(61) Wilhelm, S. M.; Yun, K. S.; Ballenger, L. W.; Hackerman, N. Semiconductor properties of iron oxide electrodes. *J. Electrochem. Soc.*, 1979, *126*, 419-424.

(62) Balko, B. A.; Tratnyek, P. G. Photoeffects on the reduction of carbon tetrachloride by zero-valent iron. *J. Phys. Chem B.*, 1998, *102*, 1459-1465.

(63) Searson, P. C.; Latanision, R. M.; Stimming, U. Analysis of the photoelectrochemical response of the passive film on iron in neutral solutions. *J. Electrochem. Soc.*, 1988, *135*, 1358-1363.

(64) Stimming, U. Photoelectrochemical studies of passive films. *Electrochim. Acta,* 1986, *31*, 415-429.

(65) Stimming, U. Tunnel processes in photoelectrochemical reactions of passive films. *Langmui,r* 1987, *3*, 423-428.

(66) Newmark, A. R.; Stimming, U. Photoinduced electron transfer involving localized electronic states. *Electrochim. Acta,* 1987, *32*, 1217-1221.

(67) Gerischer, H. Remarks on the electronic structure of the oxide film on passive iron and the consequences for its electrode behavior. *Corr. Sci.*, 1989, *29*, 191-195.

(68) Schmickler, W. Electron transfer reactions at oxide electrodes involving tunnelling through a space charge barrier. *Ber. Bunsenges. Phys. Chem.*, 1978, *82*, 477-487.

(69) Hummel, R. E. *Electronic Properties of Materials;* 2nd ed.; Springer: New York, 1993.

(70) Leiva, E.; Meyer, P.; Schmickler, W. Electron transfer through thin films: role of localized electronic states. *Corr. Sci.*, 1989, *29*, 225-236.

(71) Schmickler, W. A theory of resonance tunnelling at film-covered metal electrodes. *J. Electroanal. Chem.,* 1977, *82*, 65-80.

(72) Stimming, U.; Schultze, J. W. A semiconductor model of the passive layer on iron electrodes and its application to electrochemical reactions. *Electrochem. Acta,* 1979, *24*, 858-869.

(73) Meisterjahn, P.; Schultze, J. W.; Siemensmeyer, B.; Stimming, U.; Dean, M. H. Electron transfer reaction on passive iron electrodes. *Chem. Phys.,* 1990, *141*, 131-141.

(74) Schultze, J. W.; Stimming, U. Tunnelprozesse an passivierten eisenelektroden. *Z. Phys. Chem., N. F.* 1975, *98*, 285-302.

(75) Klausen, J.; Trüber, S. P.; Haderlein, S. B.; Schwarzenbach, R. P. Reduction of substituted nitrobenzenes by Fe(II) in aqueous mineral suspensions. *Environ. Sci. Technol.,* 1995, *29*, 2396-2404.

(76) Stucki, J. W. Structural iron in smectites. *Nato Adv. Sciences Inst. Ser., Ser. C,* 1988, *217*, 625-75.

(77) Kriegman-King, M. R.; Reinhard, M. Reduction of hexachloroethane and carbon tetrachloride at surfaces of biotite, vermiculite, pyrite, and marcasite. In *Organic Substances and Sediments in Water*; Baker, R., Ed; Lewis: MI, 1991; Vol. 2; pp. 349-364.

(78) Kriegman-King, M. R.; Reinhard, M. Transformation of carbon tetrachloride in the presence of sulfide, biotite, and vermiculite. *Environ. Sci. Technol.,* 1992, *26*, 2198-2206.

(79) Kriegman-King, M. R.; Reinhard, M. Transformation of carbon tetrachloride by pyrite in aqueous solution. *Environ. Sci. Technol.,* 1994, *28*, 692-700.

(80) Pecher, K.; Haderlein, S. B.; Schwarzenbach, R. P. Transformation of polyhalogenated alkanes in suspensions of ferrous iron iron oxides*; 213th National Meeting,* San Francisco, CA, American Chemical Society, 1997; Vol. 37, No. 1, pp. 185-187.

(81) Butler, E. C.; Hayes, K. F. Effects of solution composition on the reductive dechlorination of hexachloroethane by iron sulfide*; 213th National Meeting,* San Francisco, CA, American Chemical Society, 1997; Vol. 37, pp. 113-115.

(82) Peterson, M. L.; White, A. F.; Brown, G. E.; Parks, G. A. Surface passivation of magnetite by reaction with aqueous Cr(VI): XAFS and TEM results. *Environ. Sci. Technol.,* 1997, *31*, 1573-1576.

(83) Hansen, H. C. B.; Koch, C. B.; Nancke-Kroge, H.; Borggaard, O. K.; Sørensen, J. Abiotic nitrate reduction to ammonium: key role of green rust. *Environ. Sci. Technol.,* 1996, *30*, 2053-2056.

(84) Zepp, R. G.; Wolfe, N. L. Abiotic transformation of organic chemicals at the particle-water interface. In *Aquatic Surface Chemistry: Chemical Processes at the Particle-Water Interface*; Stumm, W., Ed; Wiley: New York, 1987; pp. 423-455.

(85) Scherer, M. M.; Tratnyek, P. G. Dechlorination of carbon tetrachloride by iron metal: Effect of reactant concentrations; *209th National Meeting,* Anaheim, CA, American Chemical Society, 1995; Vol. 35, No. 1, pp. 805-806.

(86) Morel, F. M. M.; Hering, J. G. *Principles and Applications of Aquatic Chemistry*; Wiley: New York, 1993.

(87) Stumm, W. *Chemistry of the Solid-Water Interface: Processes at the Mineral-Water and Particle-Water Interface of Natural Systems*; Wiley: New York, 1992.

(88) Dzombak, D. A.; Morel, F. M. M. *Surface Complexation Modeling: Hydrous Ferric Oxide*; John Wiley & Sons: New York, 1990.

(89) Furrer, G.; Stumm, W. The coordination chemistry of weathering: I. Dissolution kinetics of α-Al_2O_3 and FeO. *Geochim. Cosmochim. Acta,* 1986, *50*, 1847-1860.

(90) Wieland, E.; Wehrli, B.; Stumm, W. The coordination chemistry of weathering: III. A generalization on the dissolution rates of minerals. *Geochim. Cosmochim. Acta* 1988, *52*, 1969-1981.

(91) Zinder, B.; Furrer, G.; Stumm, W. The coordination chemistry of weathering: II. Dissolution of Fe(III) Oxides. *Geochim. Cosmochim. Acta,* 1986, *50*, 1861-1869.

(92) Stumm, W. Reactivity at the mineral-water interface: Dissolution and inhibition. *Colloids and Surfaces. A: Physicochemical and Engineering Aspects* 1997, *120*, 143-166.

(93) Burris, D. R.; Campbell, T. J.; Manoranjan, V. S. Sorption of trichloroethylene and tetrachloroethylene in a batch reactive metallic iron-water system. *Environ. Sci. Technol.,* 1995, *29*, 2850-2855.

(94) Allen-King, R. M.; Halket, R. M.; Burris, D. R. Reductive transformation and sorption of cis- and trans-1,2-dichloroethene in a metallic iron-water system. *Environ. Toxicol. Chem.,* 1997, *16*, 424-429.

(95) Bizzigotti, G. O.; Reynolds, D. A.; Kueper, B. H. Enhanced solubilization and destruction of tetrachloroethylene by hydroxypropyl-β-cyclodextrin and iron. *Environ. Sci. Technol.,* 1997, *31*, 472-478.

(96) Huennekens, F. M.; Chance, B. Enzyme reactions. In *Investigation of Rates and Mechanisms of Reactions*; Friess, S. L.; Lewis, E. S.; Weissberger, A., Eds; Interscience: New York, 1963; Vol. 8, Part 2; pp. 1231-1314.

(97) Hingston, F. J.; Posner, A. M.; Quirk, J. P. Competitive adsorption of negatively charged ligands on oxide surfaces. *Discuss. Faraday Soc.,* 1971, *52*, 334-342.

(98) Davis, J. A.; Kent, D. B. Surface complexation modeling in aqueous geochemistry. In *Mineral-Water Interface Geochemistry*; Hochella, J., M.F.; White, A. F., Eds; Mineralogical Society of America: 1990; Vol. 23; pp. 177-260.

(99) Wehrli, B.; Sulzberger, B.; Stumm, W. Redox processes catalyzed by hydrous oxide surfaces. *Chem. Geol.,* 1989, *78*, 167-179.

(100) Fruchter, J. S.; Amonette, J. E.; Cole, C. R.; Gorby, Y. A.; Humphrey, M. D.; Istok, J. D.; Spane, F. A.; Szecsody, J. E.; Teel, S. S.; Vermeul, V. R.; Williams, M. D.; Yabusaki, S. B. In Situ Redox Manipulation Field Injection Test Report - Hanford 100-H Area, Pacific Northwest National Laboratory, 1996.

(101) Loiselle, S.; Branca, M.; Mulas, G.; Cocco, G. Selective mechanochemical dehalogenation of chlorobenzenes over calcium hydride. *Environ. Sci. Technol.,* 1997, *31*, 261-265.

(102) Morlando, R.; Manahan, S. E.; Larsen, D. W. Iron-catalyzed cocurrent flow destruction and dechlorination of chlorobenzene during gasification. *Environ. Sci. Technol.,* 1997, *31*, 409-415.

(103) Choi, W. Y.; Hoffmann, M. R. Novel photocatalytic mechanisms for $CHCl_3$, $CHBr_3$, and $CCl_3CO_2^-$ degradation and the fate of photogenerated trihalomethyl radicals on TiO_2. *Environ. Sci. Technol.,* 1997, *31*, 89-95.

(104) Hudlicky, M. *Reductions in Organic Chemistry*; Ellis Horwood: Chichester, 1984.

(105) Lai, Y.-H. Grignard reagents from chemically activated magnesium. *Synthesis,* 1981,8:585-604.

(106) Smentkowski, V. S.; Cheng, C. C.; Yates, J. T. J. The interaction of carbon tetrachloride with Fe(110): A system of tribological importance. *Langmuir,* 1990, *6*, 147-158.

(107) Bockris, J. O. M.; Khan, S. U. M. *Surface Electrochemistry. A Molecular Level Approach*; Plenum: New York, 1993, pp. 1014.

(108) Archer, W. L. Aluminum—1,1,1-trichloroethane. Reactions and Inhibition. *Ind. Eng. Chem. Prod. Res. Dev.* 1982, *21*, 670-672.

(109) Choi, W.; Termin, A.; Hoffman, M. R. The role of metal ion dopants in quantum-sized TiO_2: Correlation between photoreactivity and charge carrier recombination dynamics. *J. Phys. Chem.,* 1994, *98*, 13669-13679.

(110) Blesa, M. A.; Morando, P. J.; Regazzoni, A. E. *Chemical Dissolution of Metal Oxides*; CRC Press: Ann Arbor, 1994.

(111) Wei, D.; Osses-Asare, K. Semiconductor electrochemisty of particulate pyrite: Dissolution via hole and electron pathways. *J. Electrochem. Soc.,* 1996, *143*, 3192-3198.

(112) Anderman, M.; Kennedy, J. H. Iron oxide (Fe_2O_3). In *Semiconductor Electrodes*; Finklea, H. O., Ed; Elsevier: Amsterdam, 1988; pp. 147-202.

(113) Kormann, C.; Bahnemann, D. W.; Hoffmann, M. R. Environmental photochemistry: Is iron oxide (hematite) an active photocatalyst? A comparative study: α-Fe_2O_3, ZnO, TiO_2. *J. Photochem. Photobiol., A. Chem.,* 1989, *48*, 161-169.

(114) Hoffmann, M. R. Catalysis in aquatic environments. In *Aquatic Chemical Kinetics*; Stumm, W., Ed; Wiley: New York, 1990; pp. 71-111.

(115) Dimitrijevíc, N. M.; Savíc, D.; Mícíc, O. I.; Nozik, A. J. Interfacial electron-transfer equilibria and flat-band potentials of α-Fe_2O_3 and TiO_2 colloids studied by pulse radiolysis. *J. Phys. Chem.,* 1984, *88*, 4278-4283.

(116) Refait, P.; Génin, J.-M. R. The transformation of chloride-containing green rust one into sulphated green rust two by oxidation in mixed Cl^- and SO_4^{2-} aqueous media. *Corr. Sci.,* 1994, *36*, 55-65.

(117) Génin, J. M. R.; Olowe, A. A.; Refait, P.; Simon, L. On the stoichiometry and pourbaix diagram of the Fe(II)-Fe(III) hydroxy-sulphate or sulphate-containing green rust 2: an electrochemical and mossbauer spectroscopy study. *Corr. Sci.,* 1996, *38*, 1751-1762.

(118) Pierret, R. F. *Semiconductor Fundamentals*; Addison-Wesley: New York, 1988.

Table 2.1. Selected electronic properties of iron oxides

Oxide	Formula	E_{CB} (eV)[1]	E_F (eV)[1]	E_{BG} (eV)
Fe(II) only				
Siderite	$FeCO_3$			
Pyrite	FeS_2	0.17 (111)		1.0 (111)
Mixed Fe(II), Fe(III)				
Magnetite	Fe_3O_4			0.11 (112)
Green Rust I	[2]			
Green Rust II	[3]			
Fe(III) only				
Ferrihydrite	$Fe_5HO_8 \cdot 4H_2O$			
Hematite	α-Fe_2O_3	-0.245 (113), 0.242 (114)	-0.225 (57)[5], -0.28 (115), -0.17 (112), -0.285 (57)[4]	2.02 (57), 2.2 (112)
Maghemite	γ-Fe_2O_3		0.315 (57)[5]	2.03 (57)
Goethite	α-FeOOH		0.135 (57)[5]	2.10 (57)
Akaganeite	β-FeOOH		0.835 (57)[5]	2.12 (57)
Lepidocrocite	γ-FeOOH		0.705 (57)[5]	2.06 (57)
Feroxyhyte	δ'-FeOOH		0.625 (57)[5]	1.94 (57)

[1]At pH 7 versus NHE. [2]$3Fe(OH)_2 \cdot Fe(OH)_2Cl \cdot n\ H_2O$ where $3 \geq n \geq 2$ (116). [3]$[Fe(II)_4\ Fe(III)_2\ (OH)_{12}]^{2+} \cdot [SO_4 \cdot 2H_2O]^{2-}$ (117). [4]Single crystal. [5]Quasi-Fermi energy level for electrons. This is the Fermi energy level under illumination (nonequilibrium conditions). For n-type semiconductors where electrons are the majority carriers, the quasi-Fermi energy level is approximately equal to the Fermi energy level (118).

Table 2.2 Mass action equations for the surface complexation model

Protonation Reactions	
$\equiv FeOH_2 \rightleftharpoons \equiv FeOH^0 + H^+$	$K_{a1} = [\equiv FeOH^0][H^+] / [\equiv FeOH_2]$
$\equiv FeOH^0 \rightleftharpoons \equiv FeO^- + H^+$	$K_{a2} = [\equiv FeO^-][H^+] / [\equiv FeOH^0]$
Ligand Exchange Reactions	
$\equiv FeOH^0 + HL \rightleftharpoons \equiv FeL + H_2O$	$K_{L1} = [\equiv FeL] / [\equiv FeOH^0][HL]$
$2 \equiv FeOH^0 + H_2L \rightleftharpoons \equiv Fe_2L + H_2O$	$K_{L2} = [\equiv Fe_2L] / [\equiv FeOH^0][H_2L]$
Hydrophobic Partitioning	
$\equiv FeOH^0 + RX \rightleftharpoons \equiv FeOH^0\text{-}RX$	$K_{RX} = [\equiv FeOH^0\text{-}RX] / [\equiv FeOH^0][RX]$
Metal Partitioning	
$\equiv FeOH^0 + Fe^{2+} \rightleftharpoons \equiv FeOFe^+ + H^+$	$K_{M1} = [\equiv FeOFe^+][H^+] / [\equiv FeOH^0][Fe^{2+}]$
$2 \equiv FeOH^0 + Fe^{2+} \rightleftharpoons \equiv (FeO)_2Fe + 2H^+$	$K_{M2} = [\equiv (FeO_2)Fe][H^+]^2 / [\equiv FeOH^0][Fe^{2+}]$
Ternary Complex Formation	
$\equiv FeOH^0 + Fe^{2+} + L^- \rightleftharpoons \equiv FeOFeL + H^+$	$K_{T1} = [\equiv FeOFeL][H^+] / [\equiv FeOH^0][Fe^{2+}][L^-]$
$\equiv FeOH^0 + L^- + Fe^{2+} \rightleftharpoons \equiv FeLFe^+ + OH^-$	$K_{T2} = [\equiv FeLFe^+][OH^-] / [\equiv FeOH^0][Fe^{2+}][L^-]$

Table 2.3 SCM Model parameters for iron metal systems.

Iron-RX System	[≡Fe_{TOT}] (mM)	K_{RX} (mM^{-1})	k_{RX} (s^{-1})
[a]Fluka Fe^0 and CCl_4	6.6	$(5.3 \pm 2.6) \times 10^{-3}$	$(3.1 \pm 0.41) \times 10^{-2}$
[b]Fisher Fe^0 and CCl_4	8.5	$(5.4 \pm 4.4) \times 10^{-3}$	$(3.0 \pm 0.76) \times 10^{-3}$

[a] Ref. (13). [b] Ref. (15, 85).

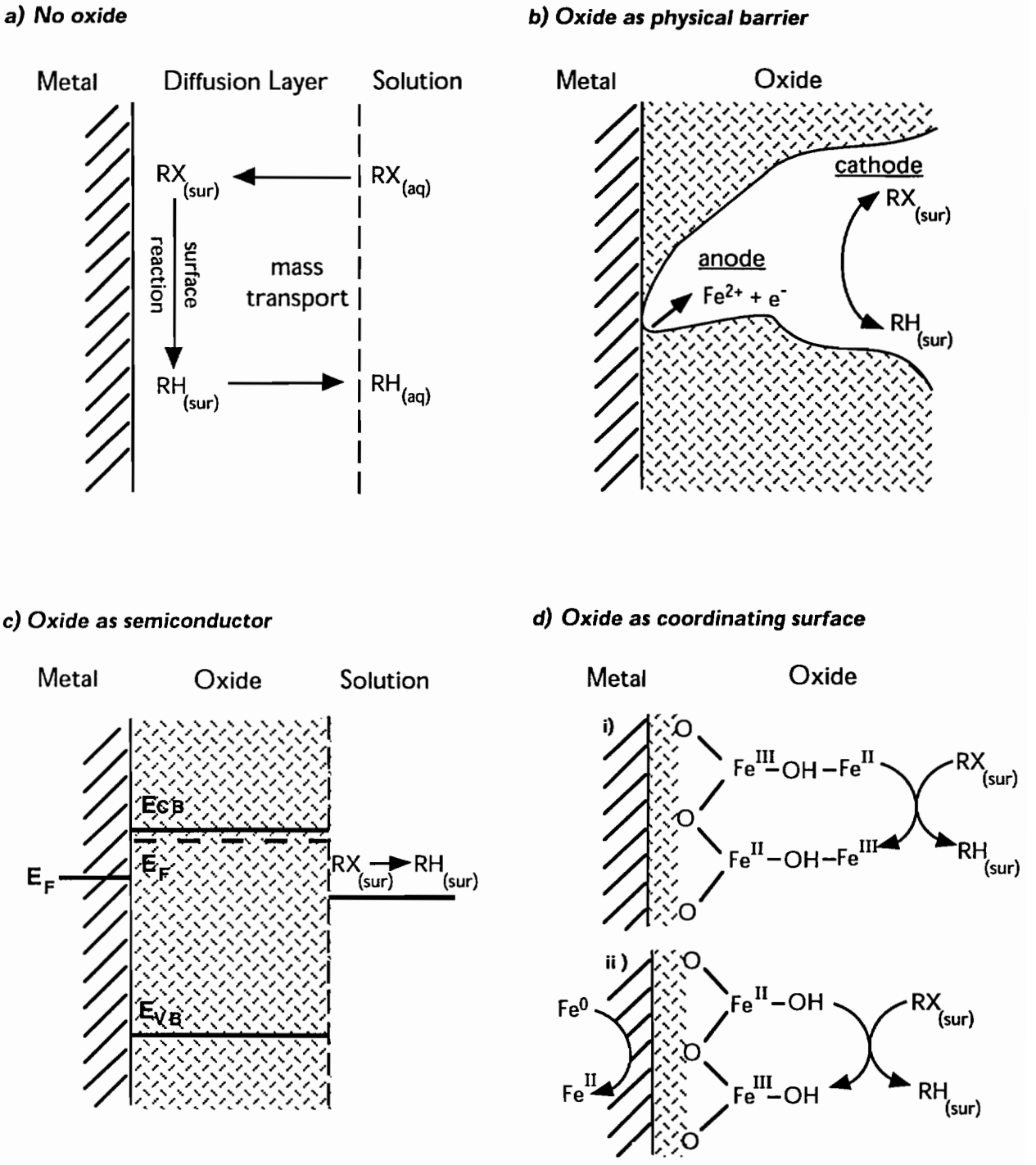

Figure 2.1. Conceptual models of processes that may be involved in reduction of chlorinated aliphatics (RX → RH) at the iron-oxide-water interface: (a) bare electrode (b) passivated electrode, (c) semiconductor surface, and (d) coordinating surface. E_F, E_{CB}, and E_{VB} refer to the Fermi, conduction band, and valence band energies, respectively.

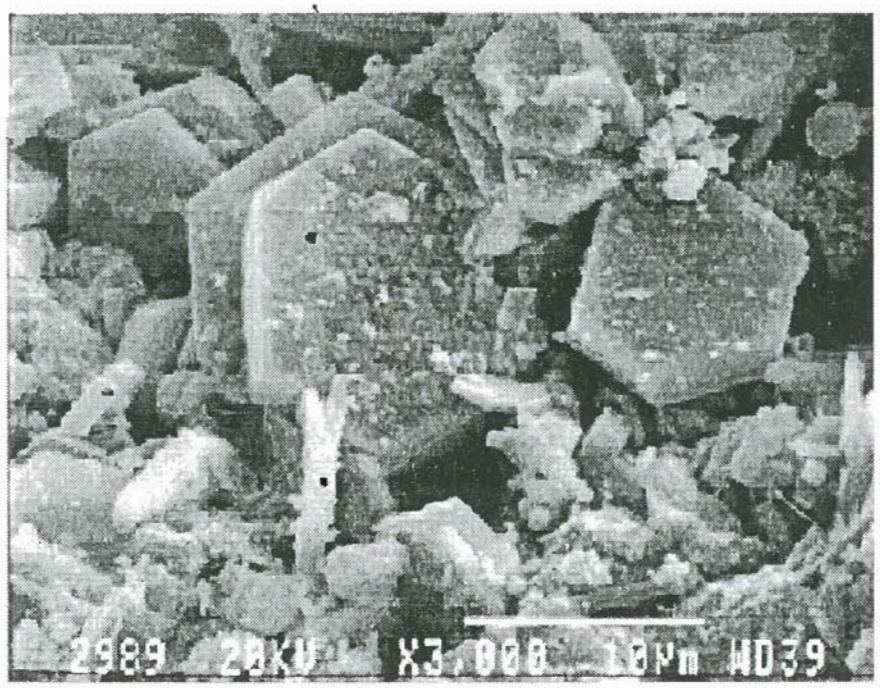

Figure 2.2. Scanning electron micrograph showing precipitates on an Fe^0 surface after long-term exposure (>1 year) to CCl_4 dissolved in deionized water (3). (magnification: x3000)

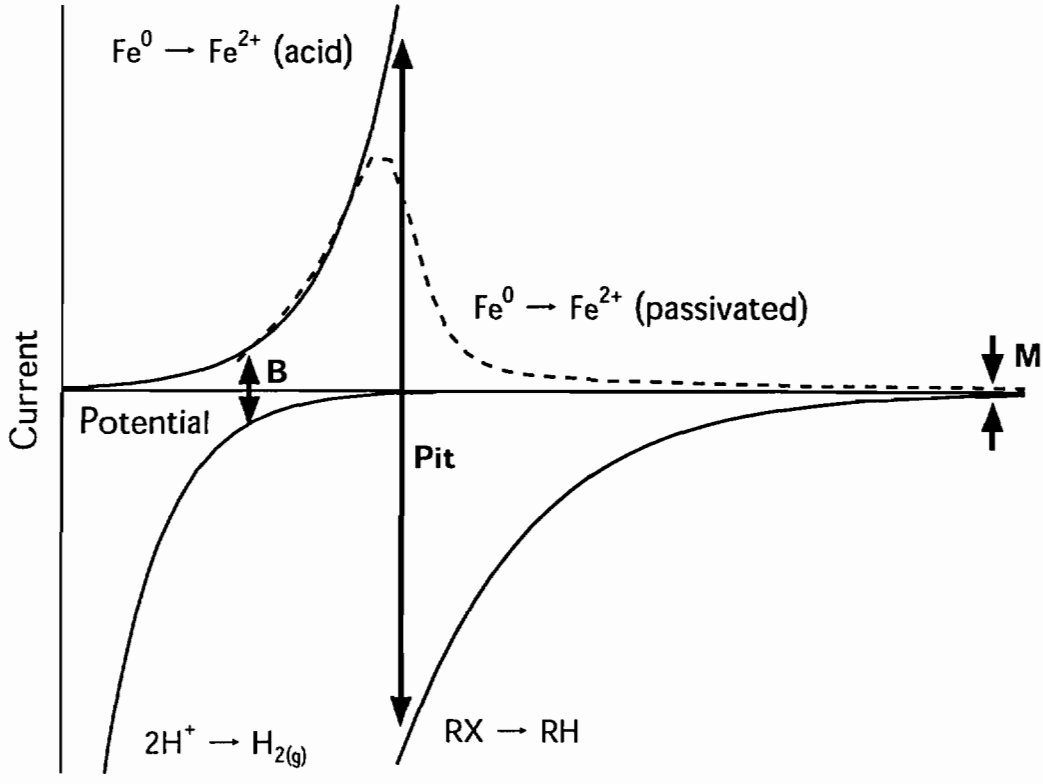

Figure 2.3. Current-potential diagram illustrating controls on the kinetics of corrosion at a pitted, oxide-covered metal. The potential range is from -700 to +300 mV/NHE. Arrows: (B) corrosion current at the bottom of the pit, controlled by $Fe^0 \rightarrow Fe^{2+}$ (acid) and $2H^+ \rightarrow H_2$; (M) corrosion current at the mouth of the pit, controlled by the partial currents for $Fe^0 \rightarrow Fe^{2+}$ (passivated) and RX → RH; (Pit) corrosion current for the short-circuited pit, controlled by $Fe^0 \rightarrow Fe^{2+}$ (acid) and RX → RH. The three solid curves are generated using the Tafel equation and exchange current densities and Tafel slopes from reference (9). The dashed curve was measured at 5 mV s^{-1} in pH 8.4 borate buffer, using methods described in reference (9).

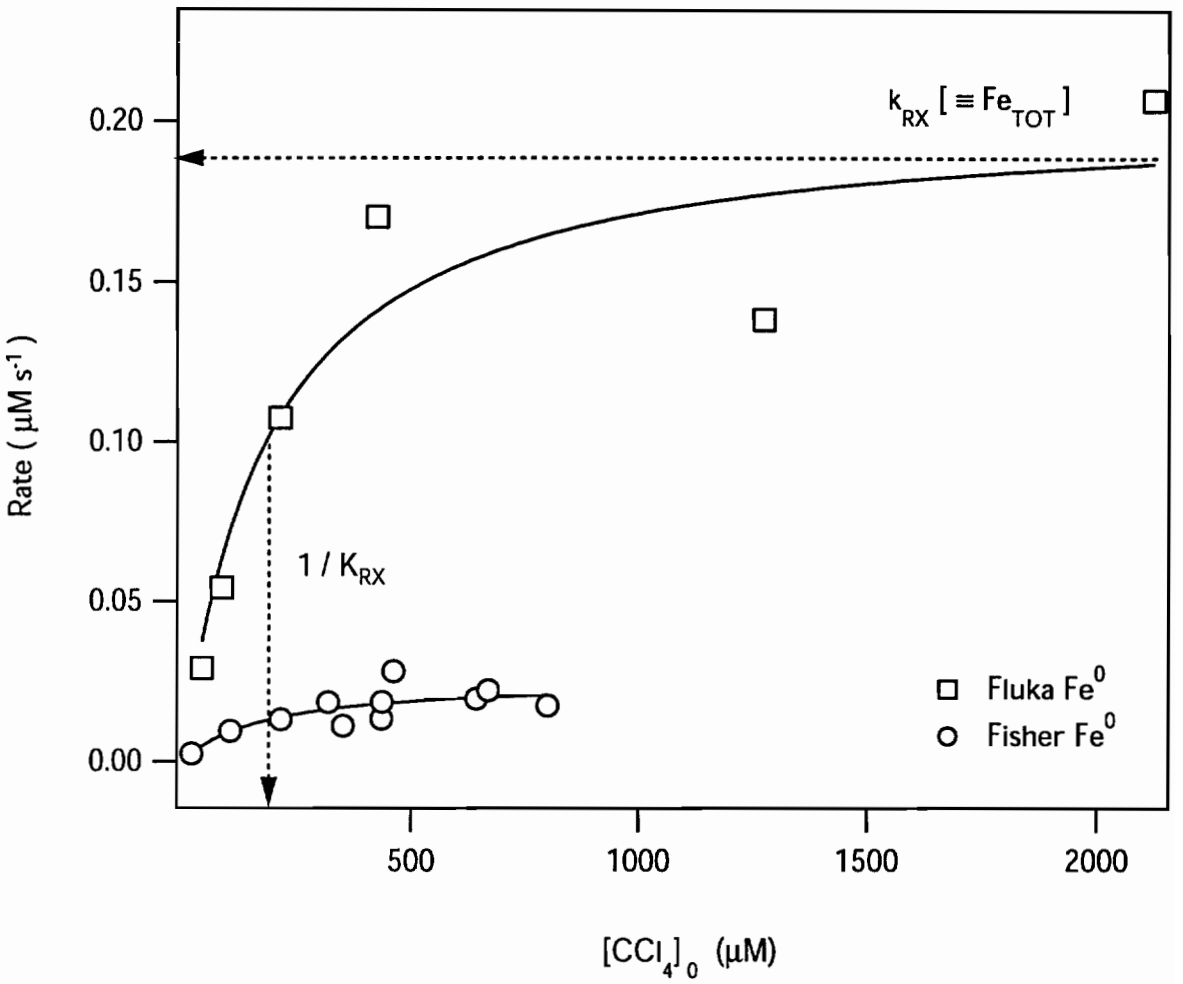

Figure 2.4. Effect of initial CCl_4 concentration, $[CCl_4]_0$, on the rate of CCl_4 reduction by Fe^0, in two well-mixed anaerobic batch systems. Squares: Fluka Fe^0 turnings ($\rho_a = 0.79\ m^2\ L^{-1}$) in deionized water buffered with 10 mM HEPES at pH 6.2 (13). Circles: Fisher Fe^0 filings ($\rho_a = 1.02\ m^2\ L^{-1}$) in unbuffered deionized water (15, 85). Solid curves are drawn from the non-competitive SCM (equation 8) using fitted values of K_{RX} and k_{RX} (given in Table 2.3).

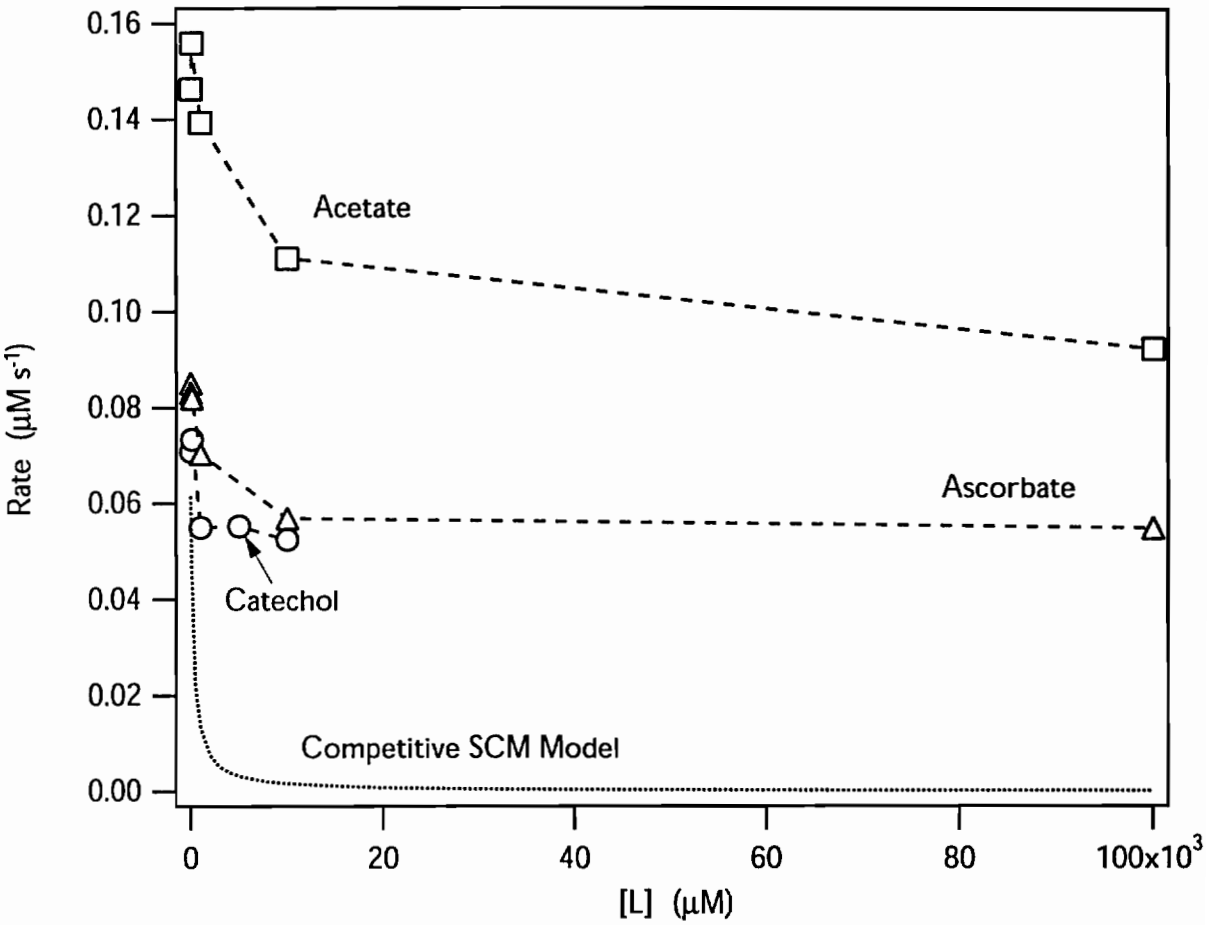

Figure 2.5. Effect of acetate, ascorbate, and catechol concentration on the rate of CCl_4 dechlorination by Fluka Fe^0 (13). Same conditions as in Figure 2.4 and Table 2.3. The dotted curve is calculated from the competitive SCM (equation 9) using values in Table 2.3 for Fluka Fe^0 and assuming $K_L = K_{RX}$.

CHAPTER 3

Kinetics of Carbon Tetrachloride Reduction at an Oxide-Free Iron Electrode[1]

3.1 Abstract

To address some of the fundamental questions regarding the kinetics of reduction of contaminants by zero-valent iron (Fe^0), we have taken advantage of the mass transport control afforded by a polished Fe^0 rotating disk electrode (RDE) in an electrochemical cell. The kinetics of carbon tetrachloride (CCl_4) dechlorination at an Fe^0 RDE were studied in a pH 8.4 borate buffer at a potential which an oxide film would not form. In this system, the cathodic current was essentially independent of electrode rotation rate, and the measured first-order heterogeneous rate constant for the chemical reaction ($k_{ct} = 2.3 \times 10^{-5}$ cm s^{-1}) was less than the estimated rate constant for mass transfer to the surface. Thus, for the conditions of this study, the rate of reduction of CCl_4 by oxide-free Fe^0 appears to be dominated by reaction at the metal-water interface rather than by transport to the metal surface. Activation energies for reduction of CCl_4 and hexachloroethane by oxide covered granular Fe^0 (measured in batch systems) also indicate that overall rates are limited by reaction kinetics. Since mass transport rates vary little among the chlorinated solvents, it is likely that variation in k_{ct} is primarily responsible for the wide range of dechlorination rates that have been reported for batch and column conditions.

3.2 Introduction

Studies of the use of zero-valent metals to remediate contaminated sites have grown to cover a wide range of organic and inorganic contaminants, metal and metal/catalyst reductants, and modes of full-scale implementation (1). Among these, the most thoroughly

---

[1] Reprinted with permission from Scherer, M.M, J.C. Westall, M. Ziomek-Moroz, and P.G. Tratnyek. 1997. Kinetics of carbon tetrachloride reduction at an oxide-free iron electrode. *Environmental Science & Technology* 31(8):2385-2391. Copyright 1997 American Chemical Society.

studied is the reduction of chlorinated solvents in groundwater by in-situ permeable barriers containing granular iron metal (Fe^0). The kinetics of contaminant degradation in these systems are of particular interest because they bear directly on the design of full-scale treatment operations. Major kinetic issues that have been addressed in recent studies include (i) parameterization of degradation kinetics (2, 3), (ii) the kinetics of associated processes such as adsorption (4), and (iii) the coupling of models for reaction kinetics with models for transport in permeable barriers (5, 6).

There are, however, a variety of issues that limit progress toward a comprehensive understanding of the kinetics of this treatment process. For example, there is uncertainty over how to incorporate the kinetics of growth of the oxide film on the metal surface and the effect of the oxide film on the degradation rate. An even more fundamental concern is the relative rates of mass transfer to the reactive sites and chemical reaction (charge-transfer) at the reactive sites. This distinction has important practical implications because of its potential to narrow the search for enhancements that will improve the performance of full-scale remediation installations.

In the batch and column studies reported to date, traditional tests have been applied to distinguish between processes that are limited by mass transfer and those that are limited by reaction kinetics. Many researchers have found that reduction rates increase with mixing intensity in batch systems (7-9) and average linear velocity in flow-through systems (10, 11). Temperature-effect studies indicate modest activation energies, for example, 15 - 18 kJ mol^{-1} for TCE (12). Others (2-4, 13) have observed that lower concentrations of substrate yield slower degradation rates. All of these results have been interpreted as indications that dechlorination is influenced by mass transport of the organic oxidant to the metal surface. In contrast, the wide variation in reaction rates among the various chlorinated solvents, despite the narrow range in diffusivities is evidence for a dependence on molecular properties that implies reaction limited kinetics (2). This apparent contradiction pervades much of the literature to date on remediation with zero-valent metals, and suggests that batch and column experiments do not provide enough hydrodynamic control to resolve mass transport rates and reaction rates in these processes.

An alternative experimental approach is to monitor dechlorination kinetics by recording electrical current at an iron rotating disk electrode (RDE). The control of mass transport afforded by the RDE allows separation of the mass transport and reaction contributions to the overall degradation rate, making it possible to derive more fundamental kinetic parameters for dechlorination by Fe^0.

The objectives of this study were to (i) introduce an experimental protocol for studying dechlorination of organic solutes in aqueous solution at an Fe^0 RDE, (ii) describe the electrochemical basis for interpreting the behavior of such systems, and (iii) determine the heterogeneous rate constants for reactions in the Fe^0-CCl_4-H_2O system. For the present, we have limited our scope to CCl_4 as a model chlorinated solvent, high purity Fe^0 in the potential region where iron oxides are not formed, and borate buffer. These well defined conditions provide continuity with the vast literature on electrochemistry of iron corrosion and a basis for future studies, in which these restrictions will be relaxed to explore other aspects of contaminant reduction by zero-valent metals.

3.3 Background

3.3.1 Conceptual Model of the Fe^0-RCl-H_2O System

The reduction of chlorinated aliphatic compounds (RCl) by Fe^0 is a heterogeneous process involving the oxidation and dissolution of iron in conjunction with the reduction and dechlorination of RCl (3, 8):

$$Fe^0 + RCl + H^+ \rightarrow Fe^{2+} + RH + Cl^- \quad (1)$$

A major issue that has not been resolved is the extent to which the overall rate of the reaction in eq. 1 is controlled by *chemical reaction* (i.e., electron transfer, dechlorination, proton transfer, etc.) versus the extent to which it is controlled by *mass transport* of RCl from the well-mixed bulk solution to the Fe^0 surface.

3.3.2 Chemical Reactions

The objective of this section is to present a theory from which heterogeneous rate constants for the chemical reaction (eq. 1) can be derived from experimental current versus voltage data obtained with the electrochemical cell. The overall dechlorination reaction (eq. 1) can be broken into two half-reactions, namely, the oxidation of Fe^0:

$$Fe^0 \rightarrow Fe^{2+} + 2\,e^- \quad (2)$$

and the reduction of RCl:

$$RCl + H^+ + 2\,e^- \rightarrow RH + Cl^- \quad (3)$$

The conditions of interest are anoxic, so reduction of O_2 can be neglected, but the reduction of water occurs at an Fe^0 electrode and must be considered:

$$2\,H_2O + 2\,e^- \rightarrow H_2(g) + 2\,OH^- \quad (4)$$

The net current density (i, A m^{-2}) that is observed at an iron electrode in this system is the sum of the partial current densities (j_X, A m^{-2}) for each of the processes described in eq. 2-4:

$$i = j_{Fe} + j_{RCl} + j_H \tag{5}$$

where *Fe*, *RCl*, and *H*, refer to the partial current densities associated with reactions in eq. 2, 3, and 4, respectively. Equation 5 is based on the sign convention where anodic (oxidation) currents are positive and cathodic (reduction) currents are negative.

The partial current densities can be described by the Tafel equation, which can be related to the Arrhenius equation for a single-step process, but is often used as an approximation to describe multistep processes, as probably occur here. For eq. 2-4, the corresponding Tafel equations are:

$$j_{Fe} = j_{Fe}^{0} \exp\{(E - E_{Fe}^{eq})/b_{Fe}\} \tag{6}$$

$$j_{RCl} = -j_{RCl}^{0} \exp\{-(E - E_{RCl}^{eq})/b_{RCl}\} \tag{7}$$

$$j_H = -j_H^{0} \exp\{-(E - E_H^{eq})/b_H\} \tag{8}$$

where j_x^0 (for reaction x) is the exchange current density, which refers to the partial current density under specified conditions ($E = E_x^{eq}$ and concentrations of reactants at the electrode surface at "standard" values), E is the electrode potential (relative to a specified reference electrode), E_x^{eq} (reaction x) is the equilibrium potential for the half reaction, and b_x (reaction x) is an empirical parameter known as the Tafel slope. Equations 6-8 are applicable in the absence of mass transfer effects, when the concentrations of reactants and products at the electrode surface, C^s, are equal to those in the bulk of solution C^b.

A combination of eq. 5-8 allows the observed current density, i, to be expressed in terms of the applied potential, E. If this kinetic model is a good approximation of the behavior of the system, and the values of the parameters j_x^0 and b_x can be determined from experimental data, then the electrochemical reaction kinetics are characterized. In particular, if the value of j_{RCl} can be determined from the model, it can be re-expressed in terms of a first-order heterogeneous rate constant for charge transfer in the RCl reaction, k_{ct},

$$j_{RCl} = -n \, \mathrm{F} \, k_{ct} \, C_{RCl}^{s} \tag{9}$$

where n is the number of electrons in the reaction, F is the Faraday constant (96485 C mol^{-1}), and C_{RCl}^s is the concentration of RCl at the surface. As formulated above, the value of k_{ct} is dependent on applied potential.

A special case of this i vs. E relation (eq. 5-8) occurs when the net current (eq. 5) is equal to zero, as is the case for an iron particle that is not part of an electrochemical cell. The potential at which this zero-current condition is fulfilled is known as the corrosion potential, E_{corr}. Although the net current density at E_{corr} is equal to zero, the partial current densities are non-zero, and define the corrosion current density i_{corr}:

$$i_{corr} = j_{Fe} = -j_{RCl} - j_H \tag{10}$$

If j_H is negligible compared to j_{RCl}, then $j_{RCl} \sim i_{corr}$ and the heterogeneous rate constant for reaction of RCl can be calculated from eq. 9. The value of k_{ct} at E_{corr} is relevant for Fe^0 surfaces not under potential control, as in most groundwater remediation operations.

3.3.3 Mass Transport

Transport to the surface of the RDE is controlled by forced convection and diffusion, but is functionally equivalent to transport to an electrode which is separated from the well mixed solution by a stagnant boundary layer, as shown in Figure 3.1. Under steady-state or quasi steady-state conditions, the mass transport limited current density due to reduction of species x at an RDE can be approximated by the Levich equation (14):

$$j_x = -nF(D_x / \delta_x)(C_x^b - C_x^s) \tag{11}$$

where D_x is the molecular diffusion coefficient and δ_x is given by:

$$\delta_x = 1.61\, D_x^{1/3}\, \omega^{-1/2}\, \nu^{1/6} \tag{12}$$

in which ν is the kinematic viscosity of the electrolyte, and ω is the angular velocity of the rotating disk ($\omega = 2\pi f$, where f = rotation rate in rev s^{-1}). A more exact treatment of mass transport to an RDE is available (15) , but eq. 11-12 are sufficient for this work. Thus, the current under mass transport limited conditions is expected to vary inversely with the square root of the rotation rate. At sufficiently high rotation rates, the reactant is transported to the surface faster than it can be consumed and the current density reaches a value that is limited by the chemical reaction rate and independent of disk rotation rate.

In order to facilitate comparison of the rates of mass transport and electrochemical reaction, it is convenient to express two of the factors in eq. 11 as a first-order heterogeneous rate constant for mass transport of species x to the surface, k_{mt}:

$$k_{mt} = D / \delta \tag{13}$$

This definition allows direct comparison of measured k_{ct} values to estimated k_{mt} values.

3.3.4 Mixed Control

For the case of intermediate kinetics, where both reaction and transport processes control the reaction rate, eq. 9 and 11-12 can be combined to describe the relative contributions of k_{mt} and k_{ct}. Under steady state conditions (where current due to mass transport (eq. 11) is equal to the current due to reaction (eq. 9)), the mixed control equation for reduction of species x is:

$$\frac{1}{j_x} = -\frac{1}{nFk_{ct}C_x^b} - \frac{1}{nFk_{mt}C_x^b} \tag{14}$$

where the first term on the right side represents the reaction controlled portion of the overall kinetics and the second term represents the mass transport contribution.

3.4 Experimental Section

3.4.1 Electrochemical Experiments

Experiments were carried out in a custom three- electrode glass cell, which is shown in Figure 3.2. The working electrode was an Fe^0 RDE that was custom fabricated by Pine Instruments (Grove City, PA) from a 99.5% pure Fe^0 rod (Metal Samples, Munford, AL). The diameter of the Fe^0 disk was 3.0 mm, providing a geometric surface area of 0.071 cm^2. A double-junction Ag/AgCl reference electrode, immersed in 0.1 M KNO_3, was connected to the cell through a Luggin capillary salt bridge that was filled with the same borate buffer solution used in the cell as the supporting electrolyte. The counter electrode was a Pt mesh welded to a Pt wire. Electrode potential and current were controlled with a potentiostat (Pine Instruments, Model AFCBP1). Potentials are reported relative to the standard hydrogen electrode (SHE) and currents are reported in accord with IUPAC convention (anodic current is positive and cathodic current is negative). Preliminary experiments validated the performance of our cell against the ASTM standard method for making potentiostatic and potentiodynamic corrosion measurements (16).

Before each experiment, the Fe^0 electrode was mechanically polished with 600 and 800 grit silicon carbide paper and 1 μm diamond paste to achieve a mirror-like finish. The current-voltage (*i-E*) curves were measured in pH 8.4 borate buffer made from 0.15 M H_3BO_3 and 0.0375 M $Na_2B_4O_7$. The cell was deaerated by bubbling Ar into the cell for at least one hour at the beginning of each sequence of experiments. To reduce any oxide film that may have formed by exposure to air, the electrode was reduced at -720 mV for about 30 minutes immediately prior to each experiment. It has been shown that the iron surface is

free of an oxide film under these conditions (17). Following cathodic pretreatment, CCl_4 was introduced by bubbling Ar gas saturated with CCl_4 into the cell solution for approximately 15 minutes.

Three types of electrochemical experiments were carried out. First, conventional cyclic voltammograms were obtained with a stationary Fe^0 electrode at scan rates of 5.0 and 0.2 mV s^{-1}. The scan limits were set to avoid hydrogen evolution at potentials more negative than -700 mV and oxygen evolution at potentials more positive than 800 mV. These cyclic votammograms were obtained with and without CCl_4 in solution in order to verify the condition of the Fe^0 surface and to observe the effect of CCl_4. Second, coulometry was used to assess the current efficiency, that is, the fraction of the current passed that results in the transformation of CCl_4. Third, in order to observe mass transfer effects, the current was recorded as a function of rotation rate while the electrode was held at a constant potential. The potential was chosen to minimize oxide formation and hydrogen evolution (i.e., optimal for having $i \sim j_{RCl}$ and no oxide film).

3.4.2 Batch Experiments

Activation energies for CCl_4 reduction on oxide coated Fe° particles were determined in batch experiments at five temperature values ranging from 4 to 45 °C. The air-formed oxide film was not removed from the Fe^0 surfaces in these experiments, in contrast to those in the electrochemical experiments. Vials were filled in an N_2-atmosphere with 12 mL of 10 mM HEPES buffer (pH 6.5), 0.5 g of 20-32 mesh Fe^0 turnings (Fluka, puriss. grade, specific surface area of 0.019 m^2 g^{-1} (2)), and CCl_4 at an initial concentration of 85 μM. The vials were crimp-sealed without headspace and rotated at 30 rpm in a dark, temperature controlled chamber. CCl_4 disappearance kinetics were determined by periodically extracting the contents of duplicate bottles with hexane and analyzing the extract by ECD gas chromatography (18).

3.5 Results and Discussion

The results presented here show that both the oxide-free Fe^0 RDE and the oxide covered granular Fe^0 display kinetic behaviors typical for reaction controlled processes (19, 20): (i) minor effect of rotation rate on overall reaction rate, (ii) observed rates significantly slower than theoretical mass transport rates, (iii) high activation energies (> 20 kJ mol^{-1}), and (iv) significant influence of surface preparation on reaction rate. Having identified the conditions where the dechlorination rate is reaction controlled, we characterized the Fe^0-

RCl-H_2O system by deriving exchange currents and Tafel slopes for each reaction. The derived parameters are used in an electrochemical model for evaluating the thermodynamic and kinetic behavior of the system.

3.5.1 Cyclic Voltammetry with a Stationary Fe^0 Electrode

A cyclic voltammogram obtained with the stationary Fe^0 electrode in deaerated borate buffer (without CCl_4) is shown in Figure 3.3. The voltammogram agrees well with those previously published for this system (21, 22), confirming that the electrode is oxide-free and the solution is anoxic. The cyclic voltammogram illustrates the active and passive states of a corroding metal. Along the positive (anodic) scan, the increase in current density up to a peak at -400 mV reflects oxidative dissolution of the Fe^0 electrode to Fe^{2+} (21, 22), i.e., active corrosion. Beyond that peak, the current density declines due to accumulation of a passivating film of iron oxide. In view of the ubiquitousness of iron oxides in field and laboratory studies with Fe^0 (10, 11, 23), we believe that it is oxide covered iron that is most relevant to remediation activities. However, the composition and role of the oxide layer is complex (24, 25) and it may introduce conduction, transport, and reaction processes that will be difficult to resolve (26). Therefore, as a first step in studying the rate limiting process, we have focused on reduction of CCl_4 in the active region ($E < -400$ mV) where formation of an oxide layer is not expected. In the fully passivated region at $E > -100$ mV (Figure 3.3), current densities remain nearly constant with increasing potential until a point (usually $E > 1000$ mV, not shown) at which the transpassive state is reached, and water is oxidized to oxygen. In the negative (cathodic) scan, the increase in current density at $E < -600$ mV results from the reduction of the oxide film and reduction of water to hydrogen (21).

A linear sweep voltammogram for the Fe^0 electrode in the active region, with and without CCl_4 present, is shown in Figure 3.4. The *i*-E curves show a greater cathodic current density in the presence of CCl_4. The corrosion potential (where $i = 0$) shifts positively from -510 ± 10 mV in borate buffer to -380 ± 10 mV in borate buffer saturated with CCl_4. Replicate experiments gave reproducible shifts in the corrosion potential. The positive shift in E_{corr} is consistent with our expectation that CCl_4 is acting as an oxidant in this system.

3.5.2 Coulometry

To confirm that the observed current densities are due to the reductive dechlorination of CCl_4 by the Fe^0 RDE, the concentrations of reaction products in the cell (mainly $CHCl_3$) were compared to those expected from the total charge passed. From Faraday's law, the amount of product (N, mol) is related to the amount of charge (q, C) by $N = q / n\mathrm{F}$. A two-electron reduction of CCl_4 to $CHCl_3$ (eq. 1) at -600 mV (where the current contribution from Fe^0 oxidation and H_2 evolution should be negligible) and varying rotation rates accounts for ~ 96% of the measured charge. At more negative potentials, lower current efficiencies were observed for CCl_4 reduction because the evolution of H_2 becomes a competing cathodic reaction.

3.5.3 Effect of Electrode Rotation Rate

For a mass transport limited reaction, current should vary linearly with the square root of electrode rotation rate (eq. 11-12). However, as shown in Figure 3.5, current density varies only slightly with the rotation rate when reduction of CCl_4 is the major reaction, but varies more strongly for reduction of O_2, which is known to be mass transport limited on Fe^0 up to 3600 rpm (27, 28).

The steady-state current densities from Figure 3.5 are re-plotted against the square root of rotation rate in Figure 3.6 to allow direct comparison with the Levich equation (eq. 11). The current densities for CCl_4 reduction are significantly lower than those predicted by the Levich equation, whereas those for O_2 approach the predicted curves. At higher rotation rates, the O_2 data deviate from the Levich relationship revealing some influence of reaction limited kinetics. In contrast, the nearly zero slope for the CCl_4 data suggests that CCl_4 reduction by the bare Fe^0 RDE is not significantly influenced by mass transport.

A detailed view of the effect of rotation rate on CCl_4 reduction at two potentials in the active region is provided by Figure 3.7. Although the current densities are still significantly less than those that would be predicted for mass transport control (see Figure 3.6), the lower current densities at lower rotation rates do reveal a slight dependence on rotation rate. The Levich equation (eq. 12) predicts values of δ in the range of 20 to 70 μm for these low rotation rates (10-100 rpm), which is significantly larger than the 4 to 20 μm predicted at higher rotation rates (> 100 rpm).

These larger values of δ found at low rotation rates may be more typical of values in a porous medium, for which δ is often assumed to be roughly equal to the average particle radius (19, 29). Assumption of a mean particle size of 0.25 to 0.50 mm (that of

fine/medium sand) results in an estimated $\delta \sim 125$ to 250 μm, which agrees well with the effective radius of 220 μm that was used in a model of the Borden site aquifer material (29). Therefore, approximating Fe^0 particles as fine to medium sand results in an estimated range of δ in an Fe^0 permeable barrier that is 2 to 3 times larger than δ at the Fe^0 RDE. The comparison suggests that the mixed influence of mass transport and reaction kinetics exhibited with the RDE at low rotation rates may also apply to batch and column studies of Fe^0 reduction of chlorinated solvents. This interpretation is consistent with the weak effect of mixer rotation rate and flow velocity reported previously for batch (8, 9) and column degradation experiments (10, 11).

3.5.4 Chemical Reaction Kinetics

Having identified the conditions in our system under which mass transport effects are negligible, we can study the charge-transfer kinetics of CCl_4 reduction by measuring steady-state *i*-E curves at rotation rates > 900 rpm (see Figure 3.7). Steady-state *i*-E curves observed both in aqueous borate buffer (i_{borate}) and in aqueous borate buffer saturated with CCl_4 (i_{CCl_4}) are presented in Figure 3.8. The difference between i_{CCl_4} and i_{borate} can be attributed to the reduction of CCl_4 to $CHCl_3$, as confirmed by the current efficiency measurements described above. Thus, the partial current density due to CCl_4 reduction can be estimated from $j_{RCl} = i_{CCl_4} - i_{borate}$.

The value of j_{RCl} at E_{corr} was found to be 22 ± 1 μA cm^{-2} (from three experiments run over 2 months). Using this measured j_{RCl} value and assuming the solubility of CCl_4 in water is 5×10^{-6} mol cm^{-3} (30) and $n = 2$ for a two-electron transfer, we can calculate a surface area normalized heterogeneous charge-transfer rate constant from eq. 9. The value obtained is $k_{ct} = (2.3 \pm 0.1) \times 10^{-5}$ cm s^{-1}. Despite the presence of borate buffer in the RDE experiments (which is known to inhibit corrosion slightly), this value is ten times greater than the average reduction rate constant for previously reported batch and column experiments performed with granular iron (3.3×10^{-6} cm s^{-1} calculated from 1.2×10^{-1} L m^{-2} h^{-1}) (2). The greater reduction rate at the Fe^0 RDE may be due to the absence of an oxide film which is typically present in the conventional experiments.

From the measured steady-state *i*-E curves in Figure 3.8, a quantitative electrochemical characterization for the reaction kinetics of the Fe^0-CCl_4-H_2O system can be derived. Values of the parameters j^0 and b for CCl_4 reduction, Fe^0 oxidation, and H_2 evolution were determined by nonlinear least squares parameter adjustment with the Tafel equations (eq. 5-8) and the data in Figure 3.8. The parameters derived by this method are

presented in Table 1, and the currents calculated from the model (eq. 5) with these parameters are given by the solid lines in Figure 3.8.

The partial current densities calculated from this model, as shown in Figure 3.9, provide a basis for evaluating the thermodynamic and kinetic behavior of the system. As expected, the j-E curves share a common potential region indicating that the reduction of both CCl_4 and H_2O by Fe^0 is thermodynamically favorable. The kinetics of each reaction (position and slope of j-E curve) are controlled by j^0 and b, which, in the presence of multiple couples, dictate the corrosion potential and overall corrosion rate. For the Fe^0-CCl_4-H_2O system studied here, H_2 evolution comprises a minor part of the total current at E_{corr}, and i_{corr} is approximately equal to $|j_{CCl_4}|$. Hence i_{corr} is proportional to the reductive dechlorination rate. The relatively low value of j_H at E_{corr} lends support to our previous arguments that H_2 is not an important mechanistic intermediate in the reductive dechlorination of CCl_4 (31). Furthermore, the model can be used to show that mass transfer effects on the CCl_4 current density (for δ = 200 μm) are not predicted until extreme cathodic potentials (E < -1400 mV, not shown), suggesting that the rate of dechlorination is generally dominated by reaction kinetics rather than mass transport.

Additional implications regarding possible enhancement strategies arise from considering how they might effect the j-E curves in Figure 3.9. Imposition of a cathodic overpotential on Fe^0 particles will increase the rate of H_2 evolution as well as increase the reduction of RCl. As the imposed potential is made more negative, the H_2 evolution becomes an increasingly large portion of the overall corrosion current ($b_H < b_{RCl}$). Another enhancement strategy that has been proposed is the addition of more noble metals such as Pd and Ni to form a bimetallic surface that is more reactive than Fe^0 alone (32). This enhancement may be due to the addition of a catalytic hydrogenation pathway for contaminant degradation. However, an alternative explanation for the observed enhancement is that j_{RCl}^0 is greater on the noble metals (which shifts the RCl j-E curve on the potential axis), causing i_{corr} to increase (and E_{corr} to become more positive) thereby enhancing the rate of degradation by Fe^0 observed in presence of Pd and Ni.

3.5.5 Effect of Surface Preparation and Temperature

The preceding discussion pertained to the reduction of RCl at bare Fe^0 electrodes. We conclude with some observations about reduction of RCl at oxide covered Fe^0 particles. One simple–and often overlooked–criterion for distinguishing mass-transport from chemical reaction kinetics, which can be applied to batch and column studies, is the degree

to which surface preparation and conditioning influence reaction rates (20). A process limited by mass transport should show little influence of surface condition, whereas a process controlled by chemical reaction is often sensitive to even small surface modifications. Indeed, it is commonly found that pretreatment of oxide covered iron particles (such as sonication or acid-washing) tends to increase the reaction rate significantly (9, 33).

Another useful criterion for characterizing kinetic control is the magnitude of apparent activation energies (E_{act}) derived from the effect of temperature on disappearance rate constants. In this study, batch experiments with CCl_4 and Fluka Fe^0 filings gave E_{act} = 55.9 ± 12.0 kJ mol^{-1} over the temperature range of 4 to 45°C and hexachloroethane gave E_{act} = 40.5 ± 4.1 kJ mol^{-1} under similar conditions (Figure 3.10). These values are not significantly different, and are consistent with the similarity in disappearance rate constants reported for the two compounds previously (2). The values of E_{act} are large enough to reflect reaction rate control, and are 2-3 times greater than the 10-16 kJ mol^{-1} considered typical of mass transport controlled reactions (19). Thus, it appears that there is a significant degree of reaction control on the kinetics of dechlorination in a well-mixed batch systems, as well as in the Fe^0 RDE model system. However, as experimental conditions approach those expected under field conditions, the kinetics of dechlorination begin to show characteristics of mass transport in addition to reaction control. This tendency is evident from our analysis of diffusion layer thicknesses for field situations (above), and from previously reported effects of mixing rate and flow velocity on batch and column experiments (8-11).

3.5.6 Reduction Rates of Other Halocarbons

The majority of this study focused on CCl_4, but our major conclusions with respect to the importance of chemical reaction rates will likely apply to other chlorinated solvents as well. This prediction is based on a comparison of the calculated mass transfer rates with dechlorination rates previously reported for batch and column experiments. For each chlorinated solvent, the rate of mass transport through the aqueous boundary layer can be estimated from the corresponding molecular diffusion coefficient of the substrate and the effective value of δ in the system. For chlorinated solvents the value of D is on the order of 10^{-6} cm^2 s^{-1} (30), which translates to $k_{mt} \sim 5 \times 10^{-5}$ cm s^{-1} (eq. 13 for δ = 200 μm based on fine/medium sand assumption). Reported dechlorination rates from batch and column experiments are significantly smaller, ranging from 1.1 x 10^{-9} cm s^{-1} (4.1 x 10^{-5} L m^{-2} h^{-1}) for *cis*-1,2-dichloroethene to 3.3 x 10^{-6} cm s^{-1} (1.2 x 10^{-1} L m^{-2} h^{-1}) for CCl_4 (2).

Therefore, the wide variation in dechlorination rates between the different chlorinated solvents appears to be due to differences in k_{ct} rather than k_{mt}.

3.6 Acknowledgments

B. A. Balko made many helpful contributions to the experimental design and data analysis. This study was supported in part by the Petroleum Research Fund (29995-AC5), the National Science Foundation (BCS-9212059), the Office of Naval Research (N00014-96-1-0893), the University Consortium Solvents-In-Groundwater Research Program, and the Office of Research and Development of the U. S. Environmental Protection Agency (R-819751) through the Western Region Hazardous Substance Research Center.

3.7 List of Symbols

b_x	Tafel slope for reaction x, V
C^s	aqueous surface concentration of reactant, mol cm^{-3}
C^b	aqueous bulk concentration of reactant, mol cm^{-3}
D	molecular diffusion coefficient, $cm^2\ s^{-1}$
E	electrode potential relative to a standard reference electrode, V
$E_{eq}{}^x$	Nernst equilibrium potential for reaction x, V
E_{corr}	corrosion potential (where net current is equal to zero), V
E_{act}	activation energy, kJ mol^{-1}
f	revolutions per second, rev s^{-1}
F	Faraday constant (F = 96485 C mol^{-1})
i	observed current density, A cm^{-2}
i_{borate}	observed current density in borate buffer, A cm^{-2}
i_{CCl_4}	observed current density in CCl_4 saturated borate buffer, A cm^{-2}
i_{corr}	corrosion current density, A cm^{-2}
j_x	partial current density for reaction x, A cm^{-2}
$j_x{}^0$	exchange current density for reaction x, A cm^{-2}
k_{ct}	surface area normalized heterogeneous charge-transfer rate constant, cm s^{-1}
k_{mt}	surface area normalized heterogeneous mass transport rate constant, cm s^{-1}
n	number of electrons transferred
N	amount of product, mol
q	amount of charge, C
δ	thickness of stagnant boundary layer, cm
ν	kinematic viscosity, $cm^2\ s^{-1}$
ω	angular velocity of RDE, s^{-1}

3.8 Literature Cited

(1) Tratnyek, P. G. Putting corrosion to use: Remediation of contaminated groundwater with zero-valent metals. *Chem. Ind. (London),* 1996, 13:499-503.

(2) Johnson, T. L.; Scherer, M. M.; Tratnyek, P. G. Kinetics of halogenated organic compound degradation by iron metal. *Environ. Sci. Technol.,* 1996, *30*, 2634-2640.

(3) Gillham, R. W.; O'Hannesin, S. F. Enhanced degradation of halogenated aliphatics by zero-valent iron. *Ground Water,* 1994, *32*, 958-967.

(4) Burris, D. R.; Campbell, T. J.; Manoranjan, V. S. Sorption of trichloroethylene and tetrachloroethylene in a batch reactive metallic iron-water system. *Environ. Sci. Technol.,* 1995, *29*, 2850-2855.

(5) Hatfield, K.; Burris, D. R.; Wolfe, N. L. Analytical model for heterogenous reactions in mixed porous media. *J. of Environ. Engr.,* 1996, *122*, 676-684.

(6) Eykholt, G. R.; Sivavec, T. M. Contaminant transport issues for reactive-permeable barriers. In *Geoenvironment 2000, Vol. 2, Characterization, Containment, Remediation, and Performance in Environmental Geotechnics*; Acar, Y. B.; Daniel, D. E., Eds; American Society of Civil Engineers: New York, 1995; pp. 1608-1621.

(7) Warren, K. D.; Arnold, R. G.; Bishop, T. L.; Lindholm, L. C.; Betterton, E. A. Kinetics and mechanism of reductive dehalogenation of carbon tetrachloride using zero-valence metals. *J. Haz. Mat.,* 1995, *41*, 217-227.

(8) Matheson, L. J.; Tratnyek, P. G. Reductive dehalogenation of chlorinated methanes by iron metal. *Environ. Sci. Technol.* 1994, *28*, 2045-2053.

(9) Agrawal, A.; Tratnyek, P. G. Reduction of nitro aromatic compounds by zero-valent iron metal. *Environ. Sci. Technol.,* 1996, *30*, 153-160.

(10) Johnson, T. L.; Tratnyek, P. G. A column study of carbon tetrachloride dehalogenation by iron metal; *Proceedings of the 33rd Hanford Symposium on Health & the Environment. In-Situ Remediation: Scientific Basis for Current and Future Technologies,* Pasco, WA, Battelle Pacific Northwest Laboratories, 1994; Vol. 2, pp. 931-947.

(11) Mackenzie, P. D.; Baghel, S. S.; Eykholt, G. R.; Horney, D. P.; Salvo, J. J.; Sivavec, T. M. Pilot-scale demonstration of reductive dechlorination of chlorinated ethenes by iron metal; *209th National Meeting,* Anaheim, CA, American Chemical Society, 1995; Vol. 35, No. 1, pp. 796-799.

(12) Sivavec, T. M.; Horney, D. P. Reductive dechlorination of chlorinated ethenes by iron metal; *209th National Meeting,* Anaheim, CA, American Chemical Society, 1995; Vol. 35, No. 1, pp. 695-698.

(13) Scherer, M. M.; Tratnyek, P. G. Dechlorination of carbon tetrachloride by iron metal: Effect of reactant concentrations; *209th National Meeting,* Anaheim, CA, American Chemical Society, 1995; Vol. 35, No. 1, pp. 805-806.

(14) Bard, A. J.; Faulkner, L. R. *Electrochemical Methods. Fundamentals and Applications*; Wiley: New York, 1980, pp. 718.

(15) Newman, J. *J. Phys.Chem.,* 1966, *70*, 1327-1330.

(16) Standard reference test method for making pontentiostatic and potentiodynamic polarization measurements. *Annual Book of ASTM Standards* 1987; Vol. 3.04; pp. 73-79.

(17) Bockris, J. O. M.; Genshaw, M.; Brusic, V. Mechanism of film growth and passivation of iron as indicated by transient ellipsometry. *Symp. Faraday Soc.,* 1970, *4*, 177-191.

(18) Johnson, T. L.; Fish, W.; Gorby, Y. A.; Tratnyek, P. G. Degradation of carbon tetrachloride by iron metal: Complexation effects on the oxide surface. *J. Contam. Hydrol.,* 1998, *29*, 377-396.

(19) Spiro, M. Heterogenous catalysis of solution reactions. In *Chemical Kinetics, Vol. 28, Reactions at the Liquid-Solid Interface*; Compton, R. G., Ed; Elsevier: Amsterdam, 1989; pp. 69-166.

(20) Gardner, G. S. Velocity studies: diffusion-controlled corrosion reactions. *Corrosion,* 1963, *19*, 81t-90t.

(21) Jovancicevic, V.; Kainthla, R. C.; Tang, Z.; Yang, B.; Bockris, J. O. M. The passive film on iron: an ellipsometric-spectroscopic study. *Langmuir,* 1987, *3*, 388-395.

(22) Oblonsky, L. J.; Devine, T. M. A surface enhanced Raman spectroscopic study of the passive films formed in borate buffer on iron, nickel, chromium and stainless steel. *Corr. Sci.,* 1995, *37*, 17-41.

(23) Mackenzie, P. D.; Baghel, S. S.; Eykholt, G. R.; Horney, D. P.; Salvo, J. J.; Sivavec, T. M. Pilot-scale demonstration of chlorinated ethene reduction by iron metal: Factors affecting lifetime*; Emerging Technologies in Hazardous Waste Management VII, Extended Abstracts for the Special Symposium,* Atlanta, GA, Industrial & Engineering Chemistry Division, American Chemical Society, 1995; pp. 59-62.

(24) Stratmann, M.; Bohnenkamp, K.; Engell, H.-J. An electrochemical study of phase-transitions in rust layers. *Corr. Sci.,* 1983, *23*, 969-985.

(25) Stratmann, M.; Hoffmann, K. In Situ Mössbauer spectroscopy study of reactions within rust layers. *Corr. Sci.,* 1989, *29*, 1329-1352.

(26) Stratmann, M.; Müller, J. The mechanism of the oxygen reduction on rust-covered metal substrates. *Corr. Sci.*, 1994, *36*, 327-359.

(27) Jovancicevic, V.; Bockris, J. O. M. The mechanism of oxygen reduction on iron in neutral solution. *J. Electrochem. Soc.*, 1986, *133*, 936-938.

(28) Zecevic, S.; Drazic, D. M.; Gojkovic, S. Oxygen reduction on iron: Part III. An analysis of the rotating disk-ring electrode measurements in near neutral solutions. *J. Electroanal. Chem.*, 1989, *265*, 179-193.

(29) Ball, W. P.; Roberts, P. V. Long-term sorption of halogenated organic chemicals by aquifer material. 2. Intraparticle diffusion. *Environ. Sci. Technol.*, 1991, *25*, 1237-1249.

(30) Pankow, J. F.; Cherry, J. A. *Dense Chlorinated Solvents and Other DNAPLs in Groundwater: History, Behavior, and Remediation*; Waterloo Press: Portland, OR, 1996.

(31) Johnson, T. L.; Tratnyek, P. G. Dechlorination of carbon tetrachloride by iron metal: The role of competing corrosion reactions; *209th National Meeting,* Anaheim, CA, American Chemical Society, 1995; Vol. 35, No. 1, pp. 699-701.

(32) Muftikian, R.; Fernando, Q.; Korte, N. A method for the rapid dechlorination of low molecular weight chlorinated hydrocarbons in water. *Wat. Res.*, 1995, *29*, 2434-2439.

(33) Tratnyek, P. G.; Johnson, T. L.; Schattauer, A. Interfacial phenomena affecting contaminant remediation with zero-valent iron metal; *Emerging Technologies in Hazardous Waste Management VII,* Atlanta, GA, American Chemical Society, 1995; pp. 589-592.

(34) Hayduk, W.; Minhas, B. S. Correlations for prediction of molecular diffusivities in liquids. *Can. J. Chem. Eng.*, 1982, *60*, 295-299.

(35) Reid, R. C.; Prausnitz, J. M.; Poling, B. E. *The Properties of Gases and Liquids,* Fourth Edition; McGraw Hill: New York, 1987.

(36) Vogel, T. M.; Criddle, C. S.; McCarty, P. L. Transformations of halogenated aliphatic compounds. *Environ. Sci. Technol.*, 1987, *21*, 722-736.

Table 3.1. Electrochemical Kinetic Parameters for Fe^0-CCl_4-H_2O System.

Redox Couple	$E_x^{eq\ (a)}$ (V)	j_x^0 ($A\ cm^{-2}$)	b_x (V)
$Fe^0 \rightarrow Fe^{2+}$	-0.620 (14)	1.5×10^{-6}	0.077
$2H^+ \rightarrow H_2(g)$	-0.500 (14)	5.5×10^{-6}	0.061
$CCl_4 \rightarrow CHCl_3$	+0.720 (36)	2.2×10^{-9} (b)	0.127

[a]Equilibrium potentials were estimated using the Nernst equation for the conditions pH 8.4, $[Cl^-] = [Fe^{2+}] = 10^{-6}$ M, $[CCl_4] = [CHCl_3]$, and $pH_2 = 1$ atm.

[b]Relative standard deviation based on three replicate experiments is 27%.

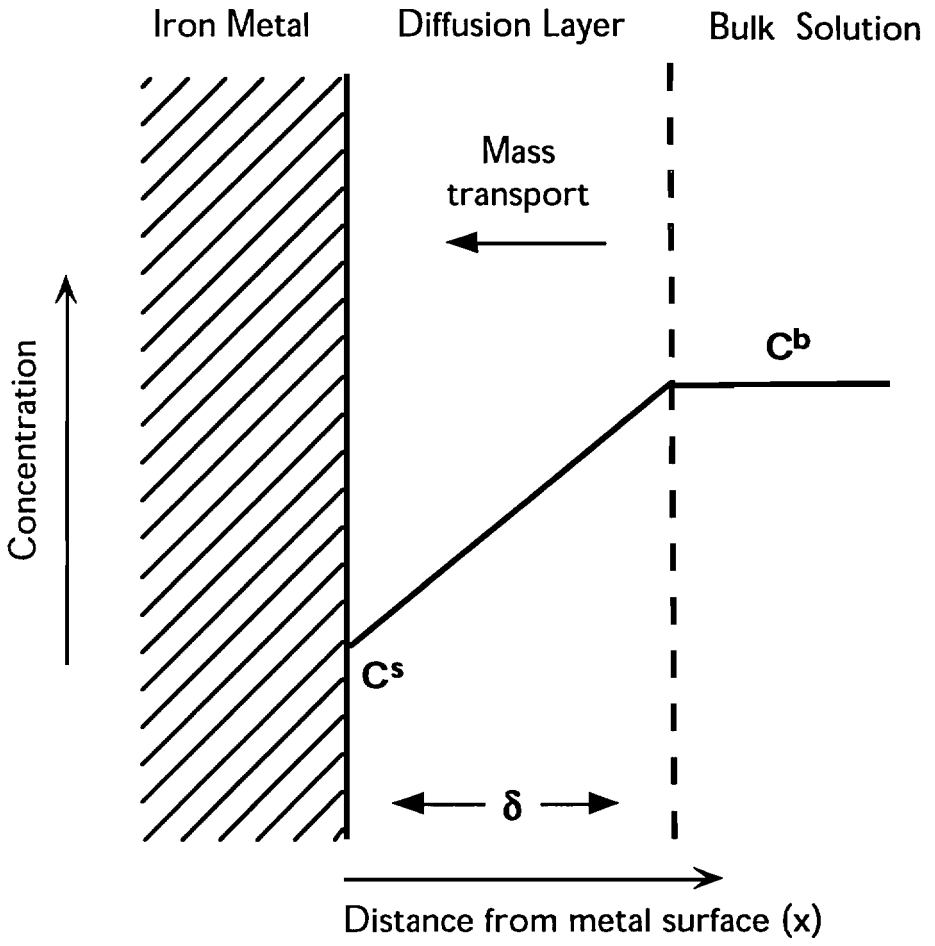

Figure 3.1. Conceptual diagram of an electrode-solution interface with a linear concentration gradient through the diffusion layer; the model is consistent with the RDE and eq. 11-12.

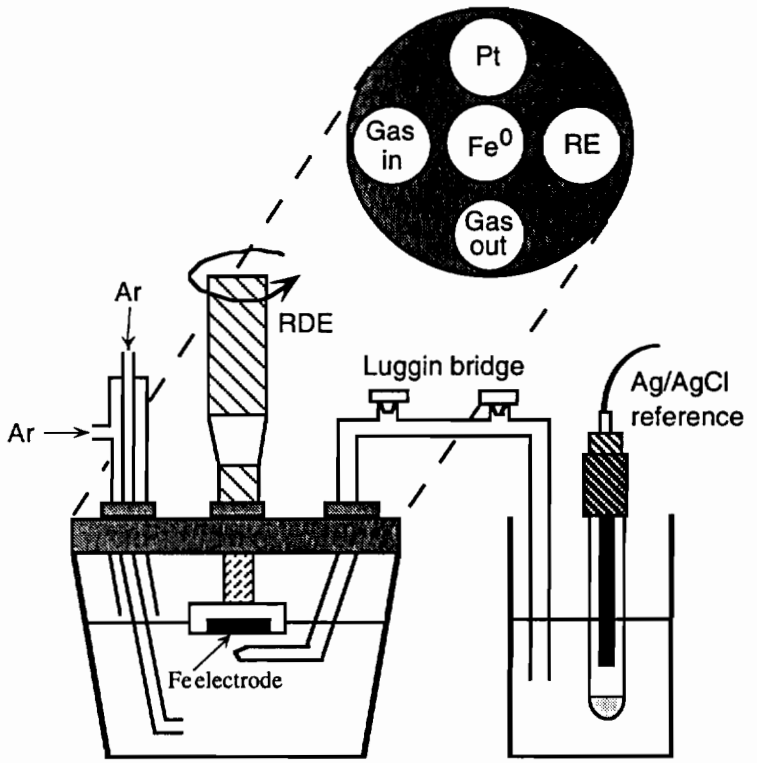

Figure 3.2. Schematic of electrochemical cell used to study dechlorination of aqueous CCl_4 at an Fe^0 rotating disk electrode.

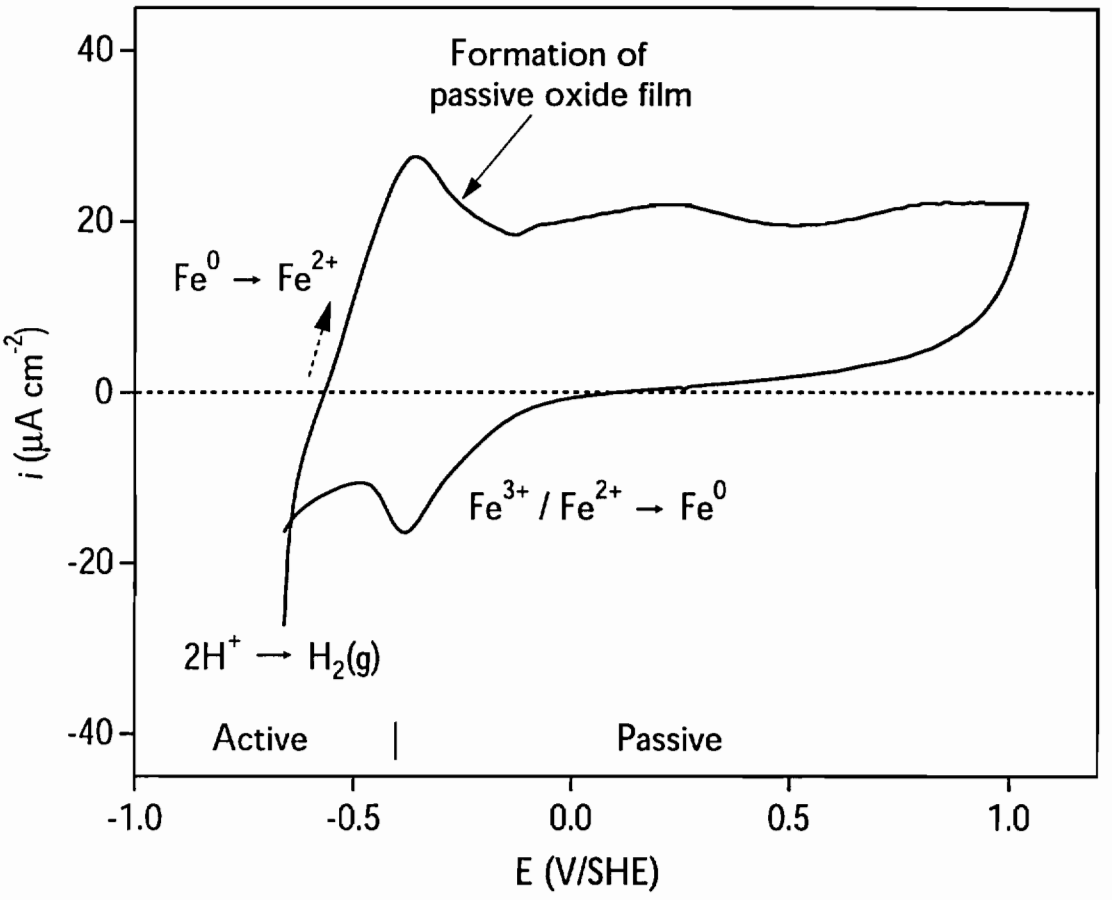

Figure 3.3. Typical cyclic voltammogram at a stationary Fe^0 disk electrode ($\omega = 0$) in deaerated pH 8.4 borate buffer at a scan rate of 5 mV s^{-1}.

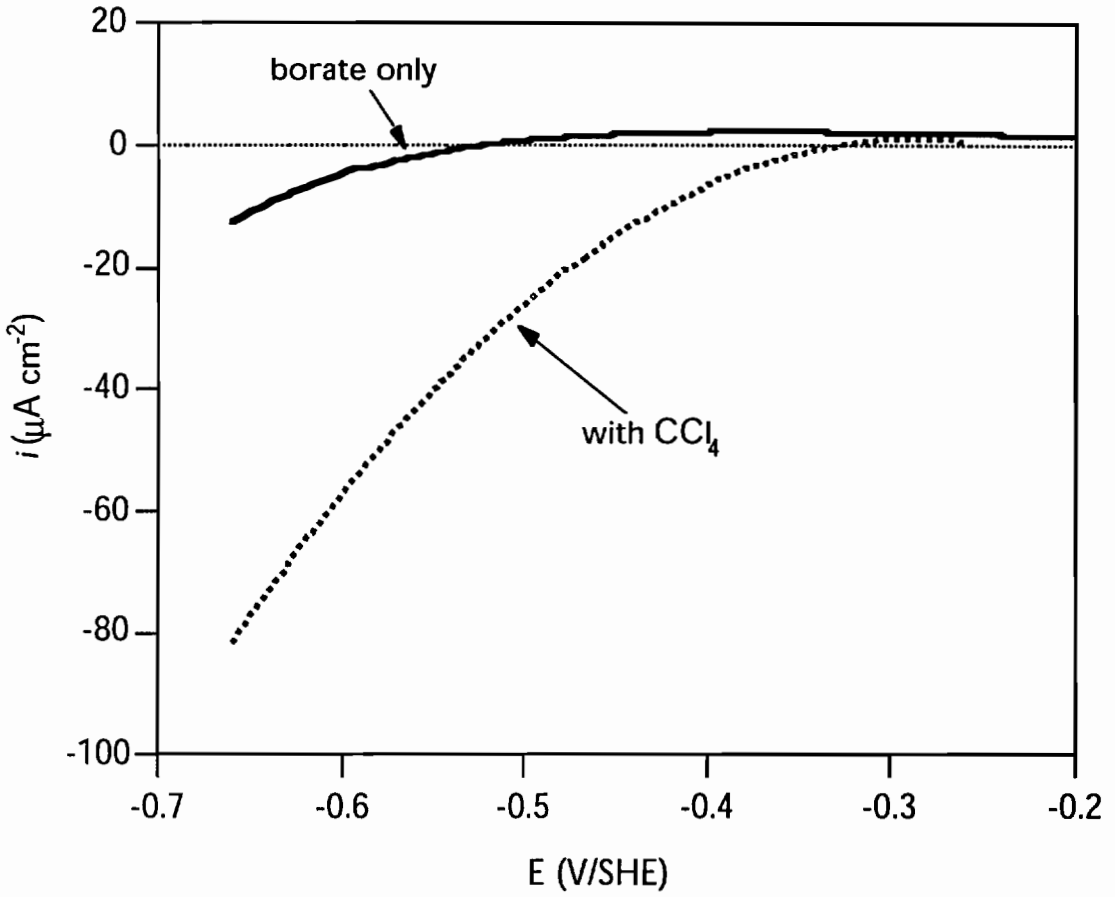

Figure 3.4. Effect of CCl_4 on *i*-E curves at a stationary Fe^0 disk electrode ($\omega = 0$) in the active region. Experiments were carried out in deaerated pH 8.4 borate buffer at a scan rate of 0.2 mV s^{-1}. E_{corr} is -510±10 mV in the absence CCl_4 (solid line) and -380±10 mV in the presence of CCl_4 (dashed line).

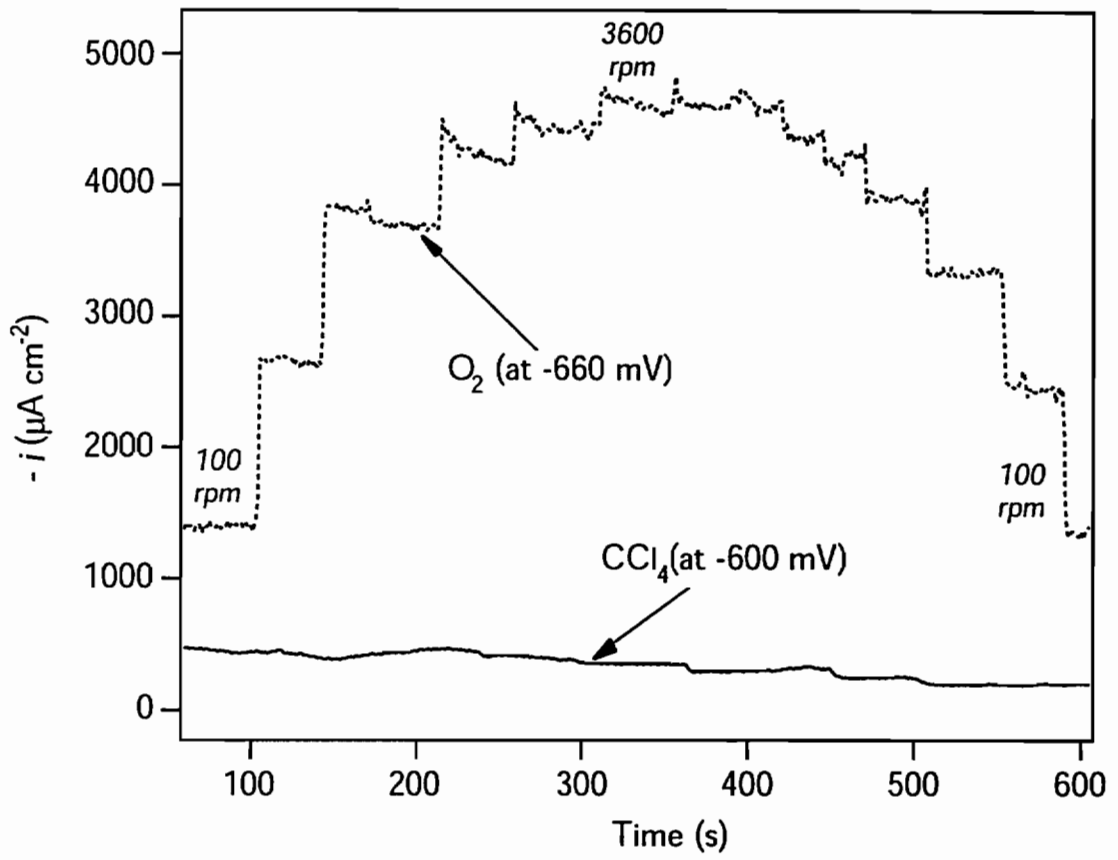

Figure 3.5. Time traces for constant potential reduction of O_2 and CCl_4 at an Fe^0 RDE with stepwise variation in rotation rate. Current densities at -660 mV for p_{O_2} = 1 atm (dashed line), rotation rate stepped from 100 to 3600 rpm and back down. Current densities at -600 mV for CCl_4 saturated borate buffer (solid line), rotation rate varied between 20 and 2500 rpm.

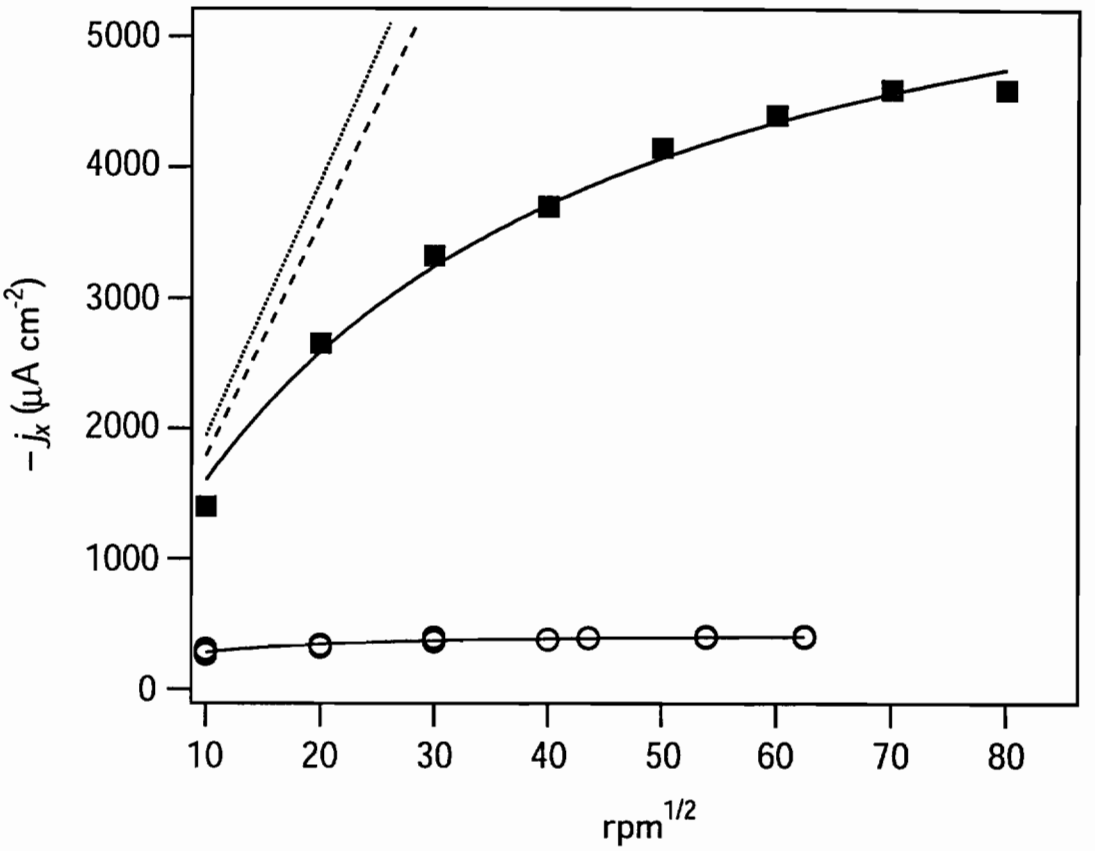

Figure 3.6. Effect of rotation rate on O_2 and CCl_4 current densities at an Fe^0 RDE. Steady-state current densities at -660 mV for pO_2 = 1 atm (squares), steady-state current densities at -600 mV for CCl_4 saturated borate buffer (circles), theoretical line for O_2 under mass transport control (dotted line) calculated using data for the solubility (4 x 10^{-6} mol cm^{-3}) and diffusion coefficient (5 x 10^{-6} cm^2 s^{-1}) of O_2 in borate buffer (27), theoretical line for CCl_4 under mass transport control (dashed line) calculated using a CCl_4 diffusion coefficient (8.6 x 10^{-6} cm^2 s^{-1}) estimated by the Hayduk and Minhas method (34, 35) and solubility of CCl_4 in water (5 x 10^{-6} mol cm^{-3}). Solid lines represent fits to the mixed control equation (eq. 14) using nonlinear least squares parameter adjustment of k_{ct}.

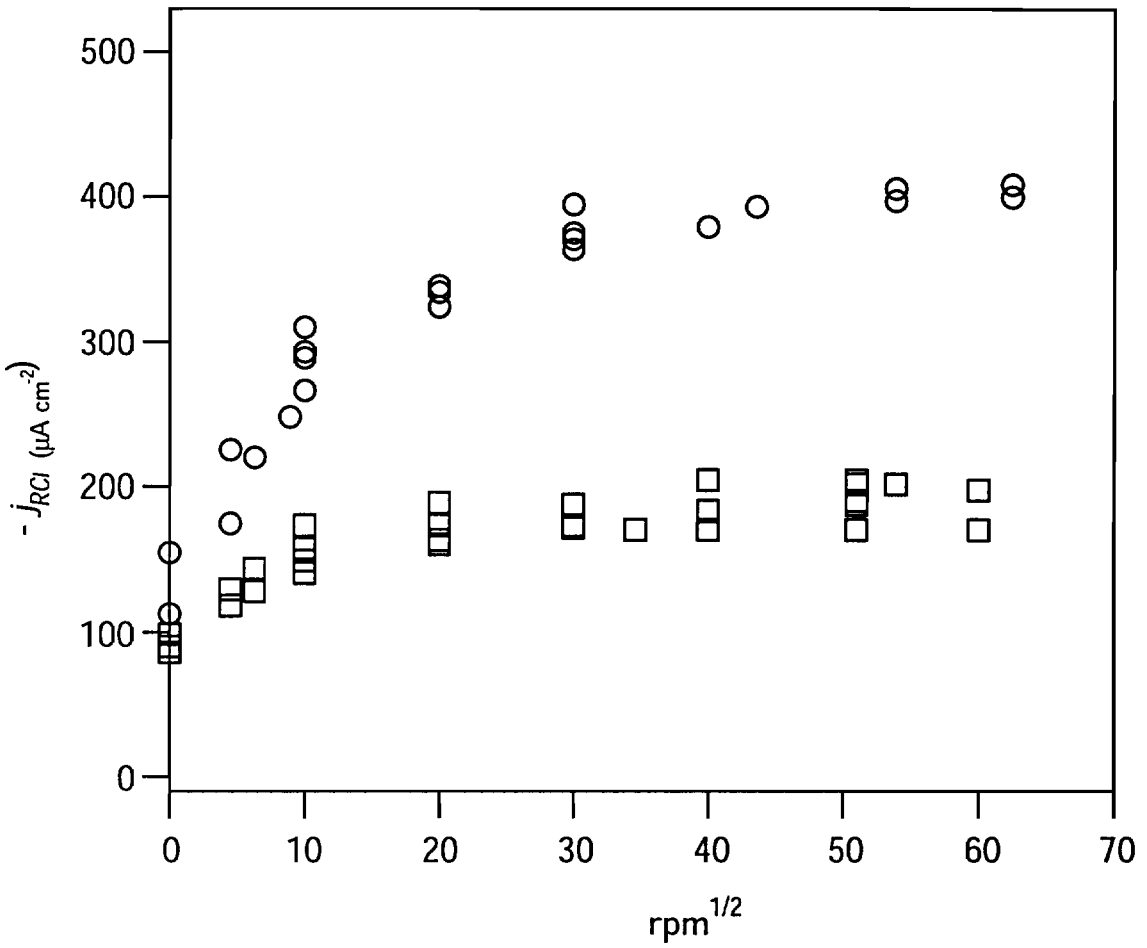

Figure 3.7. Effect of rotation rate on potentiostatic CCl_4 current densities at Fe^0 RDE in active region. E = -640 mV (circles), E = -580 mV (squares).

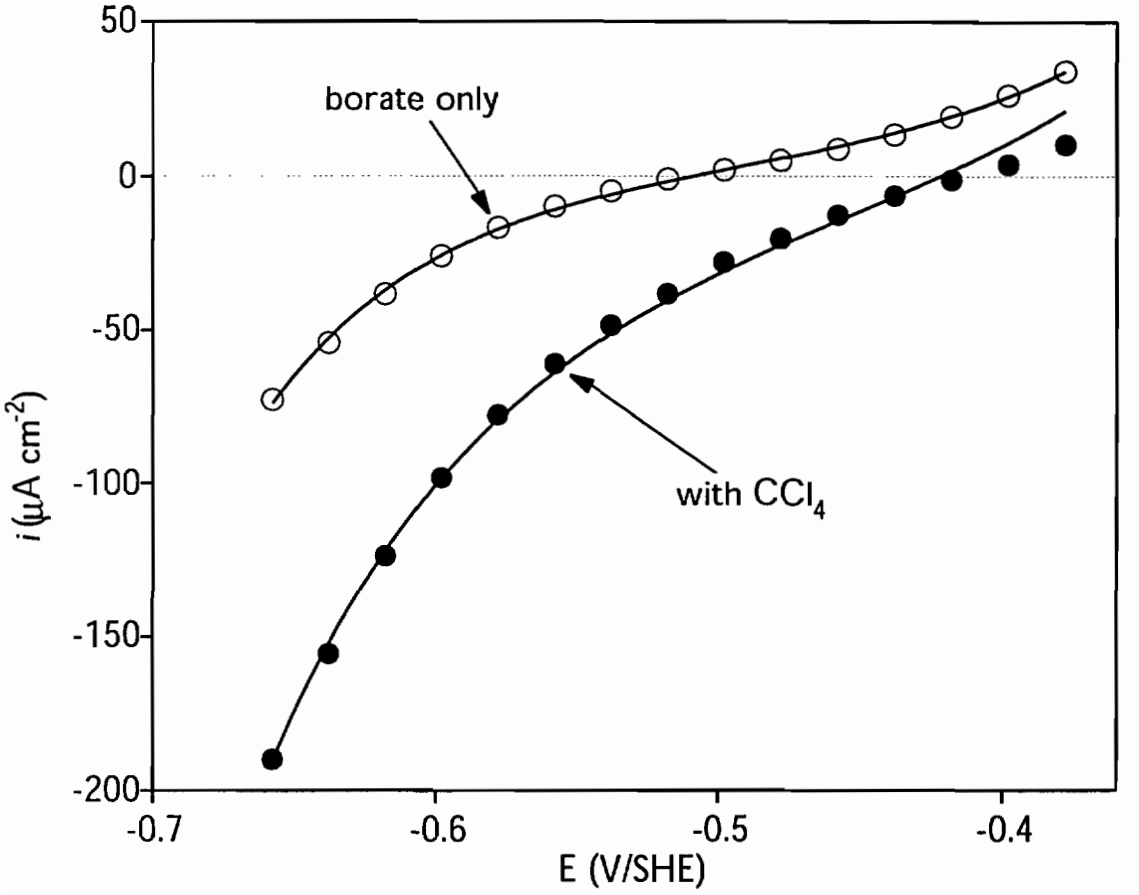

Figure 3.8. Effect of CCl_4 on steady-state *i*-E curves at an Fe^0 RDE rotating at 3000 rpm, where mass transfer effects are negligible (the data were collected as conventional linear sweep voltammograms but are presented as discrete points to distiguish between the model and the data). Experiments were carried out in deaerated pH 8.4 borate buffer at a scan rate of 0.2 mV s^{-1} in the absence CCl_4 (open circles) and in the presence of CCl_4 (closed circles). Charge transfer kinetics are modeled with eq. 5-8 and the parameters given in Table 1. The sum of the *j*-E curves provides a reasonably good fit to the the observed *i*-E data.

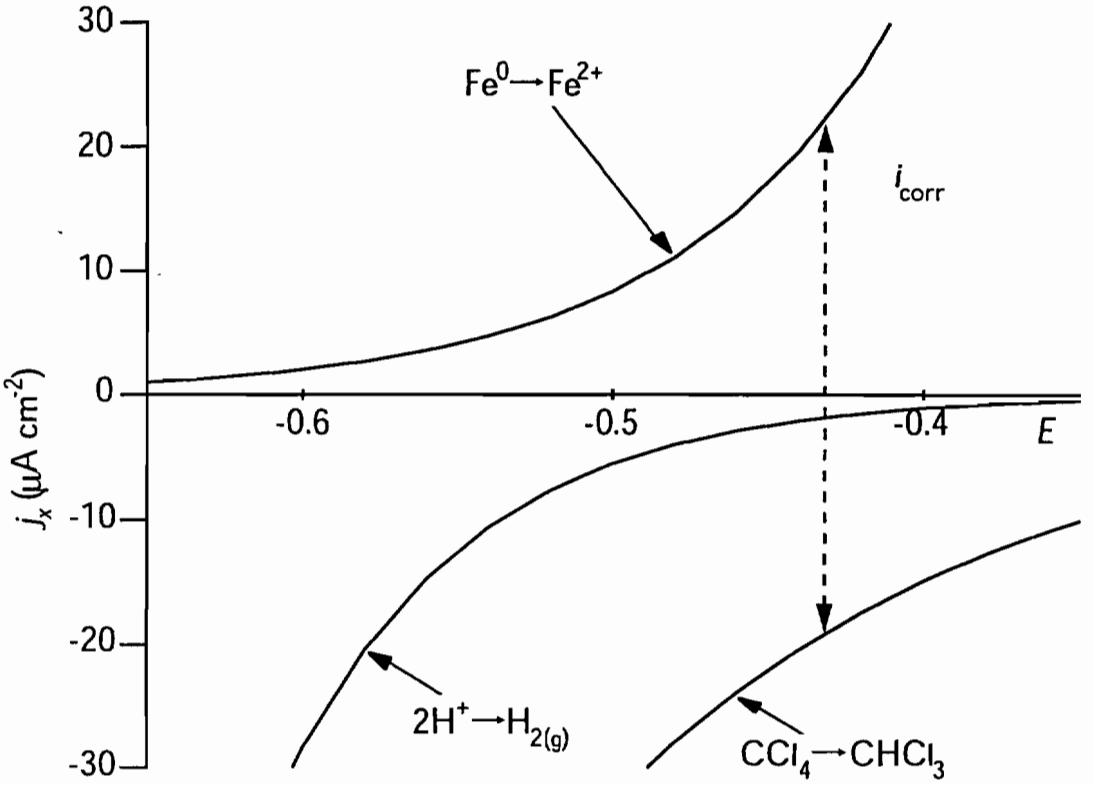

Figure 3.9. Mixed potential diagram showing calculated partial current densities for the Fe^0-CCl_4-H_2O system derived from the Tafel equations (eq. 5-8) and the parameters listed in Table 1. The predicted corrosion current (where $|j_{RCl} + j_H| = j_{Fe}$) is 21 μA cm^{-2}, which agrees well with the measured value of 22 ± 1 μA cm^{-2}.

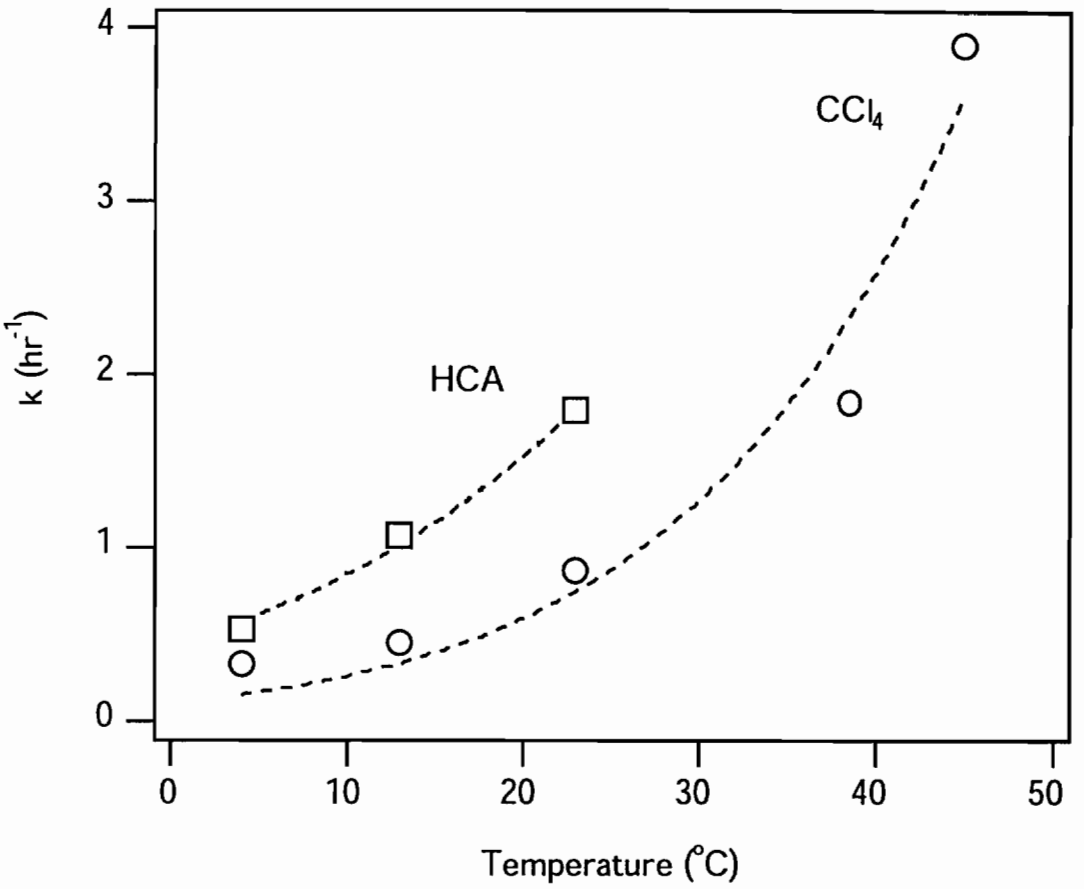

Figure 3.10. Effect of temperature on observed reaction rate constants for the reduction of CCl_4 and hexachloroethane (HCA) by Fe^0. Dashed lines represent nonlinear least squares parameter adjustment of A and E_a using the Arrhenius equation ($k = Ae^{-Ea/RT}$).

CHAPTER 4

Kinetics of Nitrobenzene Reduction at an Oxide-Free Iron Electrode

4.1 Introduction

The reduction of nitro groups is often the first step in the remediation of nitroaromatic pollutants, such as the explosives 2,4,6-trinitrotoluene (TNT) and hexahydro-1,3,5-trinitro-1,3,5-triazine (RDX) (1). Although nitro reduction by microorganisms is the most common treatment method (2, 3), abiotic reduction by iron metal (Fe^0) has recently emerged as a promising alternative (4-6). Presently, the most common application of Fe^0 for environmental remediation is in permeable reactive barriers (PRBs) which have proven to be a passive, cost-effective treatment technology for reducing chlorinated solvents (7), metals (8, 9), and radionuclides (10). Application of Fe^0 PRBs to nitroaromatics, however, will require an additional treatment step because the amine compounds formed from nitro reduction are still of significant environmental concern (11). Recent progress has been made in this area with a sequential treatment process with Fe^0 as a reductant, followed by hydrogen peroxide as an oxidant, to remove TNT and RDX from explosives-contaminanted water and soil (5).

Since it appears that the use of Fe^0, in combination with oxidative or biotic treatment, may provide a basis for remediating nitroaromatic compounds, a better understanding of the kinetics of nitro reduction by Fe^0 is desirable. A detailed study (4) of the reduction of nitrobenzene ($ArNO_2$) by Fe^0 in batch experiments led to three findings of particular interest: (i) precipitation of siderite ($FeCO_3$) on the iron surface inhibits the rate of $ArNO_2$ reduction; (ii) the rate of $ArNO_2$ reduction is not influenced by substituent effects or pH; and (iii) a linear relationship exists between the $ArNO_2$ reaction rate constant and the square root of the batch mixing rate ($rpm^{1/2}$). The latter two findings were interpreted as an indication that, in the batch system used, the rate of $ArNO_2$ reduction was controlled primarily by mass transport to the Fe^0 surface.

We recently developed an alternative experimental approach to study the kinetics of contaminant reduction by Fe^0 (12). The experimental design consists of an electrochemical cell with an Fe^0 rotating disk electrode (RDE). The controlled hydrodynamics of an RDE are well understood (13, 14), and can be used to quantify the mass transport and reaction contributions to the observed reduction rate. In the Fe^0-CCl_4-H_2O system, results with the RDE clearly showed that the reduction of CCl_4 by Fe^0 was controlled by surface reaction (precursor complex formation or electron transfer) rather than mass transport (12, 15). In this study, the RDE is used evaluate the role of mass transport in the reduction of nitroaromatic compounds by Fe^0.

4.2 Background

4.2.1 Chemical Reactions

The complete reduction of $ArNO_2$ to $ArNH_2$ by Fe^0 involves six electrons and can be written as:

$$ArNO_2 + 3Fe^0 + 6H^+ \rightarrow ArNH_2 + 3Fe^{2+} + 2H_2O \quad (1)$$

Eq. 1 represents the sum of several two-electron half-reactions: the oxidation of Fe^0,

$$Fe^0 \rightarrow Fe^{2+} + 2\,e^- \quad (2)$$

and the sequential reduction of $ArNO_2$ to nitrosobenzene (ArNO), phenyl hydroxylamine (ArNHOH), and aniline ($ArNH_2$):

$$ArNO_2 + 2H^+ + 2\,e^- \rightarrow ArNO + H_2O \quad (3)$$

$$ArNO + 2H^+ + 2\,e^- \rightarrow ArNHOH \quad (4)$$

$$ArNHOH + 2H^+ + 2\,e^- \rightarrow ArNH_2 + H_2O \quad (5)$$

Although the first intermediate, ArNO, is normally difficult to isolate (16, 17), it was the major intermediate observed in the granular Fe^0 batch systems discussed above (4). In addition to the reduction of $ArNO_2$ and oxidation of Fe^0, the reduction of water occurs and must be considered when evaluating current densities at an Fe^0 RDE:

$$2\,H_2O + 2\,e^- \rightarrow H_2(g) + 2\,OH^- \quad (6)$$

4.2.2 Electrochemical Measurements

Current densities measured at an electrode can be used to monitor the rate of an overall reaction. The net current density (i, A m^{-2}) observed at an Fe^0 RDE in the presence of dissolved $ArNO_2$ is the sum of the partial current densities (j_x, A m^{-2}) for each of the reactions described in eqs. 2-6:

$$i = j_{Fe} + j_{NB} + j_{NO} + j_{NHOH} + j_H \quad (7)$$

where *Fe*, *NB*, *NO*, *NHOH*, and *H*, refer to the partial current densities associated with each reaction, respectively. When the net current is equal to zero ($i = 0$), the system is at electrochemical steady state ($\sum$ anodic current = $-\sum$ cathodic current). The potential at which this zero-current condition is fulfilled is known as the corrosion potential, E_{corr}. Although the net current density at E_{corr} is equal to zero, the partial current densities are non-zero and define the corrosion current density (i_{corr}). If the reduction of $ArNO_2$ to ArNO (j_{NB}) is the major cathodic reaction, then at the zero-current condition, i_{corr} is equal to the rate of nitrobenzene reduction:

$$i_{corr} = j_{Fe} = -j_{NB} \quad (8)$$

A great deal can be learned about the behavior of a system at E_{corr} by observing the the change in current with a change in applied potential. The *i-E* relationship for a chemical reaction can be derived by describing the individual partial current densities with the Tafel equations (18):

$$j_{Fe} = j_{Fe}^0 \exp\{(E - E_{Fe}^{eq})/b_{Fe}\} \quad (9)$$

$$j_{NB} = -j_{NB}^0 \exp\{-(E - E_{NB}^{eq})/b_{NB}\} \quad (10)$$

where j_x^0 is the exchange current density, which refers to the partial current density under equilibrium conditions ($E = E_x^{eq}$); E is the electrode potential; E_x^{eq} is the equilibrium potential for the half reaction; and b_x is an empirical parameter known as the Tafel slope. If *i-E* data is available as a function of the concentration of substance x at the electrode surface, C_x^s, then the exchange current density can be re-expressed in terms of a standard heterogeneous rate constant, k_x^0, that is independent of potential and concentration:

$$j_x^0 = nFk_x^0 C_x^s \quad (11)$$

where, n is the number of electrons in the reaction, and F is the Faraday constant (96485 C mol^{-1}).

A combination of eqs 7–11 allows the observed current density, i, to be expressed in terms of the applied potential, E. If this kinetic model is a good approximation of the behavior of the system, then the values of k_x^0 and b_x can be determined from the experimental data. Specifically, if the value of j_{NB} can be determined from the model, it can be re-expressed in terms of a first-order heterogeneous rate constant for charge transfer in the $ArNO_2$ reaction, k_{ct}:

$$j_{NB} = -nFk_{ct}C_{NB}^{s} \tag{12}$$

Equations 7–11 are applicable in the absence of mass transfer effects, when the concentrations of reactants and products at the electrode surface, C^s, are equal to those in the bulk solution, C^b.

4.2.3 Mass Transport

Transport to the surface of the RDE is controlled by forced convection and diffusion, but is equivalent to an electrode which is separated from a well mixed solution by a stagnant water layer at the electrode surface (12). Under steady-state or quasi steady-state conditions, the mass transport limited current density due to reduction of species x at an RDE can be approximated by the Levich equation (18):

$$j_x = -nF(D_x / \delta_x)(C_x^b - C_x^s) \tag{13}$$

where D_x is the molecular diffusion coefficient and δ_x is the thickness of the stagnant water layer, given by:

$$\delta_x = 1.61\, D_x^{1/3}\, \omega^{-1/2}\, \nu^{1/6} \tag{14}$$

in which ν is the kinematic viscosity of the electrolyte, and ω is the angular velocity of the rotating disk ($\omega = 2\pi f$, where f = rotation rate in s^{-1}). Thus, the current under mass transport limited conditions is expected to vary inversely with the square root of the rotation rate. At sufficiently high rotation rates, the reactant is transported to the surface faster than it can be consumed and the current density reaches a value that is limited by the chemical reaction rate and independent of disk rotation rate.

In order to facilitate comparison of the rates of mass transport and electrochemical reaction, it is convenient to express two of the terms in eq. 13 as a first-order heterogeneous rate constant for mass transport of species x to the surface, k_{mt}:

$$k_{mt} = D_x / \delta_x \tag{15}$$

This definition allows direct comparison of measured k_{ct} values with estimated k_{mt} values.

4.2.4 Mixed Control

For the case of intermediate kinetics, where both reaction and transport processes influence the reaction rate, eqs. 12-15 can be combined to describe the relative contributions of k_{mt} and k_{ct}. Under steady state conditions, the mixed control equation due to reduction of species x is:

$$\frac{1}{j_x} = -\frac{1}{nFk_{ct}C_x^b} - \frac{1}{nFk_{mt}C_x^b} \tag{16}$$

where the first term on the right side represents the surface reaction contribution to the overall kinetics and the second term represents the mass transport contribution.

4.3 Experimental Section

4.3.1 Electrochemical Cell

Experiments were carried out in a custom three-electrode glass cell, which has been described previously (12). The cell consisted of an Fe^0 RDE working electrode (surface area = 0.071 cm^2), a double-junction Ag/AgCl reference electrode connected to the cell through a Luggin capillary salt bridge, and a Pt mesh counter electrode. Potentials are reported relative to the standard hydrogen electrode (SHE), and currents are reported in accord with IUPAC convention (anodic current is positive and cathodic current is negative).

4.3.2 Fe^0 RDE Experiments

Before each experiment, the Fe^0 electrode was mechanically polished with 600 and 800 grit silicon carbide paper and 1 μm diamond paste to achieve a mirror-like finish. The current-voltage (*i-E*) curves were measured in pH 8.4 borate buffer (0.11 M) containing 6% methanol. The cell was deaerated by bubbling Ar into the cell for at least one hour at the beginning of each sequence of experiments. To reduce any oxide film that may have formed by exposure to air after polishing, the electrode was reduced at -720 mV for about 30 minutes immediately before each experiment. It has been shown that the iron surface is free of an oxide film under these conditions (19). Following cathodic pretreatment, $ArNO_2$ was introduced into the cell by injection of a known volume of deaerated aqueous stock solution through a septum.

Linear sweep voltammograms (LSVs) were obtained with and without $ArNO_2$ with an Analytical Instrument Systems potentiostat (Model DLK). Coulometry was used to assess the current efficiency, that is, the fraction of the current passed that results in the transformation of $ArNO_2$. To observe the effects of mass transfer on the reaction rate, the current was recorded as a function of rotation rate with a Pine Instruments potentiostat (Model AFCBP1) while the electrode was held at a constant potential. The potential was chosen to minimize oxide formation and hydrogen evolution (i.e., optimal for having $i \approx j_{NB}$ and no oxide film).

4.3.3 Chemical Analysis

Nitrobenzene and its reduction products were quantified periodically by removal of 200 µL samples from the cell and determination of the concentration by isocratic HPLC with UV absorbance detection at 278 nm (4). The 3.9 x 300 mm analytical column consisted of 10 µM particle packing with a C-18 stationary phase. The eluent was 40/60 acetonitrile and unbuffered, deionized water at a flow rate of 0.9 mL min^{-1}. Selected samples were analyzed at 235 nm to obtain a detection limit for aniline of 1 µM.

4.4 Results and Discussion

4.4.1 Linear Sweep Voltammetry at Fe^0 RDE

Linear sweep voltammograms measured with the Fe^0 RDE in borate buffer, with and without $ArNO_2$, are shown in Figure 4.1. For comparison to our previous work (12), an LSV in the presence of CCl_4 is also shown. In the potential region where the passive film did not form (i.e., the active region, E < -400 mV), the presence of 5 mM CCl_4 caused a significant increase in cathodic current density compared to the those observed in borate buffer alone. The presence of $ArNO_2$ (0.75 mM) gave much greater current densities than 5 mM CCl_4, suggesting significantly faster reduction kinetics for $ArNO_2$ compared to CCl_4. This observation is consistent with reduction rates observed with granular Fe^0 metal, where the surface area normalized rate constant reported for $ArNO_2$ (k_{SA} = 1.56 L m^{-2} hr^{-1} (4)) is more than ten times greater than the average value reported for CCl_4 (k_{SA} = 0.12 L m^{-2} hr^{-1} (15)).

4.4.2 Coulometry

To confirm that the observed current densities are due to the reduction of $ArNO_2$ by the Fe^0 RDE, the concentrations of reaction products in the cell solution were compared to

those expected from the total cathodic charge passed. From Faraday's law, the amount of product (N, mol) is related to the amount of charge (q, C) by $N = q/\text{nF}$. For nitrobenzene reduction, however, the comparison must take into account the formation of the nitroso and hydroxylamine intermediates, as well as the final amine product. Therefore,

$$q_{tot} = (2N_{NO} + 4N_{NHOH} + 6N_{NH_2}) \text{ x F} \quad (17)$$

where 2, 4, and 6 represent the number of electrons transferred to form the product from the reduction of $ArNO_2$. A comparison of the products measured by HPLC and the total charge provides an estimate of the current efficiency. Approximately 72% of the total cathodic charge (q_{tot} = 2.08 C) could be accounted for by nitrosobenzene and aniline (quantified by HPLC) in a long term electrolysis experiment (26 hours with E_{appl} = -600 mV). An unidentified peak at a retention time of 4.4 min (cf. ~ 5.4 min for aniline, 8.6 min for nitrobenzene, and 9.1 min for nitrosobenzene) may correspond to the hydroxylamine intermediate (4), and could account for the remaining 28% of the measured charge. RDE and LSV experiments conducted over shorter time periods (< 3 hours) produced little product (q_{tot} < 400 mC), making it difficult to quantify the current efficiency in these experiments.

4.4.3 Effect of Electrode Rotation Rate

In our previous work (12), rotation rate had little effect on the reduction of CCl_4 at an Fe^0 RDE. This result confirmed what the wide range in reported reduction rates among chlorinated aliphatic compounds had suggested (15): the rate of CCl_4 reduction is limited by surface reaction rather than mass transport. Nitro reduction rates, on the other hand, are unaffected by chemical structure, suggesting the possibility of some influence of mass transport (4). The sharp, reproducible changes in current in response to a change in rotation rate confirm that the rate of $ArNO_2$ reduction is influenced by mass transport as shown in Figure 4.2. However, if the reaction was solely controlled by mass transport, then replotting the data from Figure 4.2 against the square root of electrode rotation rate would give a linear relationship (eq. 13). The nonlinearity observed in Figure 4.3 suggests that the reaction kinetics of nitro reduction by Fe^0 are influenced by both mass transport *and* surface reaction (i.e., mixed-control).

From the data in Figure 4.3, a quantitative electrochemical characterization for the reaction kinetics of the Fe^0-$ArNO_2$-H_2O system can be derived. Values of the parameters k_{NB}^0, b_{NB}, and D_{NB} were determined by nonlinear least squares parameter adjustment with the expression describing mixed control (eq. 16). All of the data available in Figure 4.3 (E,

C_{NB}, j_{NB}, and rpm) were evaluated simultaneously. The parameters derived by this method are presented in Table 4.1, and the currents calculated from the model (eq. 16) with these parameters are shown by the solid lines in Figure 4.3. The calculated values of j_{NB} are in good agreement with the current densities at the two most negative potentials (-630 and -580 mV) but are slightly offset at the more positive potentials (-530 and -480 mV). If the model consistently predicted current densities larger than the experimental data, then one possible explanation could be some influence of passivation at the more positive potentials.

4.4.4 Mixed Control Kinetics

The partial current densities calculated from this model, as shown in Figure 4.4, provide a basis for evaluating the thermodynamic and kinetic behavior of the system. The effect of mixed-control is illustrated by j_{NB} (mix), the partial current density influenced by both mass transport and surface reaction (eq. 16), and j_{NB} (ct), the partial current density in the absence of mass transport effects (eqs 10-11). Since the reduction of water (j_H) is negligible compared to the reduction of $ArNO_2$ (j_{NB}), i_{corr} is approximately equal to j_{NB} and can be used to estimate the rate of nitro reduction at equilibrium conditions (i.e., an Fe^0 particle in the ground). The rate of nitro reduction estimated with j_{NB} (mix) is significantly less than that estimated with j_{NB} (ct), suggesting that increasing mass transport rates is a logical basis for improving nitro reduction rates in groundwater remediation applications.

The ratio of rate constants for mass transport (k_{mt}) and surface reaction (k_{ct}) characterizes the degree to which mixed-control affects the overall kinetics. The calculated effect of k_{ct} / k_{mt} on the overall kinetics is illustrated in Figure 4.5. Although the plot is generated for an RDE system, where current is measured as a function of electrode rotation rate, additional axes are given to emphasize the relationship between rotation rate and thickness of the diffusion layer (δ), and between current density (j) and kinetic parameters such as rate (mol s^{-1} cm^2) and first-order heterogeneous rate constant (k_{SA}, L m^{-2} h^{-1}). The derivation is based on the general form of eq. 11 ($j = nFkC$) and an assumed environmental contaminant concentration of 50 μM. When k_{ct} is much less then k_{mt} (i.e., $k_{ct} / k_{mt} <$ 0.1), mass transport has no influence on the observed reaction rate and a slope of nearly zero is observed, consistent with reaction kinetics that are controlled entirely by charge transfer. This behavior was observed in the Fe^0-H_2O-CCl_4 system and led to the conclusion that the dechlorination of CCl_4 was controlled by the surface chemical reaction rather than mass transport (12). At the other extreme, when k_{ct} is much greater than k_{mt} (i.e., $k_{ct} / k_{mt} > 100$), the reaction is limited by mass transport to the surface, and a linear

relationship is observed in which the slope is only a function of the molecular diffusivity of the reacting substrate (recall eq. 13). A continuum of possibilities exist between these two extremes where both chemical reaction and mass transport influence the observed kinetics (i.e., mixed control kinetics). The Fe^0-$ArNO_2$-H_2O is an example of an environmentally relevant system that exhibits mixed control (Figure 4.4).

From the kinetic parameters in Table 4.1, k_{ct} / k_{mt} values can be calculated for the CCl_4 and $ArNO_2$ systems to compare with Figure 4.5. For the Fe^0-$ArNO_2$-H_2O system, k_{ct} / k_{mt} values vary from 1.2 (E_{appl} = -480 mV) to 3.7 (E_{appl} = -630 mV), consistent with the region in Figure 4.5 where the observed kinetics exhibit mixed control. The Fe^0-CCl_4-H_2O system, on the other hand, has a much smaller value of k_{ct} / k_{mt} (0.01), which is consistent with the evidence that the reduction of CCl_4 by Fe^0 is charge transfer controlled (12). Given the slower reduction rates observed for other chlorinated aliphatic compounds (15), the k_{ct} / k_{mt} values will be significantly less than the 0.01 calculated for CCl_4. Conversely, di and tri-nitroaromatics such as 2,4-DNT and TNT are likely to have k_{ct} / k_{mt} ratios even greater than that of $ArNO_2$ (17), and therefore we expect mass transport limited nitro reduction under most conditions.

4.5 Literature Cited

(1) Haderlein, S. B.; Schwarzenbach, R. P. Environmental processes influencing the rate of abiotic reduction of nitroaromatic compounds in the subsurface. In *Biodegradation of Nitroaromatic Compounds*; Spain, J. C., Ed; Plenum: New York, 1995; pp. 199-225.

(2) Gorontzy, T.; Drzyzga, O.; Kahl, M.; Bruns-Nagel, D.; Breitung, J.; von Loew, E. Microbial degradation of explosives and related compounds. *Crit. Rev. Microbiol.*, 1994, *20*, 265-284.

(3) Hughes, J. B.; Wang, C. Y.; Rudolph, F. B. Reduction of 2,4,6-trinitrotoluene by *Clostridium acetobutylicum* through hydroxylamino-nitrotoluene intermediates. *Environ. Toxicol. Chem.*, 1998, *17*, 343.

(4) Agrawal, A.; Tratnyek, P. G. Reduction of nitro aromatic compounds by zero-valent iron metal. *Environ. Sci. Technol.*, 1996, *30*, 153-160.

(5) Hundal, L. S.; Singh, J.; Bier, E. L.; Shea, P. J.; Comfort, S. D.; Power, W. L. Removal of TNT and RDX from water and soil using iron metal. *Environ. Poll.*, 1997, *97*, 55-64.

(6) Devlin, J. F.; Klausen, J.; Schwarzenbach, R. P. Kinetics of nitroaromatic reduction on granular iron in recirculating batch experiments. *Environ. Sci. Technol.*, In press.

(7) O'Hannesin, S. F.; Gillham, R. W. Long-term performance of an in situ "iron wall" for remediation of VOCs. *Ground Water,* 1998, *36*, 164-170.

(8) Puls, R. W.; Paul, C. J.; Clark, P. J. Remediation of chromate-contaminated ground water using an in-situ permeable reactive mixture: Field pilot test, Elizabeth City, North Carolina*; 213th National Meeting,* San Francisco, CA, American Chemical Society, 1997; Vol. 37, No. 1, pp. 241-243.

(9) Cantrell, K. J.; Kaplan, D. I.; Wietsma, T. W. Zero-valent iron for the in situ remediation of selected metals in groundwater. *J. Haz. Mat.,* 1995, *42*, 201-212.

(10) Del Cul, G. D.; Bostick, W. D.; Trotter, D. R.; Osborne, P. E. Technetium-99 removal from process solutions and contaminated groundwater. *Sep. Sci. and Tech.,* 1993, *28*, 551-564.

(11) Parris, G. E. Environmental and metabolic transformations of primary aromatic amines and related compounds. *Res. Rev.,* 1980, *76*, 1-30.

(12) Scherer, M. M.; Westall, J. C.; Ziomek-Moroz, M.; Tratnyek, P. G. Kinetics of carbon tetrachloride reduction at an oxide-free iron electrode. *Environ. Sci. Technol.,* 1997, *31*, 2385-2391.

(13) Riddiford, A. C. The rotating disk system. In *Advances in Electrochemistry and Electrochemical Engineering*; Delahay, P., Ed; Wiley: New York, 1966; Vol. 4; pp. 47-111.

(14) Levich, V. G. *Physicochemical Hydrodynamics*; Prentice-Hall, Inc.: 1962.

(15) Johnson, T. L.; Scherer, M. M.; Tratnyek, P. G. Kinetics of halogenated organic compound degradation by iron metal. *Environ. Sci. Technol.,* 1996, *30*, 2634-2640.

(16) Shindo, H.; Nishihara, C. Detection of nitrosobenzene as an intermediate in the electrochemical reduction of nitrobenzene on Ag in a flow reactor. *J. Electroanal. Chem.,* 1989, *263*, 415-420.

(17) Fry, A. J. Electrochemistry of nitro compounds. In *The Chemistry of Amino, Nitroso, and Nitro Compounds and their Derivatives*; Patai, S., Ed; Wiley-Interscience: Chichester, 1982; Vol. 1; pp. 319-337.

(18) Bard, A. J.; Faulkner, L. R. *Electrochemical Methods. Fundamentals and Applications*; Wiley: New York, 1980, pp. 718.

(19) Bockris, J. O. M.; Genshaw, M.; Brusic, V. Mechanism of film growth and passivation of iron as indicated by transient ellipsometry. *Symp. Faraday Soc.,* 1970, *4*, 177-191.

(20) Vogel, T. M.; Criddle, C. S.; McCarty, P. L. Transformations of halogenated aliphatic compounds. *Environ. Sci. Technol.,* 1987, *21*, 722-736.

Table 4.1. Electrochemical Kinetic Parameters for Fe^0-$ArNO_2$-H_2O and Fe^0-CCl_4-H_2O Systems.

Redox Couple	$E_x^{eq\ (a)}$ (V)	j_x^0 (A cm^{-2})	k_x^0 (cm s^{-1})	b_x (V)	D (cm^2 s^{-1})
$ArNO_2 \rightarrow ArNO$	-0.400	[c]NA	7.03×10^{-3}	0.139	4.4×10^{-5}
[b]$CCl_4 \rightarrow CHCl_3$	+0.720 (20)	2.2×10^{-9}	[d]2.3×10^{-9}	0.127	8.6×10^{-6}
[b]$Fe^0 \rightarrow Fe^{2+}$	-0.620 (18)	1.5×10^{-6}	[e]7.8×10^{-3}	0.077	NA
[b]$2H^+ \rightarrow H_2(g)$	-0.500 (18)	5.5×10^{-6}	[f]7.2	0.061	NA

[a] Equilibrium potentials were estimated using the Nernst equation for the conditions pH 8.4, $[Cl^-] = [Fe^{2+}] = 10^{-6}$ M, $[CCl_4] = [CHCl_3]$, and $pH_2 = 1$ atm. [b] Data from ref. (12). [c] Not applicable. [d] Calculated using $[CCl_4] = 5$ mM, as reported in ref. (12). [e] Calculated with $[Fe^{2+}] = 1$ μM. [f] Calculated with a pH value of 8.4.

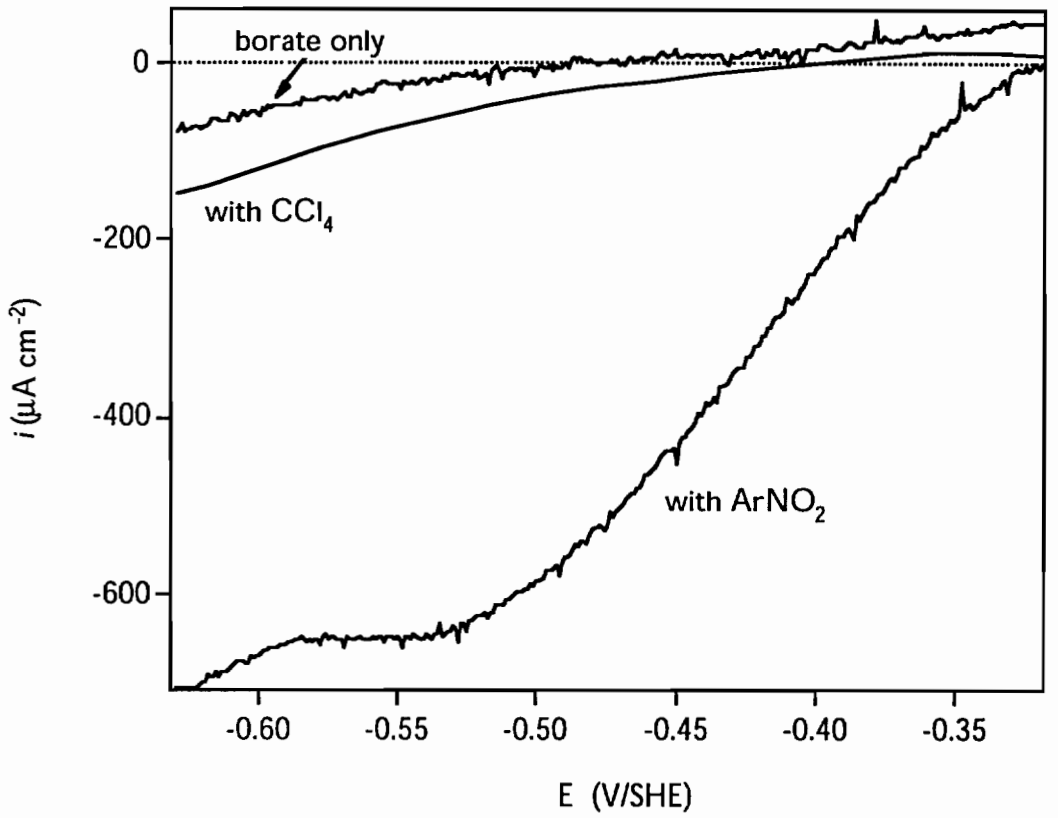

Figure 4.1 Effect of $ArNO_2$ and CCl_4 on *i-E* curves at an Fe^0 RDE. Linear sweep voltammograms were measured in deaerated pH 8.4 borate buffer at a scan rate of 0.2 mV s^{-1} and an electrode rotation rate of 2400 rpm. E_{corr} was -510 ± 10 mV in borate buffer alone, -340 ± 10 mV in the presence of 0.75 mM $ArNO_2$, and -380 ± 10 mV in the presence of 5 mM CCl_4. Note that current densities in the presence of $ArNO_2$ are influenced by mass transport effects at this rotation (2400 rpm).

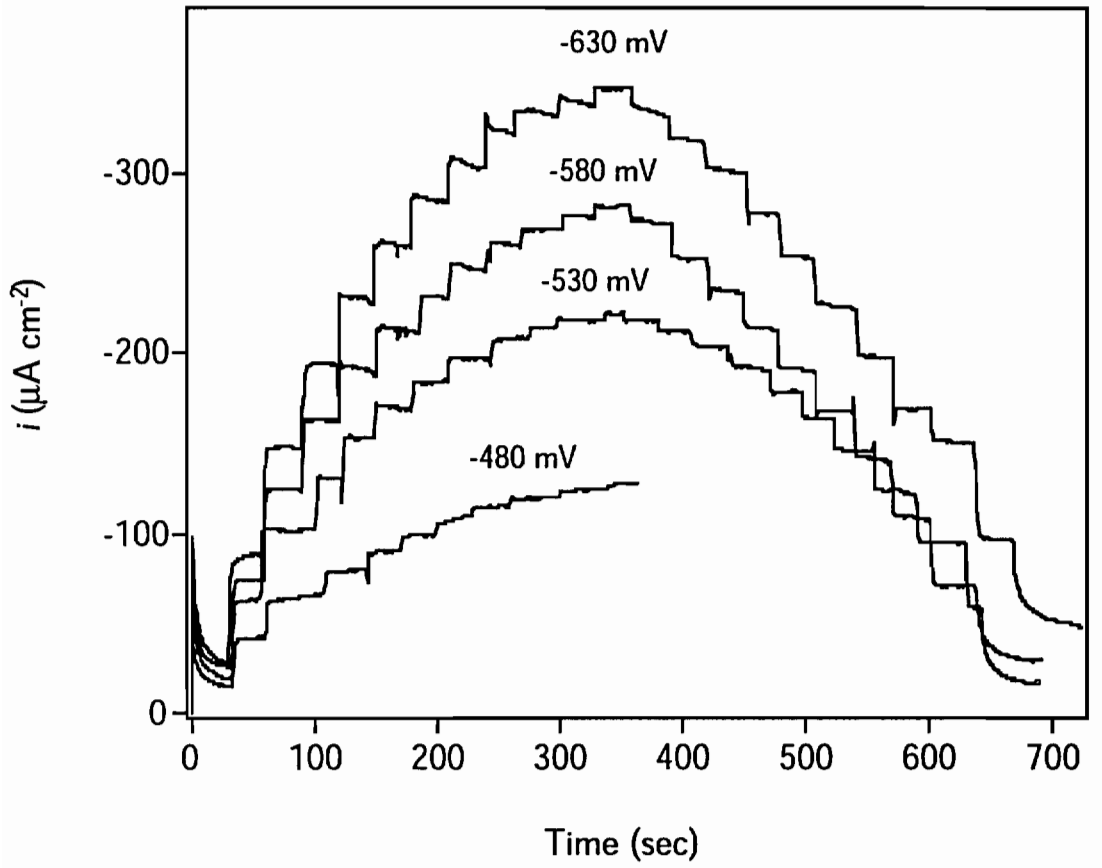

Figure 4.2 Time traces for constant potential reduction of $ArNO_2$ at an Fe^0 RDE with stepwise variation in rotation rate from 100 to 9400 rpm and back down to 100 rpm. Current densities at -630 mV for C_{NB} = 87 μM, -580 mV for C_{NB} = 83 μM, -530 mV for C_{NB} = 75 μM, and -480 mV for C_{NB} = 75 μM.

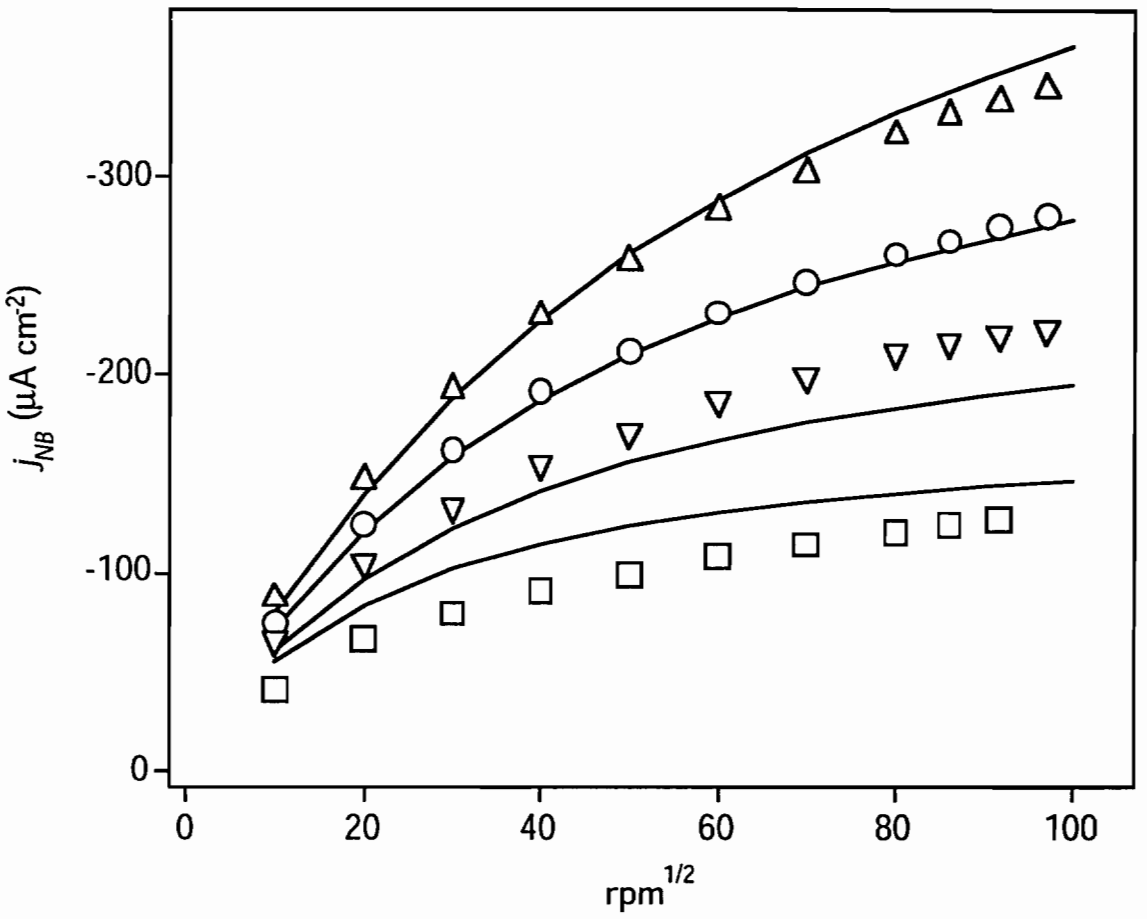

Figure 4.3 Effect of rotation rate and applied potential on $ArNO_2$ current densities at an Fe^0 RDE. Steady-state current densities at: -630 mV for C_{NB} = 87 μM (up triangles), -580 mV for C_{NB} = 83 μM (circles), -530 mV for C_{NB} = 75 μM (down triangles), and -480 mV for C_{NB} = 75 μM (squares). Solid curves represent the mixed control model (eq. 16) using the parameters in Table 4.1.

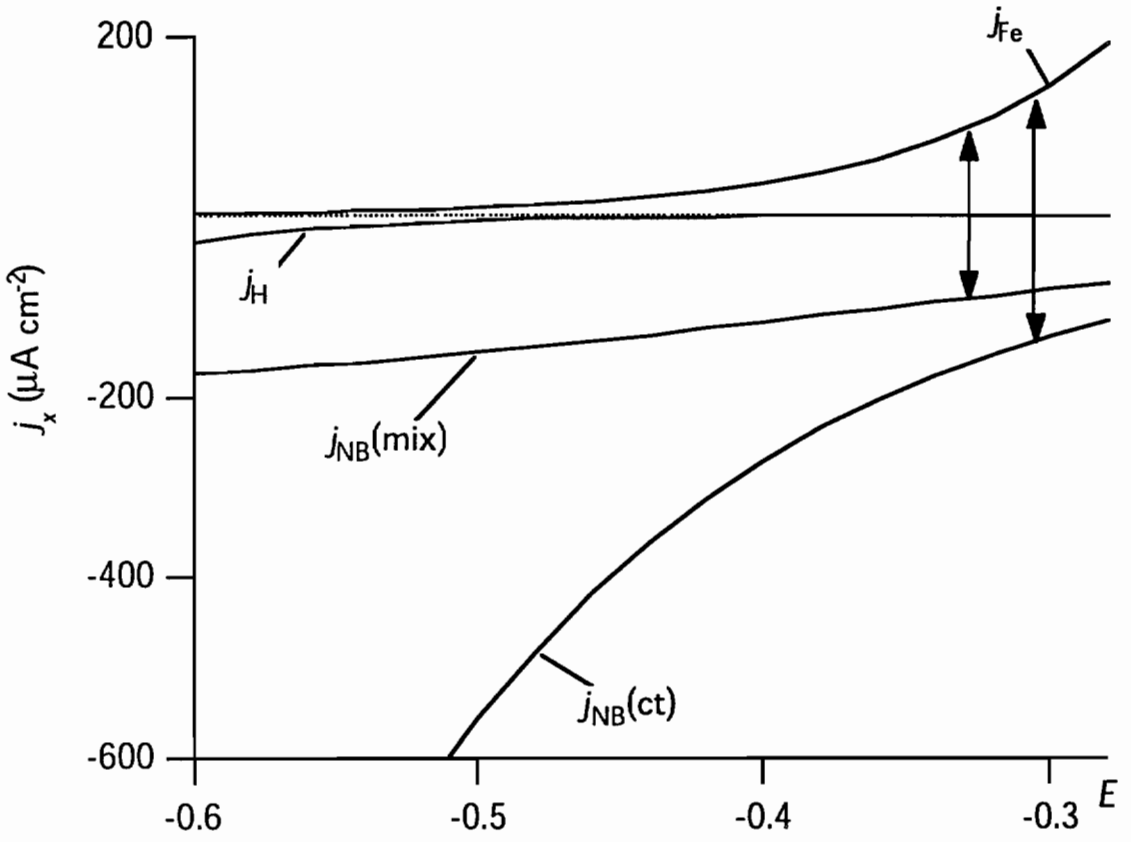

Figure 4.4 Parial current densities for the Fe^0-$ArNO_2$-H_2O system. Derived using the mixed-control model (eq. 16) and the kinetic parameters given in Table 4.1. Rotation rate is 100 rpm (δ = 40 μm) and C_{NB} = 200 μM. The arrows represent i_{corr}.

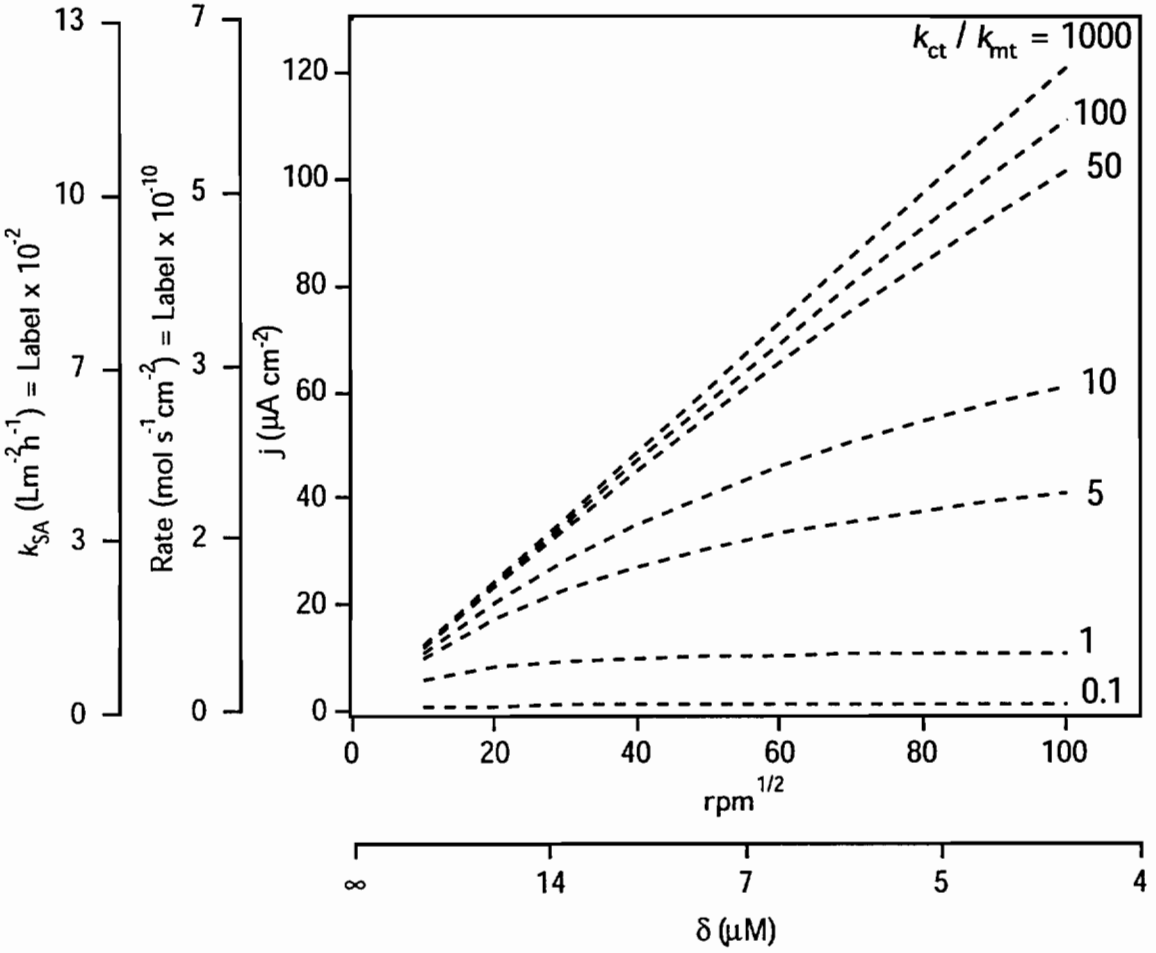

Figure 4.5 Influence of the first-order heterogeneous charge-transfer rate constant (k_{ct}) and the mass transport rate constant (k_{mt}) on observed reaction kinetics. Lines are derived from eq. 15 using n = 2, C = 50 μM, and D = 5 x 10^{-6} cm^2 s^{-1}. The k_{ct} / k_{mt} ratio is calculated for rpm$^{1/2}$ = 10, which corresponds to δ = 40 μM and k_{mt} = 10^{-3} cm s^{-1}.

CHAPTER 5

Correlation Analysis of Rate Constants for Dechlorination by Zero-Valent Iron[1]

5.1 Abstract

Dehalogenation is among the most important processes involved in contaminant fate, but despite all the work that has been done on the kinetics of dehalogenation, there are few linear free energy relationships (LFERs) that can be used to explain or predict rates of dehalogenation by environmental reductants. Previously, we summarized kinetic data for dehalogenation of chlorinated alkanes and alkenes by zero-valent iron (Fe^0), and showed that correlation analysis of these data with published two-electron reduction potentials did not give a simple relationship. In this study, we report successful LFERs based on estimated lowest unoccupied molecular orbital (LUMO) energies calculated from semi-empirical (AM1 and PM3) and ab initio methods (6-31G*), and one-electron reduction potentials. Solvation effects can be modeled with COSMO and incorporated into semi-empirical estimates of E_{LUMO}, but this did not improve the correlation with k. The best LFER ($\log k = -5.7 - 1.5\ E_{LUMO}$) explains 83% of the variability in surface-area normalized rate constants, k, with ab initio LUMO energies. The LFER is improved by correcting for statistical bias introduced by back transformation from log-linear regression models. New kinetic data for 6 compounds are compared with rate constants predicted using the unbiased LFER.

5.2 Introduction

Correlation analysis in the chemical sciences typically involves regression of substrate property or reactivity data (defined as the response variable) for a series of related

[1] Scherer, M.M., B.A. Balko, D.A., Gallagher, and P.G. Tratnyek. 1998. Correlation analysis of rate constatns for dechlorination by zero-valent iron. *Environmental Science & Technology*. In press.

compounds with one, or several, convenient descriptor variables. The resulting linear free energy relationship (LFER) can then be used to estimate values of reactivity for compounds that were not included in the original data set. The predictive power of LFERs makes them enormously important in regulatory decision-making regarding new chemicals in the environment (1). In addition, correlation analysis is also an important tool for data validation and mechanistic investigations.

In practice, the major impediment to LFER development for environmental applications is the lack of reliable data from which they can be derived. For example, most quantitative kinetic data for contaminant redox reactions is not derived from a well-defined kinetic model (2), making it difficult to compare rate constants among different studies. When reliable kinetic data are reported, there are often not enough compounds studied under equivalent conditions to provide adequate statistical power. Additional problems arise in finding values of each descriptor variable for each substrate included in the correlation. The lack of data for descriptor variables is particularly difficult in correlation analysis of kinetic data, because the descriptor variables for which data are most scarce are often those that are most fundamental (i.e., have the most unambiguous relationship to the process measured by the response variable k).

The lack of completely successful LFERs for dehalogenation kinetics is particularly notable because dehalogenation is one of the most important and widely studied of all contaminant degradation pathways. The abundance of dehalogenation studies is due, in part, to the variety of general reaction types available for cleaving carbon-halogen bonds. While the rates of these processes are often fast enough to affect the environmental fate of halogenated hydrocarbons, they tend to vary with substrate, and chemical and microbiological conditions. As a basis for remediation technologies, dehalogenation mediated by microorganisms has received a great deal of attention, and there is growing interest in several processes that produce dehalogenation under abiotic conditions, such as reactions involving cyanocobalamin or zero-valent iron (Fe^0). Recently, kinetic data on dechlorination by Fe^0 have become quite abundant (3), and they now make up one of the most extensive data sets available for pursuing correlation analysis of contaminant dehalogenation rates.

We have performed correlation analysis using this Fe^0 data set in order to (i) explore the reliability of the available data, (ii) develop LFERs for predicting dechlorination rates by Fe^0, and (iii) improve our understanding of the factors controlling reduction

kinetics by Fe^0 and dehalogenation kinetics in general. The goal was to develop a LFER that offers a statistically robust predictive tool and is consistent with the combination of statistical and mechanistic criteria that reflect the mixed purposes of environmental scientists and engineers (4). Satisfactory correlations were obtained with a variety of measures of electron affinity as the descriptor variable, and LFERs derived from the best correlations may be suitable for use as predictive models. The analysis also has implications regarding the reduction of solutes by Fe^0 and the degradation of chlorinated aliphatics by competing reduction pathways.

5.3 Methods

5.3.1 Training Set Data

The data set of surface-area normalized rate constants (k) reported by Johnson et al. (3) was used to derive the correlations described in this study. The scope of the data set is limited to chlorinated aliphatic compounds reacting with granular zero-valent iron, and does not include halogenated aromatic compounds, zero-valent metals other than Fe^0, bimetallic reductants, or non-aqueous systems. Other experimental variables, such as mixing efficiency, iron type, and adsorption to non-reactive sites (5, 6) are known to affect the rate of dehalogenation (3, 7), but quantitative corrections for these factors are not yet practical. Therefore, the original rate data, reported by Johnson et al. (3) were used for correlation analysis, and the effects of uncorrected experimental variables were evaluated statistically as possible sources of variance in dehalogenation rates.

Three types of descriptor variables were used for LFER development: (i) LUMO energies calculated by molecular modeling with semi-empirical and ab initio methods, (ii) thermodynamic estimates of one- and two-electron reduction potentials compiled from the literature (8-10), and (iii) diffusion coefficients estimated using the method of Hayduk and Minhas (11, 12). Additional descriptor variables (solubility, sediment-water partitioning coefficient, and vapor pressure) were investigated, but gave poor correlations ($r^2 < 0.5$).

Molecular descriptor variables were calculated using the CAChe WorkSystem software (Oxford Molecular Group Inc., Beaverton, OR). Energies of the LUMO were obtained with the semi-empirical method MOPAC (13, 14) and Mulliken II (15, 16) using version 3.9 of CAChe's Macintosh Project Leader interface (running on an IBM RS6000). For comparison, MOPAC was run using the AM1 and PM3 parameter sets (13, 14) for gas

phase calculations and the Conductor-like Screening Model (COSMO) for incorporating solvent effects (17). The minimum energy conformation for compounds with more than one plausible geometry was found by comparing heats of formation calculated with the PM3 parameter set. The calculated values of E_{LUMO} for all chlorinated methanes, ethanes, ethenes, and propanes are provided in Table 5.4.

5.3.2 Validation Set Data

New data for disappearance kinetics came from batch tests performed in a manner similar to methods described previously (18, 19) and rate constants published in the literature after November, 1995. The two chlorinated ethanes tested in this study were 1,1,1-trichloroethane (Aldrich, 99.5%, anhydrous) and 1,1-dichloroethane (Chem Service). Kinetic experiments were conducted with 10 g of 18-32 mesh (0.5 - 1.0 mm size fraction) iron turnings (Fluka, puriss. grade) in vials containing 12 mL of deionized water. The iron, used without treatment to clean or activate the metal surface, had a specific surface area of 0.019 $m^2\ g^{-1}$ (3). Mixing was achieved by rotation at room temperature (23 ±1 °C). Substrate disappearance kinetics were determined by periodic sampling of the aqueous phase of removed bottles and analysis by gas chromatography with direct aqueous injection and ECD detection (19). Volatilization losses were determined by running a series of control bottles with no iron metal.

5.4 Results and discussion

5.4.1 Definition of the Response Variable

For degradation of chlorinated aliphatic compounds by zero-valent metals, a surface area normalized, first-order kinetic model has proven to be practical and appropriate (3). Thus, the rate of disappearance for a compound P is described by:

$$\frac{d[P]}{dt} = -k\rho_a[P] \tag{1}$$

where k is the surface area normalized rate constant (L hr^{-1} m^{-2}) and ρ_a is the surface area concentration of Fe^0 (m^2 L^{-1} of solution). By averaging all values of k available as of November 1995, Johnson *et al.* (3) defined a set of representative rates constants ($\bar{k}$) for 13 chlorinated aliphatic compounds. The values of $\bar{k}$ were used in this study for exploratory correlation analysis, and are summarized in Table 5.1. The original data set

was used for calculating LFERs, and it can be found in the Supporting Information to Johnson et al. (3). New values of k, from this study and others, were used only for LFER validation.

5.4.2 Descriptor Variables from Thermodynamics

There are many descriptor variables that might correlate with k, including one- and two-electron reduction potentials, half-wave potentials, molecular orbital energies, and electron affinities. Correlations between four descriptor variables and $\bar{k}$ are summarized as a matrix of scatter plots in Figure 5.1. The descriptor variables include two-electron reduction potentials (E_2), one-electron reduction potentials (E_1), and lowest unoccupied molecular orbital energies (E_{LUMO}) calculated by semi-empirical methods with solvation (AM1/H_2O) and ab initio methods without solvation (CAChe's Mulliken and the 6-31G* basis set).

E_2 corresponds to the overall reduction potential for dehalogenation, from non-radical reactants to non-radical products by hydrogenolysis ($RX + H^+ + 2\ e^- \rightarrow RH + X^-$) or vicinal dehalogenation (e.g., 1,2-dihaloalkanes + 2 e^- → alkenes + 2 X^-). The E_2 values used here correspond to reduction by hydrogenolysis (as discussed in greater detail below). Since these half-reactions are not reversible, E_2 is not amenable to direct measurement. There are, however, several methods by which E_2 can be estimated (10, 20). For many years, the set of E_2 values estimated by Vogel *et al.* (10) was the only published set of descriptor data that included all chlorinated aliphatic compounds of environmental importance. Various researchers have attempted to use these data in correlation analysis of dechlorination kinetics (e.g., 21), including our preliminary effort at correlation analysis of k data for reaction with Fe^0 (3), but the results have never lead to the successful derivation of LFERs. The perspective provided by Figure 5.1 shows that E_2 is moderately correlated with $\bar{k}$, E_1, and E_{LUMO}. The E_2 for vinyl chloride (labeled 1 in Fig. 1) is the only value that appears to be an outlier in all three correlations. Presumably, the major reason that E_2 does not give robust LFERs for dechlorination kinetics is that the rate limiting step generally does not involve concerted transfer of two electrons, as implied by the use of E_2, but instead involves initial transfer of a single electron (22, 23).

E_1 is a more promising descriptor for dechlorination kinetics, in so far as it represents the potential of the rate-limiting initial electron transfer step. For hydrogenolysis of simple aliphatics, dechlorination is initiated by dissociative electron transfer (i.e., RX +

$e^- \rightarrow R\bullet + X^-$) not simple electron transfer ($RX + e^- \rightarrow RX^{-\bullet}$), so it is E_1 for the former half-reaction that is of greatest interest (22, 23). Again, these reactions are not reversible, so measured potentials are generally not available and estimation methods offer the only possibility of obtaining a complete and consistent set of data for use in correlation analysis. Estimates of E_1 for all of the chlorinated methanes, ethanes, and ethenes have now been published (8, 9) and these data are included in . The resulting correlations involving E_1 are sufficiently improved over those involving E_2 that we have chosen to present a LFER for k versus E_1 in the following section.

E_1 and E_2, however, are defined for specific reactions with particular products, which makes them inconvenient descriptors for compounds that can dechlorinate by more than one pathway. The dependence on reaction products applies to branching among hydrogenolysis pathways, as well as branching between hydrogenolysis and reductive elimination. The former is illustrated by the hydrogenolysis of 1,1,1,2-TeCA, which can yield 1,1,1-TCA or 1,1,2-TCA. In this case, correlations based on the assumption that reduction at the perhalogenated carbon is favored resulted in a better correlation coefficient (for both E_1 and E_2). A more difficult case involves hydrogenolysis of TCE, which can yield cis-1,2-DCE, trans-1,2-DCE, or 1,1-DCE. In principle, this complication can be accommodated with a descriptor for TCE disappearance that is the weighted sum of the reduction potentials for the three contributing reduction pathways. However, this refinement is not yet practical because we do not have estimates of the reduction potentials of TCE to cis-1,2-DCE or data on the branching ratios for formation of trans-1,2-DCE and 1,1-DCE. For the present, we have used the values of E_1 and E_2 that correspond to formation of trans-1,2-DCE because they give a slightly better correlation with $\bar{k}$ data for TCE.

A quantitative accounting of the effect of branching between hydrogenolysis and reductive elimination would require a more fundamental correction because the two pathways involve different mechanisms. Ideally, the correction should be applied before correlation analysis by extracting separate rate constants for each pathway, but there is not yet enough data to make these calculations. As an alternative, we have selected values of E_1 and E_2 for hydrogenolysis, so that the resulting correlations can be used to test for significant deviations that might be attributable to reductive elimination. The results in Figure 5.1 show that compounds susceptible to reductive elimination (those with vicinal halogen substituents, compounds labeled c,d,e,g,h,i,j) do not correlate differently than

those that can be reduced only by hydrogenolysis (compound labels are listed in Table 5.1). It is not known how experimental conditions effect branching ratios, however, so the effect of branching ratios on descriptor variables like E_1 and E_2 is still a potential source of difficulty in future applications of LFERs for reduction of halogenated aliphatic compounds.

5.4.3 Descriptor Variables from Molecular Modeling

Molecular descriptors calculated by computer have the advantage that large, consistent sets of calculations can be performed with commercially available software, and they include some quantum-chemical descriptors that are not directly accessible by experimentation. Of the quantum-chemical descriptors that have been used in LFER analysis (24), E_{LUMO} is the most easily justified for reduction of chlorinated aliphatics. This is because the LUMO is the frontier molecular orbital into which electron transfer takes place, and the energy of this orbital helps determine the driving force for reaction (25). An additional advantage of molecular orbital energies as descriptor variables in correlation analysis is that there is only one value per reactant, so the complications arising from branching pathways may be circumvented.

We have correlated $\bar{k}$ and E_{LUMO}'s calculated by a variety of methods and found that all combinations exhibit a high degree of covariance. Semi-empirical calculations with AM1 and PM3 parameters are highly correlated ($r^2 = 0.98$) and result in similar correlations (not shown) with $\bar{k}$ ($r^2 = 0.81$ and 0.76, respectively). The incorporation of solvation effects and the use of ab initio methods significantly improved the correlation with $\bar{k}$. Figure 5.1 includes two of the best correlations: $\bar{k}$ versus E_{LUMO} from MOPAC with AM1 parameters and solvation by COSMO (AM1/H_2O), and $\bar{k}$ versus E_{LUMO} by ab initio methods with 6-31G* parameters but no solvation. The scatter plots for both these combinations reveal strong linear correlations, despite important differences in the way the two sets of E_{LUMO}'s were calculated.

The effect of solvation on E_{LUMO}'s calculated from the semi empirical method is illustrated in Figure 5.2. Regression on E_{LUMO}'s calculated with and without solvation gives slopes slightly less than one and slightly negative intercepts for both AM1 and PM3 parameter sets. Thus, the solvation correction results in values of E_{LUMO} that are systematically more negative and span a narrower range. These effects do not favor an improved correlation between E_{LUMO} and $\bar{k}$, and the lack of scatter about the regression

lines in Figure 5.2 suggest that there is little compound-specific variation that is accounted for by the solvation correction. Although the correlation between log k and E_{LUMO} does improve slightly when the solvation-corrected values are used (r^2 increases from 0.81 to 0.85 for AM1, and 0.76 to 0.79 for PM3), the regression lines are not statistically different. Therefore, incorporating solvation *does not* make E_{LUMO} a significantly improved descriptor of dehalogenation rates for simple chlorinated aliphatic compounds. This result is consistent with commonly proposed mechanisms for dechlorination (e.g., 8, 19), which do not involve charged species.

In the absence of strong solvation effects, the greater accuracy of ab initio methods offers the best opportunity for improving the correlation between $\bar{k}$ and E_{LUMO}. The results can be seen in Figure 5.1, which includes the best correlations we obtained to E_{LUMO}'s from semi-empirical methods (MOPAC with AM1 parameters and COSMO) and ab initio methods (Mulliken with 6-31G* basis set). The distribution of data in the two scatter plots are very similar, but there is slightly less scatter with the ab initio descriptor (r^2 = 0.85 for AM1/H_2O versus 0.86 for 6-31G*). Based on these statistical considerations, and considering the increased availability of ab initio methods in commercially available molecular modeling software, we conclude that ab initio methods (despite large computational requirements), offer an improved way to calculate E_{LUMO}'s for use as the descriptor variable in LFERs for dehalogenation kinetics.

5.4.4 Regression and Regression Diagnostics

Considering the substantial uncertainties in $\bar{k}$, it is difficult to envision further refinements in descriptor variables that would improve on the correlations in Figure 5.3. Instead, the next step is to derive LFERs from the best correlations and explore the application of these as tools for interpreting dehalogenation kinetics by Fe^0. Raw k data, rather than $\bar{k}$, have been used to obtain LFERs that are unbiased due to the large variability in (i) number of data available for each compound (N = 1 to 12), and (ii) magnitude of k for each compound. The scatter plots for k versus two descriptors, E_1 and the ab initio values of E_{LUMO}, are shown in Figure 5.3.

To obtain LFERs from the two sets of data in Figure 5.3, we used a mechanistically-based semi-logarithmic model relating kinetic data to a single descriptor variable (4)

$$\log k = \log b_o + bx + \varepsilon \quad (2)$$

where b_0 and b are the adjustable parameters, x is the descriptor variable, and ε represents variability in k not explained by x, i.e., indeterminant error. The adjustable parameters, b and b_0, were estimated by least squares regression on all of the original data for k. The results are summarized in Table 5.2 and the regression lines based on eq. 2 are plotted as solid lines in Figure 5.3. A correlation based on E_{LUMO}'s from MOPAC with PM3 parameters and COSMO was presented previously *(26)*.

The validity of the model presented in eq. 2 can be assessed by analysis of residuals based on the log-transformed response variable (log k). Residual analysis provides a means for testing that ε is randomly and normally distributed and that no significant descriptor variable has been omitted from the model (27). To do this for the LFERs represented in Figure 5.3, we calculated the residuals (e_i) of the log-transformed response variable (represented by y_i) from

$$e_i = y_i - (\log b_o + bx) \quad (3)$$

and plotted the standardized residual (e_i/s) versus the descriptor variable (x). The results are shown in Figure 5.4 for the two descriptors variables E_{LUMO} and E_1. Inspection of the plots reveals no systematic trends in the residuals indicative of errors in the model (eq. 2) or anomalous values (outside two standard deviations) due to individual outliers.

Although the lack of systematic trends in the residuals plots suggests that the errors are randomly distributed, it does not demonstrate that the distribution is normal. This, however, can be seen in the histogram of residuals from the E_{LUMO} correlation, shown in Figure 5.5, which reveals the distinctive bell shaped pattern associated with a normal distribution. The sampling increment used to generate Figure 5.5 was selected to give five or more occurrences in most intervals, resulting in a bin width of 0.35 and a total of 7 bins. Application of the Lillefors (28, 29) and Kolmogorov-Smirnov (30) tests for normality (at the 95% confidence level) confirm that the distribution shown in Figure 5.5 is normal. Equivalent results (not shown) were obtained for the residuals from the LFER based on E_1.

Residuals plots can also be useful in assessing whether additional descriptor variables should be included in the model. As discussed earlier, other experimental

variables, such as mixing efficiency and iron type, are known to effect k (3, 7). Although most of these variables do not lend themselves to making quantitative corrections in k before correlation analysis, we can test for their effect after correlation analysis by analyzing the relationship of the residuals to other descriptors (27). For example, the role of diffusion can be assessed by plotting the standardized residuals versus the diffusion coefficient, as shown in Figure 5.4. The lack of correlation between these parameters suggests that a multiple regression model that included diffusion coefficients would not improve on the LFERs in Figure 5.3. The lack of correlation with diffusion coefficients is consistent with electrochemical evidence showing that the mass transport has little influence on the reduction rate of carbon tetrachloride by Fe^0 (31).

5.4.5 Prediction and Validation

In order to use the derived LFERs in a predictive mode, it is important to consider that eq. 2 is derived by linear transformation of an exponential model represented by eq. 4.

$$k = b_o 10^{bx} \tag{4}$$

Because the error term, ε, is not included in this equation, using it to predict k will give biased results (32, 33). To obtain unbiased estimates of k, each term, including the error term, should be included in the exponential model, as shown in eq. 5.

$$k = b_o 10^{bx} 10^{\varepsilon} \tag{5}$$

To use this model, it is necessary to estimate the expected value of 10^{ε}. For ε that is normally distributed (recall Figure 5.5), it has been shown (34) that 10^{ε} will be log-normally distributed with an expected value of

$$\mathrm{E}\left[10^{\varepsilon}\right] = 10^{\left(\mu_\varepsilon + \frac{\sigma_\varepsilon^2}{2}\right)} \tag{6}$$

where μ_ε is the mean error and σ_ε^2 is the mean variance. To evaluate eq. 6 for a normal distribution, an appropriate procedure (35) is to assume that $\mu_\varepsilon = 0$ and σ_ε^2 can be estimated from

$$\sigma_{\varepsilon}^{2} = \frac{\sum_{i=1}^{N} e_i^2}{N-2} \tag{7}$$

where e_i^2 is the sum of squared residuals from regression. Combining eqs. 6 and 7 gives the general form of the correction factor (C.F.) necessary to use eq. 5.

$$10^{\varepsilon} = 10^{\frac{\frac{1}{2}\sum_{i=1}^{N} e_i^2}{N-2}} \tag{8}$$

The values of 10^{ε} given in Table 5.2 indicate that use of eq. 4 instead of eq. 5 to estimate k gives a 37% bias with E_{LUMO} and a 43% bias with E_1. Surprisingly, we have not seen this correction applied in the environmental literature on LFERs involving kinetics, although it has been discussed in other contexts, such as in the estimation of river loads from discharge data (36) and metal toxicity from water hardness (37). A survey of LFERs for the latter (37), showed that the bias ranged from 2 to 57%.

The model represented by eq. 5, together with the fitted parameters for each LFER (Table 5.2), can be used to calculate expected values of the rate constant, $\hat{k}$, for any chlorinated aliphatic compound. The results of these calculations are summarized in the Tables 5.4 and 5.5 for all chlorinated methanes, ethanes, and ethenes, as well as selected chlorinated propanes (those with up to three chlorines). To test these predictions, and thereby validate our predictive model, new kinetic data were measured for two chlorinated aliphatics with an unbuffered batch system containing granular Fe^0. The compounds studied were chosen to provide more data on the less reactive (i.e., less chlorinated) members of each family of congeners, because the majority of previously reported rates were for compounds that displayed fast kinetics (i.e., the more highly chlorinated compounds). Table 5.3 summarizes our two new values of k along with four recently reported literature values for TCE, VC, and 111TCA (note that 111TCA was also part of the training set), and the corresponding values of $\hat{k}$. Four of the new data conform to the same general trend in reactivity predicted by the LFERs, with e_i that are of the same magnitude as the residuals for the original training set data. The new values for TCE (38) and 111TCA (39), however, show markedly faster reaction rates than those predicted by the LFERs. The 111TCA rate constant may be anomalously high because of the high

concentrations of NaCl (0.1 M) used in the experiments. The presence of chloride at concentrations up to 0.1 mM have been shown to increase the rate of carbon tetrachloride reduction by four-fold, presumably by destabilizing the oxide film (40).

5.4.6 Insights from LFERs

In order to obtain a better perspective on how molecular structure is related to the kinetics of dechlorination by Fe^0, the values of $\hat{k}$ estimated from LFERs derived in this study are summarized graphically in Figure 5.6. As expected (3), rates decrease systematically with the number of chlorines on the most halogenated carbon(s) within each family of congeners. However, the figure also reveals remarkably little offset between each congener family. As a result, most monohalogenated aliphatics have $k \approx 10^{-5}$ L m^{-2} hr^{-1}, dihalogenated aliphatics have $k \approx 10^{-4}$ L m^{-2} hr^{-1}, trihalogenated aliphatics have $k \approx 10^{-3}$ L m^{-2} hr^{-1}, etc. Superimposed on this general trend are two other revealing patterns: (i) perhalogenation of one or more carbons apparently favors increased reactivity, and (ii) dechlorination rates for the ethenes seem to be slightly less sensitive than the alkanes to degree of chlorination.

The increase in k associated with perhalogenation of alkanes may be due to the differences in the stability of the intermediates that result from the initial electron transfer ($3^\circ > 2^\circ > 1^\circ$, etc.). The comparative insensitivity of ethenes to the effect of chlorine substituents may reflect the effect of unsaturation. The latter might be due to differences in bond strength ($sp^2 > sp^3$); however, then we would expect $\hat{k}$ to be less for all alkenes relative to the corresponding alkanes, which is not the case. An alternative explanation can be postulated by analogy to an analysis of polarographic reduction potentials by Fukui et al. (41). They concluded that electron transfer to halogenated aliphatic compounds occurs into the lowest unoccupied σ level (presumably antibonding) because the wide variation in observed reduction potentials is similar to the wide variation in the calculated energies of these orbitals. In contrast, they found that the lowest energy π levels are almost identical for the chlorinated ethenes. Thus, the comparative insensitivity of $\hat{k}$ to degree of chlorination on ethenes (seen in Figure 5.6) may reflect a greater importance of π orbitals in determining the rate of reduction of chlorinated alkenes by Fe^0. Other recent studies have presented arguments for (42, 43) and against (44) the involvement of π orbitals in electron transfer to unsaturated halogenated aliphatics.

Two final examples of useful insights that can be derived from this correlation

analysis arise from comparisons between the two sets of $\hat{k}$ data in Figure 5.6. First, note that $\hat{k}$ for HCA and PCA are notably greater when calculated from E_1 than when calculated from E_{LUMO}. Inspection of Figures 5.1 and 5.3 shows that HCA only appears to be an outlier in plots that involve E_1. (PCA is not included in either figure because no measured values of k have been reported.) A similar result was obtained by Perlinger (21), who found that PCA and HCA behaved as outliers among chlorinated and brominated alkanes in a correlation between E_1 (from Curtis) and E_{LUMO} (calculated independently of the values reported here). Second, Figure 5.6 reveals a more systematic deviation for mono- and di-chlorinated methanes and ethanes in that $\hat{k}$ tends to be higher when estimated from E_1 than when estimated from E_{LUMO}. It is tempting to interpret this difference as evidence for or against dissociative electron transfer, because E_1's should reflect the energy of C-X bond breaking (22, 23) whereas E_{LUMO}'s do not (and bond strength varies with degree of halogenation). Unfortunately, the available measured data (including the new values of k reported in Table 5.3) are not yet adequate to resolve which LFER is more accurate for the least halogenated alkanes. This issue will likely attract further investigation due to the desirability of complete dechlorination in remediation applications of Fe^0.

5.5 Acknowledgments

The work was supported by the University Consortium Solvents-In-Groundwater Research Program, the National Science Foundation through Award BCS-9212059, and the Petroleum Research Fund through award 29995-AC5.

5.6 List of Symbols

ρ_a	surface area concentration ($m^2\ L^{-1}$)
[P]	molar concentration of substrate (mol L^{-1})
k	surface-area normalized reaction rate constant (L $hr^{-1}\ m^{-2}$)
$\bar{k}$	averaged representative surface-area normalized rate constant (L $hr^{-1}\ m^{-2}$)
$\hat{k}$	predicted surface-area normalized rate constant (L $hr^{-1}\ m^{-2}$)
E_{LUMO}	energy of the lowest unoccupied molecular orbital (eV)
E_1	one-electron reduction potential (volt)
E_2	two-electron reduction potential (volt)
r^2	correlation coefficient

b, b_o	adjustable parameters from linear least-squares regression
ε	model error
e_i	regression residual (k_i - $\hat{k}$)
s	standard deviation
μ_ε	mean error
σ_ε^2	mean variance
n	number of data points

5.7 Literature Cited

(1) Donaldson, W. T. The role of property-reactivity relationships in meeting the EPA's needs for environmental rate constants. *Environ. Toxicol. Chem.*, 1992, *11*, 887-891.

(2) Hoigné, J. Formulation and calibration of environmental reaction kinetics: Oxidations by aqueous photooxidants as an example. In *Aquatic Chemical Kinetics: Reaction Rates of Processes in Natural Waters*; Stumm, W., Ed; Wiley-Interscience: New York, 1990; pp. 43-70.

(3) Johnson, T. L.; Scherer, M. M.; Tratnyek, P. G. Kinetics of halogenated organic compound degradation by iron metal. *Environ. Sci. Technol.*, 1996, *30*, 2634-2640.

(4) Tratnyek, P. G. Correlation analysis of the environmental reactivity of organic substances. In *Perspectives in Environmental Chemistry*; Macalady, D. L., Ed; Oxford: New York, 1998; pp. 167-194.

(5) Burris, D. R.; Campbell, T. J.; Manoranjan, V. S. Sorption of trichloroethylene and tetrachloroethylene in a batch reactive metallic iron-water system. *Environ. Sci. Technol.*, 1995, *29*, 2850-2855.

(6) Campbell, T. J.; Burris, D. R.; Roberts, A. L.; Wells, J. R. Trichloroethylene and tetrachloroethylene reduction in a metallic iron-water-vapor batch system. *Environ. Toxicol. Chem.*, 1997, *16*, 625-630.

(7) Tratnyek, P. G.; Johnson, T. L.; Scherer, M. M.; Eykholt, G. R. Remediating groundwater with zero-valent metals: Kinetic considerations in barrier design. *Ground Water Monit. Rem.*, 1997, 108-114.

(8) Roberts, A. L.; Totten, L. A.; Arnold, W. A.; Burris, D. R.; Campbell, T. J. Reductive elimination of chlorinated ethylenes by zero-valent metals. *Environ. Sci. Technol.,* 1996, *30*, 2654-2659.

(9) Curtis, G. P. *Reductive Dehalogenation of Hexachloroethane and Carbon Tetrachloride by Aquifer Sand and Humic Acid.* Ph.D. Thesis, Stanford University, 1991.

(10) Vogel, T. M.; Criddle, C. S.; McCarty, P. L. Transformations of halogenated aliphatic compounds. *Environ. Sci. Technol.,* 1987, *21*, 722-736.

(11) Reid, R. C.; Prausnitz, J. M.; Poling, B. E. *The Properties of Gases and Liquids,* Fourth Edition; McGraw Hill: New York, 1987.

(12) Hayduk, W.; Minhas, B. S. Correlations for prediction of molecular diffusivities in liquids. *Can. J. Chem. Eng.,* 1982, *60*, 295-299.

(13) Stewart, J. J. P. Optimization of parameters for semi-empirical methods. I. Method. *J. Comput. Chem.* 1989, *10*, 209.

(14) Stewart, J. J. P. Optimization of parameters for semiempirical methods. II. Applications. *J. Comput. Chem.,* 1989, *10*, 221.

(15) Hariharan, P. C.; Pople, J. A. *Chem. Phys. Lett.,* 1972, *66*, 217.

(16) Francl, M. M.; Pietro, W. J.; Hehre, W. J.; Binkely, J. S.; DeFrees, D. J.; Pople, J. A. Self-consistent molecular orbitals methods. XXIII. A polarization-type basis set for second-row elements. *J. Chem. Phys.,* 1982, *77*, 3654-3665.

(17) Klamt, A.; Schüürmann, G. COSMO: A new approach to dielectric screening in solvents with explicit expressions for the screening energy and its gradient. *J. Chem. Soc. Perkin Trans., 2* 1993, 799-803.

(18) Scherer, M. M.; Tratnyek, P. G. Dechlorination of carbon tetrachloride by iron metal: Effect of reactant concentrations*; 209th National Meeting,* Anaheim, CA, American Chemical Society, 1995; Vol. 35, No. 1, pp. 805-806.

(19) Matheson, L. J.; Tratnyek, P. G. Reductive dehalogenation of chlorinated methanes by iron metal. *Environ. Sci. Technol.,* 1994, *28*, 2045-2053.

(20) Dolfing, J.; Janssen, D. B. Estimation of Gibbs free energies of formation of chlorinated aliphatic compounds. *Biodegradation,* 1994, *5*, 21-28.

(21) Perlinger, J. A. *Reduction of Polyhalogenated Alkanes by Electron Transfer Mediators in Aqueous Solution.* Ph.D. Thesis, Swiss Federal Institute of Technology Zürich, 1994.

(22) Savéant, J.-M. Electron transfer, bond breaking, and bond formation. *Acc. Chem. Res.,* 1993, *26*, 455-461.

(23) Savéant, J.-M. Single electron transfer and nucleophilic substitution. *Adv. Phys. Org. Chem.,* 1990, *26*, 1-130.

(24) Karelson, M.; Lobanov, V. S.; Katritzky, A. R. Quantum-chemical descriptors in QSAR/QSPR studies. *Chem. Rev.,* 1996, *96*, 1027-1043.

(25) Fleming, I. *Frontier Orbitals and Organic Chemical Reactions*; Wiley: London, 1976, pp. 249.

(26) Tratnyek, P. G.; Scherer, M. M. Kinetic controls on the performance of remediation technologies based on zero-valent iron*; Proceedings of the 1998 National Environmental Engineering Conference: Water Resources in the Urban Environment,* Chicago, IL, American Society of Civil Engineers, 1998; pp. 110-115.

(27) Draper, N. R.; Smith, H. *Applied Regression Analysis;* 2nd ed.; Wiley: New York, 1981, pp. 709.

(28) Lilliefors, H. W. On the Kolmogorov-Smirnov test for normality with mean and variance unknown. *Amer. Statistical Assoc. J.,* 1967, *62*, 399-402.

(29) Conover, W. J. *Practical Nonparametric Statistics*; John Wiley & Sons: New York, 1971, pp. 302-306.

(30) Massey, F. J. J. The Kolmogorov-Smirnov test for goodness of fit. *Amer. Statistical Assoc. J.,* 1951, *46*, 69-78.

(31) Scherer, M. M.; Westall, J. C.; Ziomek-Moroz, M.; Tratnyek, P. G. Kinetics of carbon tetrachloride reduction at an oxide-free iron electrode. *Environ. Sci. Technol.,*

1997, *31*, 2385-2391.

(32) Miller, D. M. Reducing transformation bias in curve fitting. *The American Statistician,* 1984, *38*, 124-126.

(33) Newman, M. C. Regression analysis of log-transformed data: Statistical bias and its correction. *Environ. Toxicol. Chem.,* 1993, *12*, 1129-1133.

(34) Mood, A. M.; Graybill, T. A.; Boes, D. C. *Introduction to the Theory of Statistics,* 3rd Edition; McGraw-Hill: New York, 1974.

(35) Beauchamp, J. J.; Olson, J. S. Corrections for bias in regression estimates after logarithmic transformation. *Ecology,* 1973, *54*, 1403-1407.

(36) Ferguson, R. I. River loads underestimated by rating curves. *Wat. Res. Res.,* 1986, *22*, 74-76.

(37) Newman, M. C. A statistical bias in the derivation of hardness-dependent metals criteria. *Environ. Toxicol. Chem.,* 1991, *10*, 1295-1297.

(38) Gotpagar, J.; Gruike, E.; Tsang, T.; Bhattacharyya, D. Reductive dehalogenation of trichloroethylene using zero-valent iron. *Environmental Progress,* 1997, *16*, 137-142.

(39) Fennelly, J. P.; Roberts, A. L. Reaction of 1,1,1-trichloroethane with zero-valent metals and bimetallic reductants. *Environ. Sci. Technol.,* In press.

(40) Johnson, T. L.; Fish, W.; Gorby, Y. A.; Tratnyek, P. G. Degradation of carbon tetrachloride by iron metal: Complexation effects on the oxide surface. *J. Contam. Hydrol.,* 1998, *29*, 377-396.

(41) Fukui, K.; Morokuma, K.; Kato, H.; Yonezawa, T. The polarographic reduction and electronic structures of organic halides. *Bull. Chem. Soc. Japan,* 1963, *36*, 217-222.

(42) Yoshimura, R.; Tada, T. Ab initio MO studies on dissociative electron attachment of vinyl chloride. The simplest chlorine-containing hydrocarbon having a C=C π system. *Chemical Physics Letters,* 1994, *222*, 626-632.

(43) Reynolds, J. L.; Doshi, D.; Shechter, H. Relative reactivities and mechanistic aspects of the reactions of organic halides with alkali metals in alcohol environments. *J. Am.*

Chem. Soc., 1987, *109*, 8032-8041.

(44) Bunnett, J. F. Radical-chain, electron-transfer dehalogenation reactions. *Acc. Chem. Res.,* 1992, *25*, 2-9.

(45) Orth, S., W.; Gillham, R. W. Dechlorination of trichlorethene in aqueous solution using Fe(0). *Environ. Sci. Technol.,* 1996, *30*, 66-71.

(46) Deng, B.; Campbell, T. J.; Burris, D. R. Kinetics of vinyl chloride reduction by metallic iron in zero-headspace systems; *213th National Meeting,* San Francisco, CA, American Chemical Society, 1997; Vol. 37, No. 1, pp. 81-83.

Table 5.1. Data for Training Set Compounds

Chlorinated Aliphatic	Abbreviation	Label	$\bar{k}$ [1] ($L\ m^{-2}\ hr^{-1}$)	n	E_{LUMO} [2] (eV)	$\hat{k}$ ($L\ m^{-2}\ hr^{-1}$)	% Dev. $e_i/\hat{k}$	E_1 (volt)	$\hat{k}$ ($L\ m^{-2}\ hr^{-1}$)	% Dev. $e_i/\hat{k}$
Tetrachloromethane	PCM	a	$(1.2 \pm 1.5) \times 10^{-1}$	11	-3.054	8.9×10^{-2}	36	0.13	5.0×10^{-2}	139
Trichloromethane	TCM	b	$(9.2 \pm 7.3) \times 10^{-4}$	3	-2.277	6.2×10^{-3}	-85	-0.23	4.9×10^{-3}	-81
Hexachloroethane	HCA	c	$(3.1 \pm 3.3) \times 10^{-2}$	2	-2.555	1.6×10^{-2}	94	0.33	1.8×10^{-1}	-83
1,1,1,2-Tetrachloroethane	1112TeCA	d	1.4×10^{-2}	1	-2.390	9.1×10^{-3}	54	-0.22	5.2×10^{-3}	169
1,1,2,2-Tetrachloroethane	1122TeCA	e	1.3×10^{-2}	1	-1.982	1.8×10^{-3}	621	-0.34	2.4×10^{-3}	442
1,1,1-Trichloroethane	111TCA	f	1.1×10^{-2}	1	-2.160	4.1×10^{-3}	167	-0.23	4.9×10^{-3}	125
Tetrachloroethene	PCE	g	$(2.1 \pm 2.7) \times 10^{-3}$	4	-1.689	8.2×10^{-4}	156	-0.36	2.1×10^{-3}	0
Trichloroethene	TCE	h	$(3.9 \pm 3.6) \times 10^{-4}$	12	-1.435	3.4×10^{-4}	14	-0.62	3.9×10^{-4}	0
c-1,2-Dichloroethene	c12DCE	i	$(4.1 \pm 1.7) \times 10^{-5}$	3	-1.200	1.5×10^{-4}	-73	-0.89	6.8×10^{-5}	-40
t-1,2-Dichloroethene	t12DCE	j	$(1.2 \pm 0.4) \times 10^{-4}$	4	-1.200	1.5×10^{-4}	-22	-0.85	8.9×10^{-5}	36
1,1-Dichloroethene	11DCE	k	$(6.4 \pm 5.5) \times 10^{-5}$	3	-1.140	1.2×10^{-4}	-49	-0.72	2.1×10^{-4}	-69
Vinyl Chloride	VC	l	$(5.0 \pm 1.5) \times 10^{-5}$	3	-0.761	3.4×10^{-4}	47	-0.95	4.6×10^{-5}	8

[1] Arithmetic averages ± one standard deviation from kinetic data previously compiled in Refs. (3, 7).

[2] From ab initio calculations with the 6-31G* basis set.

Table 5.2 Parameter Estimates and Statistics on Linear Regression[a]

Descriptor	log b_o	b	N	r^2	s^b	Error, ε	C.F. = 10^{ε}
E_{LUMO}	-5.74 ± 0.20	-1.49 ±0.10	48	0.832	0.52	0.137	1.37
E_1	-1.82 ± 0.11	2.81 ± 0.20	48	0.810	0.56	0.155	1.43

[a] Analysis of variance (ANOVA tables) are provided in Tables 5.6 and 5.7.
[b] standard error of the estimate

Table 5.3 New Data for Validation Set Compounds

Chlorinated Aliphatic	Abbreviation	Measured k (L m^{-2} hr^{-1})	Ref.	E_{LUMO} (eV)	$\hat{k}$ (L m^{-2} hr^{-1})	% Dev. $e_i/\hat{k}$	E_1 (volt)	$\hat{k}$ (L m^{-2} hr^{-1})	% Dev. $e_i/\hat{k}$
1,1-Dichloroethane	11DCA	[a]1.5 x 10^{-3}	*b*	-1.267	1.9 x 10^{-4}	689	-0.40	1.6 x 10^{-3}	-6
1,1,1-Trichloroethane	111TCA	2.2 x 10^{-3}	*b*	-2.160	4.1 x 10^{-3}	-46	-0.23	4.9 x 10^{-3}	-55
1,1,1-Trichloroethane	111TCA	4.6 x 10^{-1}	(39)	-2.160	4.1 x 10^{-3}	11,310	-0.23	4.9 x 10^{-3}	9290
Trichloroethene	TCE	[c]3.2 x 10^{-2}	(38)	-1.435	3.4 x 10^{-4}	9,310	-0.62	3.9 x 10^{-4}	8100
Trichloroethene	TCE	1.0 x 10^{-3}	(45)	-1.435	3.4 x 10^{-4}	194	-0.62	3.9 x 10^{-4}	156
Vinyl Chloride	VC	7.3 x 10^{-6}	(46)	-0.761	3.4 x 10^{-5}	-78	-0.95	4.6 x 10^{-5}	-84

[a]average of two experiments. [b]measured in this study. [c]metal surface area/volume of solution = 500 m^{-1}.

Table 5.4 Summary of Molecular-Based Variables for Chlorinated Aliphatic Compounds

Chlorinated Aliphatic	Abbr.	E_{LUMO} AM1	E_{LUMO} AM1 with COSMO	E_{LUMO} PM3	E_{LUMO} PM3 with COSMO	E_{LUMO} 6-31G*	D $cm^2\ s^{-1}$	$\hat{k}^a$ $L\ m^{-2}\ h^{-1}$
Tetrachloromethane	PCM	-1.117	-1.176	-0.629	-0.671	-3.054	9.9×10^{-6}	8.9×10^{-2}
Trichloromethane	TCM	-0.303	-0.380	-0.118	-0.205	-2.277	1.1×10^{-5}	6.2×10^{-3}
Dichloromethane	DCM	0.594	0.505	0.521	0.370	-1.367	1.2×10^{-5}	2.7×10^{-4}
Chloromethane	CM	1.597	1.435	1.331	1.030	-0.256	1.5×10^{-5}	6.0×10^{-6}
Hexachloroethane	HCA	-0.967	-1.021	-0.564	-0.605	-2.555	6.7×10^{-6}	1.6×10^{-2}
Pentachloroethane	PCA	-0.681	-0.760	-0.373	-0.434	-2.476	7.4×10^{-6}	1.2×10^{-2}
1,1,1,2-Tetrachloroethane	1112TeCA	-0.486	-0.613	-0.233	-0.347	-2.390	8.3×10^{-6}	9.1×10^{-3}
1,1,2,2-Tetrachloroethane	1122TeCA	-0.230	-0.283	-0.096	-0.176	-1.982	8.3×10^{-6}	1.8×10^{-3}
1,1,1-Trichloroethane	111TCA	-0.265	-0.495	-0.071	-0.284	-2.160	9.3×10^{-6}	4.1×10^{-3}
1,1,2-Trichloroethane	112TCA	0.170	0.088	0.182	0.068	-1.711	9.3×10^{-6}	8.3×10^{-4}
1,1-Dichloroethane	11DCA	0.582	0.356	0.526	0.262	-1.267	1.1×10^{-5}	1.9×10^{-4}
1,2-Dichloroethane	12DCA	0.686	0.576	0.537	0.348	-1.183	1.1×10^{-5}	1.4×10^{-4}

Table 5.4 Continued. Summary of Molecular-Based Variables for Chlorinated Aliphatic Compounds

Chlorinated Aliphatic	Abbr.	E_{LUMO} AM1	E_{LUMO} AM1 with COSMO	E_{LUMO} PM3	E_{LUMO} PM3 with COSMO	E_{LUMO} 6-31G*	D $cm^2\ s^{-1}$	$\hat{k}^a$ $L\ m^{-2}\ h^{-1}$
Chloroethane	CA	1.499	1.244	1.237	0.815	-0.210	1.2×10^{-5}	5.1×10^{-6}
Tetrachloroethene	PCE	-0.437	-0.494	-0.321	-0.423	-1.689	9.6×10^{-6}	8.2×10^{-4}
Trichloroethene	TCE	-0.061	-0.062	-0.044	-0.094	-1.435	1.0×10^{-5}	3.4×10^{-4}
1,1-Dichloroethene	11DCE	0.379	0.402	0.327	0.303	-1.140	1.1×10^{-5}	1.2×10^{-4}
c-1,2-Dichloroethene	c12DCE	0.338	0.348	0.261	0.247	-1.200	1.1×10^{-5}	1.5×10^{-4}
t-1,2-dichloroethene	t12DCE	0.338	0.350	0.262	0.245	-1.200	1.1×10^{-5}	1.5×10^{-4}
Chloroethene	VC	0.855	0.820	0.703	0.668	-0.761	1.3×10^{-5}	3.4×10^{-5}
1,1,1-Trichloropropane	111TCP	-0.229	-0.465	-0.051	-0.261	-2.092	8.2×10^{-6}	3.3×10^{-3}
1,1,2-Trichloropropane	112TCP	0.232	0.082	0.223	0.052	-1.618	8.2×10^{-6}	6.4×10^{-4}
1,1,3-Trichloropropane	113TCP	0.330	0.234	0.305	0.181	-1.673	8.2×10^{-6}	7.8×10^{-4}
1,2,2-Trichloropropane	122TCP	0.201	0.016	0.227	0.020	-1.705	8.2×10^{-6}	8.7×10^{-4}
1,2,3-Trichloropropane	123TCP	0.758	0.638	0.616	0.380	-1.474	8.4×10^{-6}	3.9×10^{-4}

Table 5.4 Continued. Summary of Molecular-Based Variables for Chlorinated Aliphatic Compounds

Chlorinated Aliphatic	Abbr.	E_{LUMO} AM1	E_{LUMO} AM1 with COSMO	E_{LUMO} PM3	E_{LUMO} PM3 with COSMO	E_{LUMO} 6-31G*	D $cm^2\ s^{-1}$	$\hat{k}^a$ $L\ m^{-2}\ h^{-1}$
1,1-Dichloropropane	11DCP	0.610	0.367	0.537	0.253	-1.209	9.2×10^{-6}	1.6×10^{-4}
2,2-Dichloropropane	22DCP	0.575	0.253	0.541	0.189	-1.233	9.2×10^{-6}	1.7×10^{-4}
1,2-Dichloropropane	12DCP	0.685	0.509	0.525	0.278	-1.198	1.1×10^{-5}	1.5×10^{-4}
1,3-Dichloropropane	13DCP	1.019	0.905	0.832	0.605	-1.136	9.2×10^{-6}	1.2×10^{-4}
1-Chloropropane	1CP	1.517	1.227	1.245	0.867	-0.218	1.0×10^{-5}	5.3×10^{-6}
2-Chloropropane	2CP	1.407	1.087	1.165	0.711	-0.262	1.0×10^{-5}	6.1×10^{-6}

[a] Based on LFER developed with E_{LUMO} (6-31G*)

Table 5.5 Summary of Product Dependent Variables for Chlorinated Aliphatic Compounds

Chlorinated Aliphatic Abbreviation	Two-electron hydrogenolysis product	One-electron product	E_2 (V)[a]	E_1 (V)[b]	$\hat{k}^c$ L m^{-2} h^{-1}
PCM	TCM	$Cl_3C\bullet$	0.67	0.13	5.0×10^{-2}
TCM	DCM	$HCl_2C\bullet$	0.56	-0.23	4.9×10^{-3}
DCM	CM	$H_2ClC\bullet$	0.49	-0.50	8.5×10^{-4}
CM	M	$H_3C\bullet$	0.47	-0.88	7.3×10^{-5}
HCA	PCA	$Cl_3CCl_2C\bullet$	0.66	0.33	1.8×10^{-1}
PCA	1112TeCA	$Cl_3CCl_HC\bullet$	0.61	0.00	2.2×10^{-2}
PCA	1122TeCA	$Cl_2HCCl_2C\bullet$	0.66	0.31	1.6×10^{-1}
1112TeCA	111TCA	$Cl_3CH_2C\bullet$	0.51	-0.52	7.5×10^{-4}
1112TeCA	112TCA	$ClH_2CCl_2C\bullet$	0.56	-0.22	5.2×10^{-3}
1122TeCA	112TCA	$Cl_2HCCl_HC\bullet$	0.51	-0.34	2.4×10^{-3}
111TCA	11DCA	$H_3CCl_2C\bullet$	0.57	-0.23	4.9×10^{-3}
112TCA	11DCA	$Cl_2HCH_2C\bullet$	0.52	-0.74	1.8×10^{-4}

Table 5.5 Cont. Summary of Product Dependent Variables for Chlorinated Aliphatic Compounds

Chlorinated Aliphatic Abbreviation	Two-electron hydrogenolysis product	One-electron product	E_2 (V)[a]	E_1 (V)[b]	$\hat{k}$[c] L m^{-2} h^{-1}
112TCA	12DCA	$ClH_2CClHC\bullet$	0.54	-0.42	1.4 x 10^{-3}
11DCA	CA	$H_3CClHC\bullet$	0.51	-0.40	1.6 x 10^{-3}
12DCA	CA	$ClH_2CH_2C\bullet$	0.49	-0.57	5.4 x 10^{-4}
CA	EA	$H_3CH_2C\bullet$	0.35	-0.83	1.0 x 10^{-1}
PCE	TCE	$Cl_2CClC\bullet$	0.58 (0.59)	-0.36	2.1 x 10^{-3}
TCE	11DCE	$HClCClC\bullet$	0.50 (0.51)	-0.91	6.0 x 10^{-5}
TCE	c12DCE	$Cl_2CHC\bullet$	0.54 (0.53)	na	na
TCE	t12DCE	$ClHCClC\bullet$	0.53 (0.51)	-0.62	3.9 x 10^{-4}
11DCE	VC	$H_2CClC\bullet$	0.40 (0.42)	-0.72	2.1 x 10^{-4}
c12DCE	VC	$HClCHC\bullet$	0.36 (0.41)	-0.89	6.8 x 10^{-5}
t12DCE	VC	$HClCHC\bullet$	0.37 (0.43)	-0.85	8.9 x 10^{-5}
VC	EE	$H_2CHC\bullet$	0.49 (0.48)	-0.95	4.6 x 10^{-5}

[a] from (10), numbers in parantheses are from (8), conditions are pH 7, chloride activity = 1 mM
[b] from (8) and (9)
[c] Based on LFER developed with E_1

Table 5.6. ANOVA for log k versus E_{LUMO} Correlation

	df	Sum Sqrs (SS)	Mean SS	F
Regression	1	61.9	61.9	226.1
Residual	46	12.6	0.27	
Total	47	74.5		
r^2		0.83		Signif. @ 90%

Table 5.7. ANOVA for log k versus E_1 Correlation

	df	Sum Sqrs (SS)	Mean SS	F
Regression	1	60.3	60.3	195.7
Residual	46	14.2	0.31	
Total	47	74.5		
r^2		0.81		Signif. @ 90%

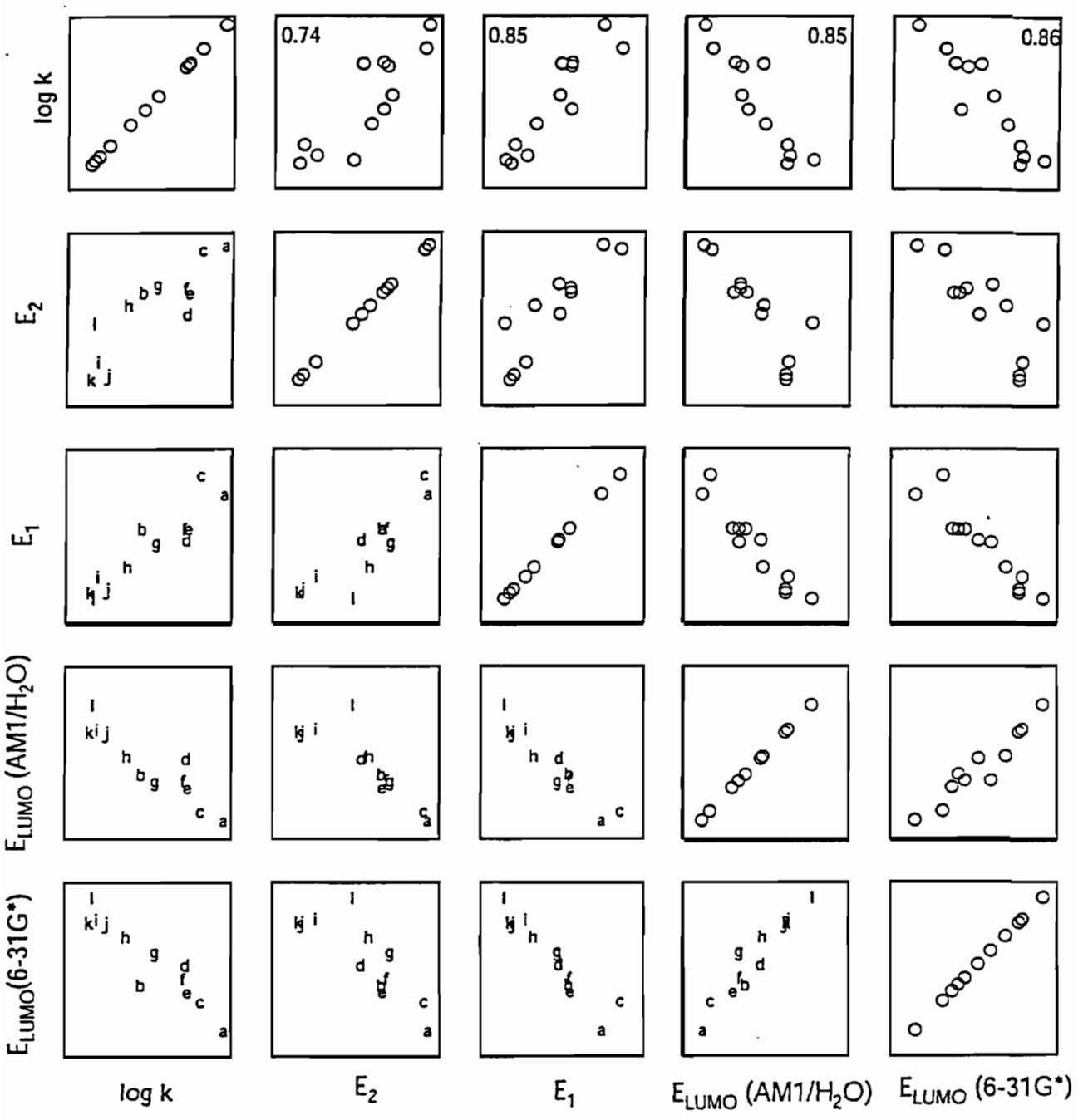

Figure 5.1. Scatter Plot matrix of log k versus selected electronic descriptor variables. E_2 values are from (10) and E_1 values are from (9) and (8). E_{LUMO} AM_1/H_2O and E_{LUMO} 6-31G* were calculated using molecular modeling software (CAChe). Correlation coefficients, r^2, are given for the top row. The compound labels are defined in Table 1.

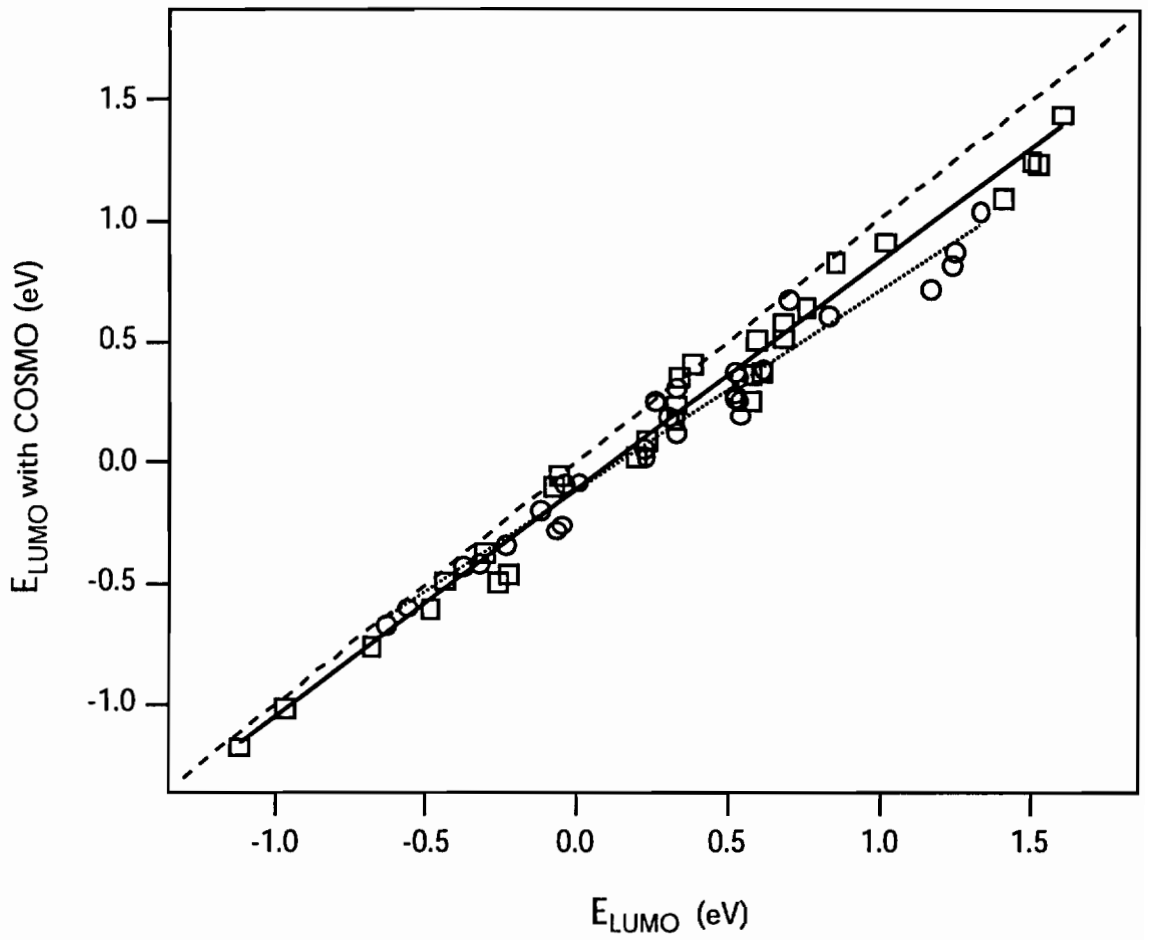

Figure 5.2. Effect of solvation on E_{LUMO}'s calculated from semi-empirical methods. (squares) E_{LUMO} values calculated using AM1 parameter set, (circles) E_{LUMO} values calculated using PM3 parameter set. Lines represent regression between E_{LUMO} values calculated with COSMO to account for solvation and E_{LUMO} values calculated without COSMO. Regression on AM1 (solid line) gives $(0.94\pm0.02)x$ - 0.11 ± 0.02 with $r^2 = 0.98$. Regression on PM3 (dotted line) gives $(0.83\pm0.03)x$ - 0.12 ± 0.02 with $r^2 = 0.96$. The dashed line is included to show perfect agreement (i.e., slope = 1.0).

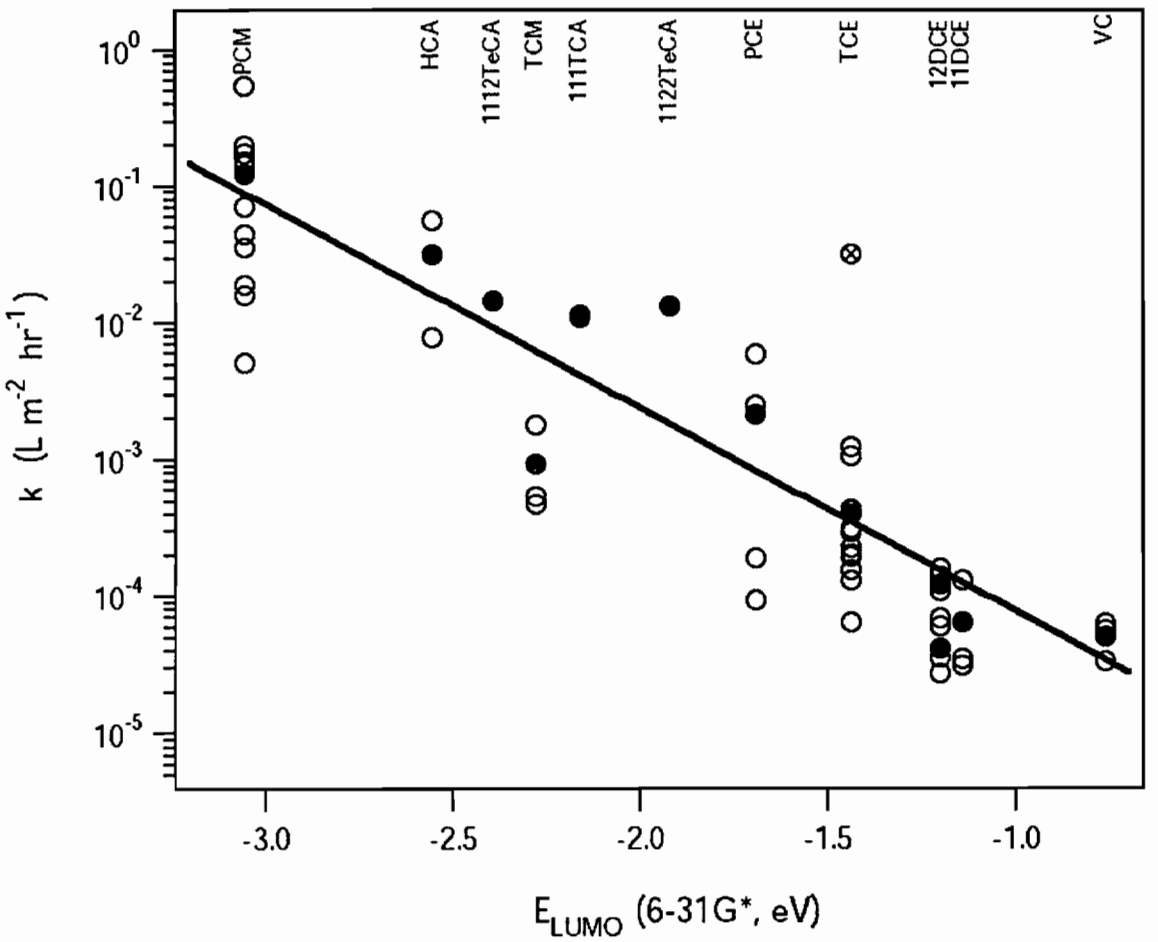

Figure 5.3A Correlation between log k and E_{LUMO}, (B) Correlation between log k and E_1. Open circles represent individual data, and solid circles indicate the average k values ($\bar{k}$) reported in Table 1. Solid lines represent the unbiased prediction using eq. 5 and parameters given in Table 2. Point marked with an X was treated as an outlier.

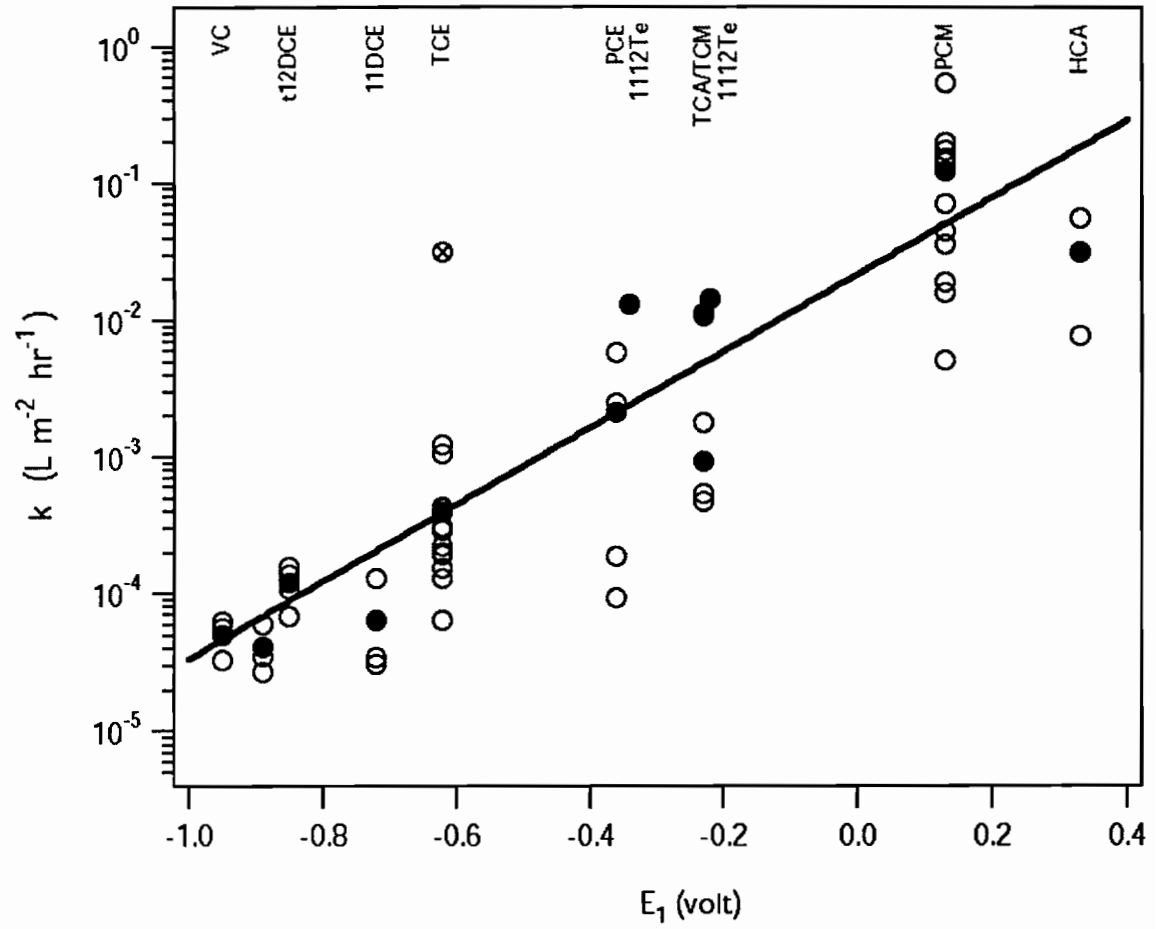

Figure 5.3B Correlation between log k and E_1. Open circles represent individual data, and solid circles indicate the average k values ($\bar{k}$) reported in Table 1. Solid lines represent the unbiased prediction using eq. 5 and parameters given in Table 2. Point marked with an X was treated as an outlier.

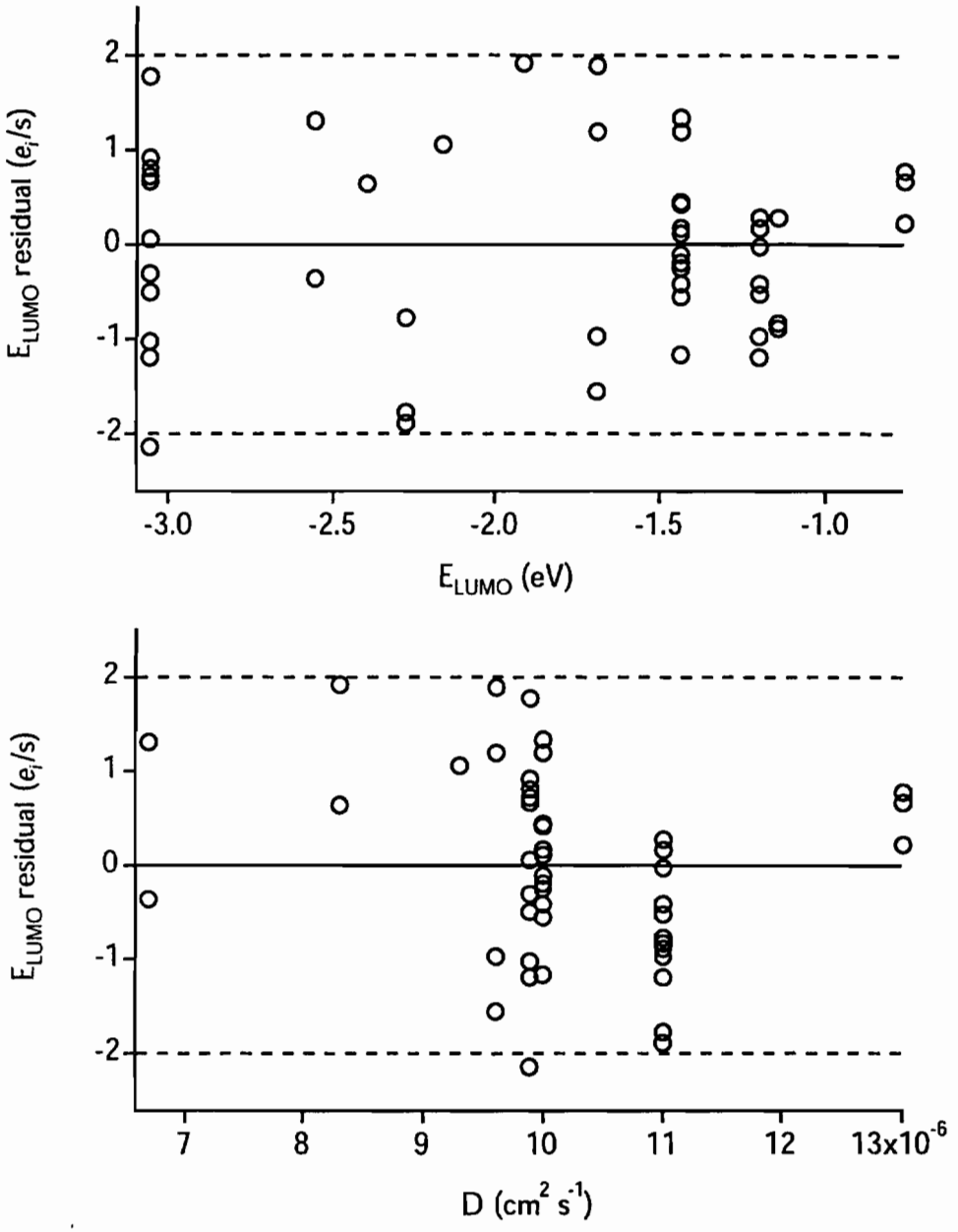

Figure 5.4A Standardized residual plots for log k versus E_{LUMO} correlation. Dashed lines are included to indicate acceptable spread in the data (± two standard deviations). Estimated diffusion coefficients are tabulated in Table 5.4.

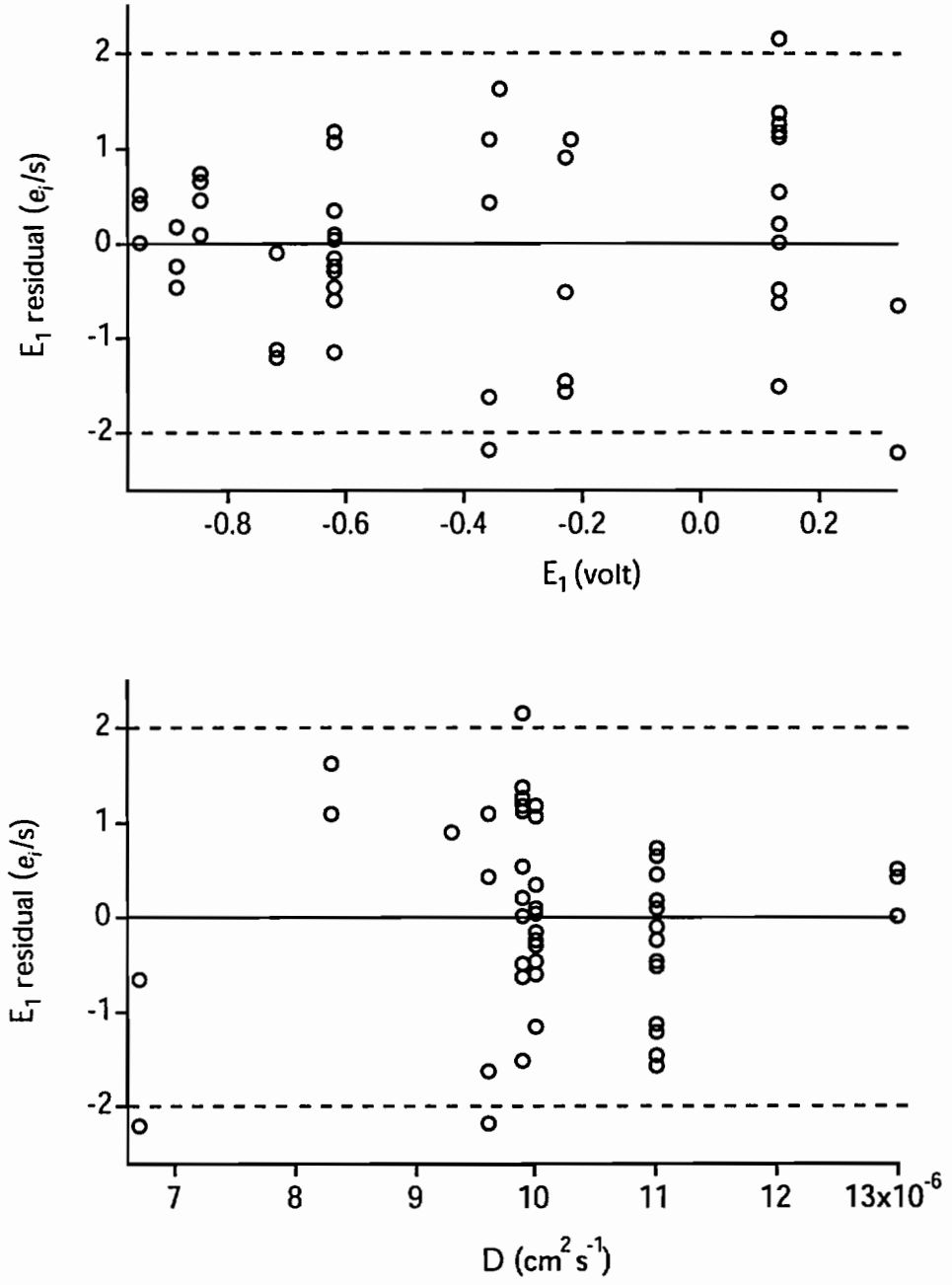

Figure 5.4B Standardized residual plots for log k versus E_1 correlation. Dashed lines are included to indicate acceptable spread in the data (± two standard deviations). Estimated diffusion coefficients are tabulated in Table 5.4.

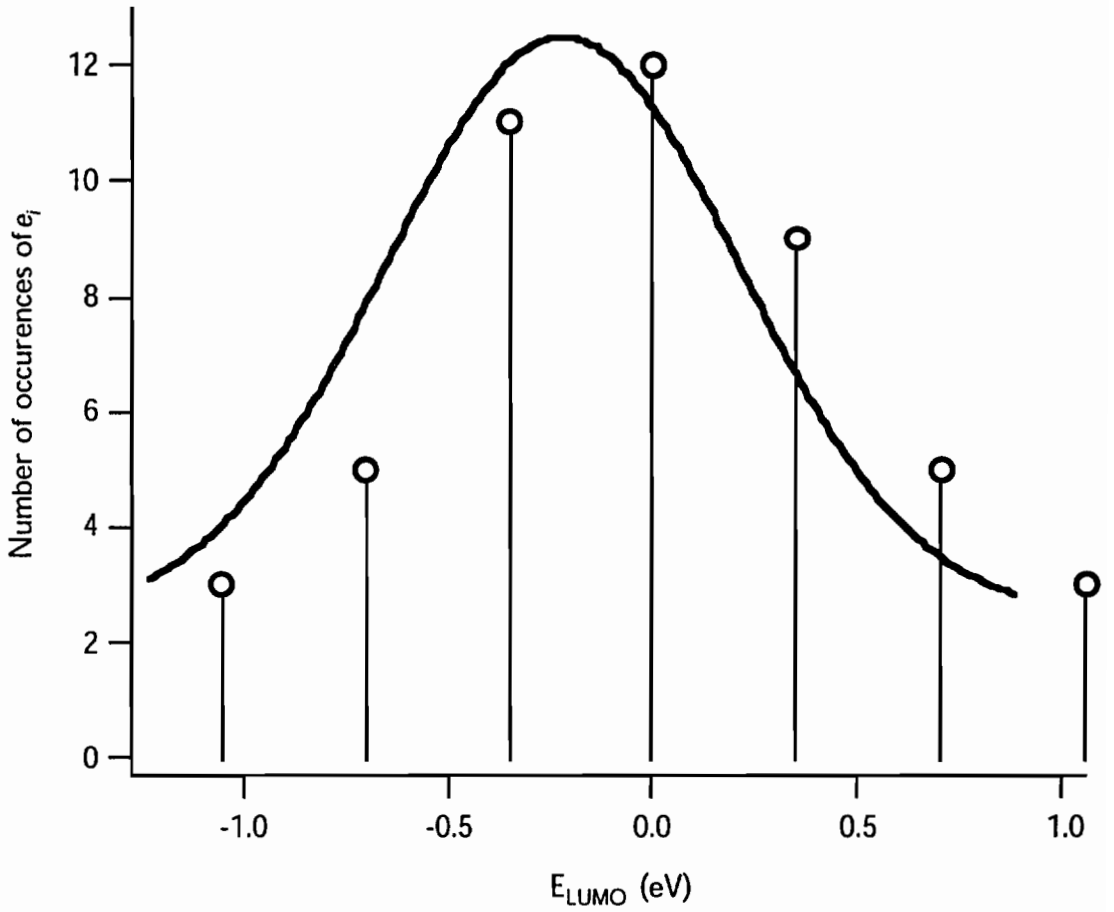

Figure 5.5. Histogram of residuals for the log k versus E_{LUMO} correlation. Circles mark the centers of each E_{LUMO} interval. The solid curve is a non-linear least squares fit to the guassian function.

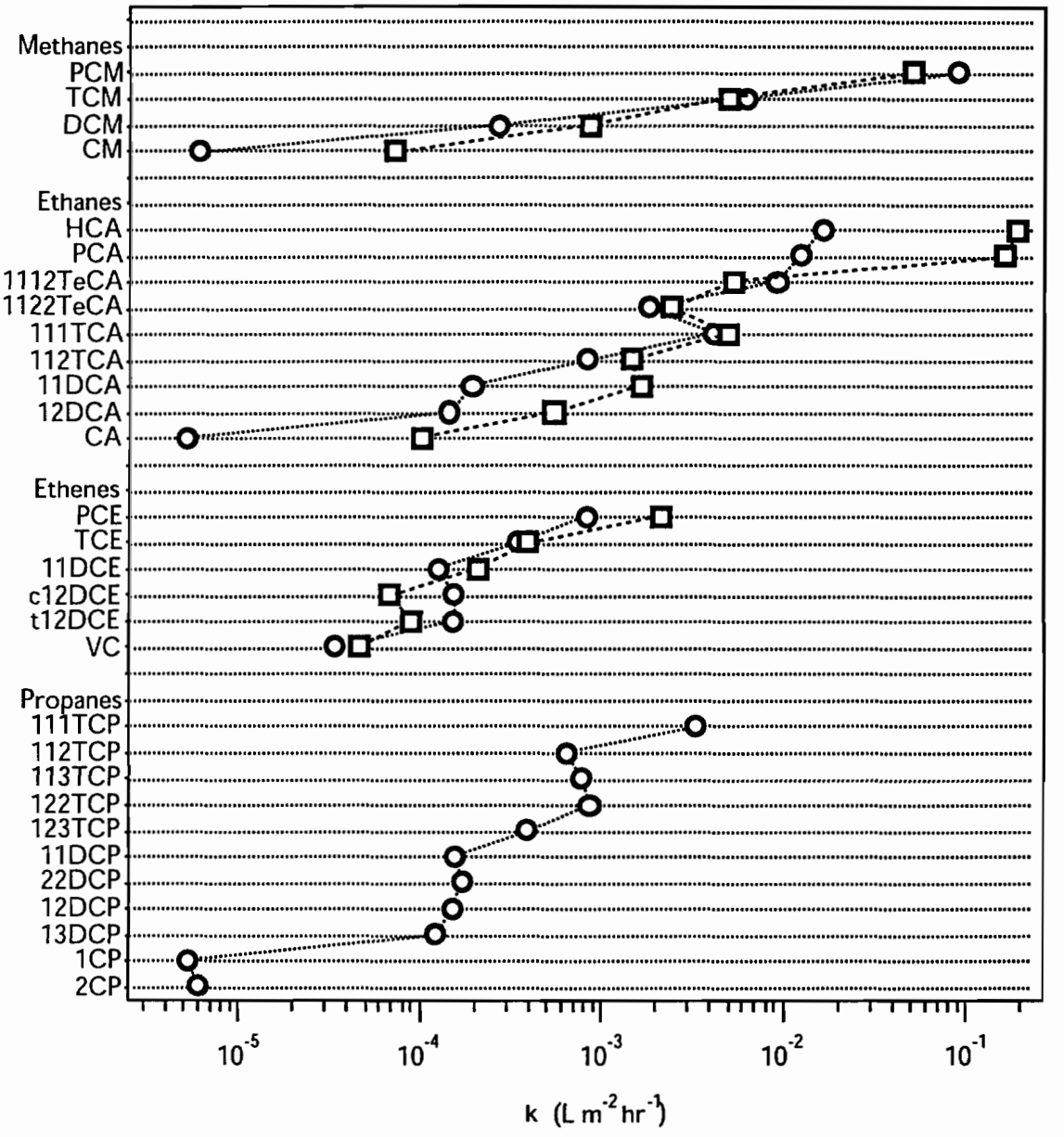

Figure 5.6. (circles) Predicted k values based on correlation between log k and E_{LUMO} and (squares) correlation between log k and E_1. Values were calculated using eq. 5 and the coefficients given in Table 2.

CHAPTER 6

The Role of Surface-Active Substances in Reduction of Contaminants by Fe^0

6.1 Introduction

Recent studies of contaminant reduction by zero-valent iron metal (Fe^0) have highlighted the role of iron oxides at the metal-water interface (Chapter 2, and refs. cited therein). The results of these studies suggest that contaminant degradation kinetics are sensitive to the presence of ligands that participate in surface complexation reactions at the oxide film, which forms on the metal surface. Analogous effects might be expected from substances that are surface active by virtue of having both hydrophilic and hydrophobic moieties (i.e., amphiphiles (1)). Amphiphiles that are of interest in this context include anthropogenic surfactants, which are sometimes used in groundwater remediation, and natural organic matter (NOM), which is ubiquitous in shallow aquifers where remediation technologies based on Fe^0 are most applicable.

The chemistry of Fe^0, NOM, and anthropogenic surfactants, suggests three ways in which amphiphilic substances might influence the kinetics of transformation of hydrophobic organic contaminants (HOCs) by Fe^0: (i) solubilization of HOCs by partitioning to micelles or other surfactant aggregates in the solution phase (Figure 6.1a), (ii) adsorption of HOCs by partitioning to the surfactant film that forms at the oxide-water interface (Figure 6.1b), and (iii) reduction of HOCs by electron transfer that is mediated by surfactants with reactive functional groups (Figure 6.1c). The goal of this chapter is to begin to assess whether these (or other) mechanisms influence the performance of remediation technologies based on reduction by Fe^0.

6.1.1 HOC Solubilized by Surfactant

In the first scenario, HOCs are made more soluble by partitioning to micelle or membrane-like hydrophobic interiors formed by surfactant aggregates (1). Sorption of HOCs into NOM has been shown to increase both the solubility and mobility of HOCs in porous media (2-4). A strong correlation between extent of sorption and HOC

hydrophobicity (measured by octanol-water partitioning coefficient or aqueous solubility) suggests that partitioning into hydrophobic interiors is the dominant mechanism of sorption (5, 6). The extent of increased solubilization depends on both the hydrophobicity of the HOC and the polarity, molecular weight, and aromaticity of the amphiphilic substance (6). Solubilization of HOCs is the desired effect in most applications of anthropogenic surfactants to remediation, and it is a well documented side-effect of the presence of dissolved NOM (7, 8). However, in systems involving remediation of HOCs with Fe^0, solubilization should result in less contact with the metal surface, and, therefore, slower rates of HOC degradation by reduction. Specific evidence for this effect includes the decreased rates of tetrachloroethene dechlorination observed in the presence of hydroxypropyl-β-cyclodextrin, which solubilizes PCE and thereby facilitates dissolution of HOC residuals (9). In fact, a kinetic model derived to fit the cyclodextrin data predicts that any substance that increases the solubility of HOCs will decrease their rate of reaction with Fe^0.

6.1.2 Sorption of HOCs to Hydrophobic Surface Coating

In the second scenario, the accumulation of surfactants (or NOM) at the oxide-water interface provides a more hydrophobic surface that favors sorption of HOCs and thereby increases the amount of HOC associated with the metal surface. Both the orientation and aggregation of adsorbed amphiphilic substances could influence the extent of HOC sorption at the interface. Properties of the film of adsorbed surfactant, will, in turn, depend on the surfactant type and concentration, the nature of the metal surface, and the solution chemistry (pH, I, E_h, T) (5). Since the oxides formed on Fe^0 in aqueous media present a polar surface, it is reasonable to expect cationic surfactants to provide strong surface interactions. Electrostatic attraction between the polar metal and ionic moiety of the surfactant will orient the hydrophobic portion of the surfactant towards the solution (10). Both cationic (11-13) and anionic (14) surfactants have been shown to sorb to oxides and natural aquifer materials and promote sorption of HOCs. Cationic surfactants, however, sorb more strongly to most natural materials because of their tendency to have a net negative surface charge (5).

The aggregation of surfactant monomers at the surface could also influence the sorption of the HOCs onto the metal surface. Both experimental and modeling studies suggest that the aggregation of surfactant monomers account for the S shaped adsorption isotherm of an ionic surfactant on a charged surface (14, 15). As illustrated in Figure 6.2, at low surfactant concentrations, adsorption is due to electrostatic forces resulting in

monomers spread out over the surface (Region I). As the surfactant concentration increases (Region II), the hydrophobic tails begin to associate and form patches of hemimicelles creating hydrophobic regions that attract further adsorption. The transition to Region III is marked by a decreasing rate of adsorption as the surface charge is neutralized, eliminating the electrostatic attraction. Beyond this point, a second layer of monomers may form, creating an admicelle with the hydophilic groups oriented towards the solution. At this level of surfactant concentration, a decrease in the extent of HOC sorption can be expected. Finally, when the surfactant concentration exceeds the critical micelle concentration (CMC) (Region IV), the organic interiors of the solution micelles will start to compete with the surface causing the extent of adsorption to level off. Enhanced HOC adsorption is most likely to occur under conditions corresponding to the transition between Region II and III, where a monolayer coverage of surfactant is achieved.

Although there is evidence that oxide-bound NOM (16, 17) and anthropogenic surfactants (12, 13, 18) significantly increase the sorption of HOCs at the oxide-water interface, it is unclear how adsorption to an organic film of surfactants covering the Fe^0 might affect electron transfer (ET) from the underlying metal to the adsorbed contaminant. Both the distance between electron donor and acceptor and the conductivity of the intervening organic film will influence whether for long range ET occurs (19). Given the low dielectric constants of organic molecules compared to water, the separation of electron donor and acceptor by an organic film may insulate the surface and inhibit ET. ET may still occur, however, if the surface film is thin enough to allow ET via a tunneling mechanism (20, 21). Thus, in most cases, we expect that the separation of electron donor and acceptor by an organic film will passivate the surface and inhibit contaminant reduction. However, at least one case has been reported in which the addition of an anthropogenic cationic surfactant (hexadecyltrimethylammonium) appears to have enhanced rates of dechlorination by Fe^0 (22).

6.1.3 HOC Electron Transfer Catalyzed by Surfactant

The third scenario is mediated ET, where reactive functional groups associated with some surfactants facilitate—or even catalyze—contaminant reduction by the metal. For example, there is evidence that quinonoid moieties associated with NOM (23, 24) or quinonoid model substances such as anthraquinone disulfonate, juglone, and lawsone (23, 25), can mediate reduction of chlorinated solvents and nitro aromatics in homogeneous systems , and such an effect might also occur in heterogeneous systems where the bulk reductant is Fe^0.

6.2 Experimental Section

6.2.1 Surface-Active Reagents

Most NOM samples were obtained from George Aiken (USGS in Boulder, CO) and included four fulvic acids (Suwannee River, 310-8 Bemidji, Lake Fryxell, and Coal Creek) and two humic acids (Suwannee River and Coal Creek). Samples were received as freeze-dried powder samples. An additional soil HA was used that had been collected and purified at OGI by B. Bonn (26). Selected properties of the NOM samples and surfactants and mediators are shown in Table 6.1 and 6.2.

6.2.2 Kinetics of HOC Reduction

Kinetics of tetrachloromethane (CCl_4) and nitrobenzene ($ArNO_2$) reduction were determined in batch experiments with untreated Fluka Fe^0 turnings (Fluka, puriss. grade, specific surface area of 0.019 $m^2\ g^{-1}$ (27)). Vials were filled with deoxygenated buffer, Fe^0 turnings, and CCl_4 at an initial concentration of 85 μM or $ArNO_2$ at an initial concentration of 250 μM. Buffers used were either 15 mM bicarbonate (pH 5.6 - 5.8), 30 mM HEPES (pH 8), 30 mM MOPS (pH 7), or 30 mM MES (pH 6)). CCl_4 disappearance kinetics were determined by periodically removing 500 μL samples from the vial and extracting the sample with hexane. The hexane extract was analyzed by gas chromatography with ECD detection (28). $ArNO_2$ and its reduction products were quantified by periodically removing 200 μL samples from the vial and measuring the concentration by isocratic HPLC with UV absorbance detection at 278 nm (29). The steel analytical column (3.9 x 300 mm) consisted of 10 μM particle packing with a C-18 stationary phase. The eluent consisted of 40/60 acetonitrile and unbuffered, deionized water at a flow rate of 0.9 mL min^{-1} (29).

6.3 Results and Discussion

6.3.1 Effect of NOM on CCl_4 Reduction Rates

In the presence of NOM, all three of the above scenarios illustrated in Figure 6.1 could be operative to varying degrees, depending on solution chemistry and the type of NOM. To gain a broad perspective on the range of effects NOM has on reduction of HOCs by Fe^0, we measured the kinetics of dechlorination in the presence of seven samples of NOM representing a range of types and sources of organic matter (Table 6.1). At a concentration of 5 mg L^{-1}, the four fulvic acids (FAs) investigated had no significant influence on the rate of reduction of CCl_4 by Fe^0 (Figure 6.3). Increasing the concentration of Coal Creek FA up to 15 mg L^{-1} also showed no significant effect on the reduction rate

(Figure 6.4). However, the three humic acids (HAs) investigated, apparently slowed down the reduction rate by almost two-fold (Figure 6.5). Two of these (Coal Creek HA and Suwannee River HA) are aquatic humic acids, whereas the OGI sample is a soil HA. The soil HA appears to have the largest effect, possibly due to stronger adsorption by the HA reflecting the greater aromatic content that is typical of soil HAs (17).

6.3.2 Effect of Surfactants on $ArNO_2$ Reduction Rates

Since there was no significant effect of NOM on the kinetics of CCl_4 reduction by Fe^0, we decided to broaden our scope of contaminants to include $ArNO_2$. The process limiting the kinetics of reduction by Fe^0 is different for each of these contaminants and may influence how surfactants effect the overall reduction kinetics. Specifically, we thought that the greater influence of mass transport on the reduction of $ArNO_2$ compared to the reduction of CCl_4 (see Chapter 4) might provide conditions where a stronger effect of surfactants on the reduction rate might be observed.

A preliminary screening of $ArNO_2$ reduction rates in the presence of one NOM and several surfactants, however, reveals no significant effect (Table 6.3). At concentrations up to 20 mg L^{-1}, Coal Creek NOM had no effect on the $ArNO_2$ reduction rate. Similar results were found with the possible mediators, lawsone (57 μM) and anthraquinone (100 μM), and a nonionic (Triton X-100, up to 10 mg L^{-1}), cationic (dodecylpyridinium chloride, up to 10 mM), and anionic (dodecyl sulfate, 100 μM) surfactants. The conditions and rate constants for each experiment are shown in Table 6.3.

6.4 Literature Cited

(1) Wershaw, R. L. Model for humus in soils and sediments. *Environ. Sci. Technol,.* 1993, *27*, 814-816.

(2) McCarthy, J. F.; Zachara, J. M. Subsurface transport of contaminants. *Environ. Sci. Technol.,* 1989, *23*, 496-502.

(3) Kan, A. T.; Tomson, M. B. Ground water transport of hydrophobic organic compounds in the presence of dissolved organic matter. *Environ. Toxicol. Chem.,.* 1990, *9*, 253-263.

(4) Magee, B. R.; Lion, L. W.; Lemley, A. T. Transport of dissolved organic macromolecules and their effect on the transport of phenanthrene in porous media. *Environ. Sci. Technol.,* 1991, *25*, 323-331.

(5) West, C. C.; Harwell, J. H. Surfactants and subsurface remediation. *Environ. Sci. Technol.,* 1992, *26*, 2324-2330.

(6) Chiou, C. T.; Malcolm, R. L.; Brinton, T. E.; Kile, D. E. Water solubility enhancement of some organic pollutants and pesticides by dissolved humic and fulvic acids. *Environ. Sci. Technol.,* 1986, *20*, 502-508.

(7) Chiou, C. T.; Kile, D. E.; Brinton, T. I.; Malcolm, R. L.; Leenheer, J. A. A comparison of water solubility enhancements of organic solutes by aquatic humic materials and commercial humic acids. *Environ. Sci. Technol.* 1987, *21*, 1231-1234.,

(8) Danielsen, K. M.; Chin, Y. P.; Buterbaugh, J. S.; Gustafson, T. L.; Traina, S. J. Solubility enhancement and fluorescence quenching of pyrene by humic substances: The effect of dissolved oxygen on quenching processes. *Environ. Sci. Technol.,* 1995, *29*, 2162-2165.

(9) Bizzigotti, G. O.; Reynolds, D. A.; Kueper, B. H. Enhanced solubilization and destruction of tetrachloroethylene by hydroxypropyl-β-cyclodextrin and iron. *Environ. Sci. Technol.,* 1997, *31*, 472-478.

(10) Ulrich, H.-J.; Stumm, W. Adsorption of Aliphatic Fatty Acids on Aquatic Interfaces. Comparison between Two Model Surfaces: The Mercury Electrode and δ-Al_2O_3 Colloids. *Environ. Sci. Technol.,* 1988, *22*, 37-41.

(11) Brownawell, B. J.; Chen, H.; Collier, J. M.; Westall, J. C. Adsorption of organic cations to natural materials. *Environ. Sci. Technol.,* 1990, *24*, 1234-1241.

(12) Wagner, J.; Chen, H.; Brownawell, B. J.; Westall, J. C. Use of cationic surfactants to modify soil surfaces to promote sorption and retard migration of hydrophobic organic compounds. *Environ. Sci. Technol.,* 1994, *28*, 231-237.

(13) Burris, D. R.; Antworth, C. P. In situ modification of an aquifer material by a cationic surfactant to enhance retardation of organic contaminants. *J. Contam. Hydrol.,* 1992, *10*, 325-337.

(14) Holsen, T. M.; Taylor, E. R.; Seo, Y.-C.; Anderson, P. R. Removal of sparingly soluble organic chemicals from aqueous solutions with surfactant-coated ferrihydrite. *Environ. Sci. Technol.,* 1991, *25*, 1585-1589.

(15) Yeskie, M. A.; Harwell, J. H. On the structure of aggregates of adsorbed surfactants: The surface charge density at the hemimicelle/admicelle transition. *J. Phys. Chem.,* 1988, *92*, 2346-2352.

(16) Murphy, E. M.; Zachara, J. M.; Smith, S. C. Influence of mineral-bound humic substances on the sorption of hydrophobic organic compounds. *Environ. Sci. Technol.,* 1990, *24*, 1507-1516.

(17) Murphy, E. M.; Zachara, J. M.; Smith, S. C.; Phillips, J. L.; Wietsma, T. W. Interaction of hydrophobic organic compounds with mineral-bound humic substances. *Environ. Sci. Technol.,* 1994, *28*, 1291-1299.

(18) Smith, J. A.; Jaffe, P. R. Comparison of tetrachloromethane sorption to an alkylammonium-clay and alkyldiammonium-clay. *Environ. Sci. Technol.,* 1991, *25*, 2054-2058.

(19) Mayo, S. L.; Ellis, W. R.; Crutchley, R. J.; Gray, H. B. Long-range electron transfer in heme proteins. *Science,* 1986, *233*, 948-952.

(20) Smith, D. P. E.; Bryant, A.; Quate, C. F.; Rabe, J. P.; Gerber, C.; Swalen, J. D. Images of a lipid bilayer at molecular resolution by scanning tunneling microscopy. *Proc. Natl. Acad. Sci.,* 1987, *84*, 969-972.

(21) Li, T. T.; Weaver, M. J. Intramolecular electron transfer at metal surfaces. 4. dependence of tunneling probability upon donor-acceptor separation distance. *J. Am. Chem. Soc.,* 1984, *106*, 6107-6108.

(22) Li, Z.; Jones, H. K.; Bowman, R., S. Incorporation of zero valent iron into pelletized surfactant-modified zeolite for groundwater remediation; *Joint Conference on the Environment,* Albuquerque, NM, 1998; Vol. pp. 3-7.

(23) Curtis, G. P.; Reinhard, M. Reductive dehalogenation of hexachlorethane, carbon tetrachloride, and bromoform by anthrahydroquinone disulfonate and humic acid. *Environ. Sci. Technol.,* 1994, *28*, 2393-2401.

(24) Dunnivant, F. M.; Schwarzenbach, R. P.; Macalady, D. L. Reduction of substituted nitrobenzenes in aqueous solutions containing natural organic matter. *Environ. Sci. Technol.,* 1992, *26*, 2133-2141.

(25) Tratnyek, P. G.; Macalady, D. L. Abiotic reduction of nitro aromatic pesticides in anaerobic laboratory systems. *J. Agric. Food Chem.,* 1989, *37*, 248-254.

(26) Bonn, B. A. *Interactions of a Soil Humic Acid with Alkali Metal Cations and Alkaline Earth Metal Cations*. Ph.D. Thesis, Oregon Graduate Institute of Science and Technology, Portland, OR, 1992.

(27) Johnson, T. L.; Scherer, M. M.; Tratnyek, P. G. Kinetics of halogenated organic compound degradation by iron metal. *Environ. Sci. Technol.,* 1996, *30*, 2634-2640.

(28) Johnson, T. L.; Fish, W.; Gorby, Y. A.; Tratnyek, P. G. Degradation of carbon tetrachloride by iron metal: Complexation effects on the oxide surface. *J. Contam. Hydrol.,* 1998, *29*, 377-396.

(29) Agrawal, A.; Tratnyek, P. G. Reduction of nitro aromatic compounds by zero-valent iron metal. *Environ. Sci. Technol.,* 1996, *30*, 153-160.

(30) Chin, Y. P.; Aiken, G.; O'Loughlin, E. Molecular weight, polydispersity, and spectroscopic properties of aquatic humic substances. *Environ. Sci. Technol.,* 1994, *28*, 1853-1858.

(31) Guha, S.; Jaffe, P. R. Bioavailability of hydrophobic compounds partitioned into the micellar phase of nonionic surfactants. *Environ. Sci. Technol.,* 1996, *30*, 1382-1391.

(32) Rosen, M. J. *Surfactants and Interfacial Phenomena;* 2nd ed.; Wiley: New York, 1989.

(33) Chandar, P.; Somasundaran, P.; Turro, N., J. Fluorescence probe studies on the sturcture of the adsorbed layer of dodecyl sulfate at the alumina-water interface. *J. Coll. and Inter. Sci.,* 1987, *117*, 31-46.

Table 6.1 Selected Properties of NOM Samples

NOM	Derived	[a]% Aromaticity	[b]H/C Ratio	[b]O/C Ratio	[b]N/C Ratio
310-8 FA (BEMIDJI)	groundwater				
Lake Fryxell FA, Antartica	microbial	13	1.19	0.48	0.05
Coal Creek FA	intermediate	27.4	1.02	0.55	0.02
Suwanee River FA, Georgia	lignin	24.8	0.84	0.54	0.01
Ogeechee River FA	intermediate		0.89	0.54	0.01
Ogeechee River HA					
Suwannee River HA, Georgia					
OGI Soil HA					

[a] from ref. (30)
[b] Hess and Chin, Colloids and Surfaces A (1996)

Table 6.2 Surfactants and Mediators

Name	Abbreviation	f_W g mol^{-1}	Type	CMC
Surfactants				
Triton X-100	TX	Ave. 647	nonionic	[a]43 mg L^{-1}
Sodium Dodecyl Sulfate	SDS	288.4	anionic	[b]8.6 mM
1-Dodecylpyridinium Chloride	DP	283.9	cationic	[b]17 mM
Hexadecyltrimethylammonium Chloride	HDTMA	320.0	cationic	[b]1.3 mM
Aerosol 22	A22	320.0		
Mediators				
5-hydroxy-1,4-napthoquinone (Juglone)	JG	174.1		
2-hydroxy-1,4-napthoquinone (Lawsone)	LW	174.1		
Anthraquinone-2,6-disulfonic acid	AQ	412.3		

[a] from ref. (31)
[b] from ref. (32)

Table 6.3. Summary of Rate Constants of $ArNO_2$ Reduction by Fe^0 with Different Treatments

Date	Treatment	$^1t_{pre}$ hr	Concentration	pH	n	R	k_{obs} min^{-1}	k_{SA} $L\ m^{-2}\ hr^{-1}$
30 Mar 98	None	0	NA	6	5	0.998	0.034	15.0
30 Mar 98	None	0	NA	6	5	0.996	0.036	15.8
3 Apr 98	^{2}NOM	2	5.9 mg L^{-1}	6	5	0.998	0.040	17.6
3 Apr 98	^{2}NOM	2	5.9 mg L^{-1}	6	5	0.989	0.035	15.4
10 Apr 98	DP	0	100 µM	6	3	1.000	0.056	24.7
10 Apr 98	DS	0	100 µM	6	5	0.990	0.046	20.3
10 Apr 98	AQ	0	100 µM	6	5	0.999	0.055	24.3
13 Apr 98	None	0	NA	6	5	0.991	0.043	19.0
13 Apr 98	Aerosol	0	1.7 mg L^{-1}	6	4	0.985	0.044	19.4
13 Apr 98	Triton	0	1.7 mg L^{-1}	6	4	0.999	0.043	19.0
13 Apr 98	Lawsone	0	57 µM	6	4	1.000	0.051	22.5
17 Apr 98	None	0	NA	6	3		0.054	23.8
17 Apr 98	^{2}NOM	120	5 mg L^{-1}	6	4		0.044	19.4

Table 6.3 Continued. Summary of Rate Constants of $ArNO_2$ Reduction by Fe^0 with Different Treatments

Date	Treatment	[1]t_{pre} hr	Concentration	pH	n	R	k_{obs} min^{-1}	k_{SA} $L\ m^{-2}\ hr^{-1}$
17 Apr 98	[2]NOM	120	20 mg L^{-1}	6	4		0.043	19.0
20 Apr 98	Aerosol	2	10 mg L^{-1}	7				
20 Apr 98	Triton	2	10 mg L^{-1}	7	5	0.998	0.050	22.1
24 Apr 98	None	0	NA	6	5	0.975	0.054	23.8
24 Apr 98	DP	48	1 mM	6	4	0.997	0.047	20.7
24 Apr 98	DP	48	5 mM	6	5	0.998	0.046	20.3
24 Apr 98	DP	48	10 mM	6	4	0.978	0.043	19.0

[1] Preequilibration time for buffer, Fe^0 and treatment.
[2] Coal Creek humic acid.

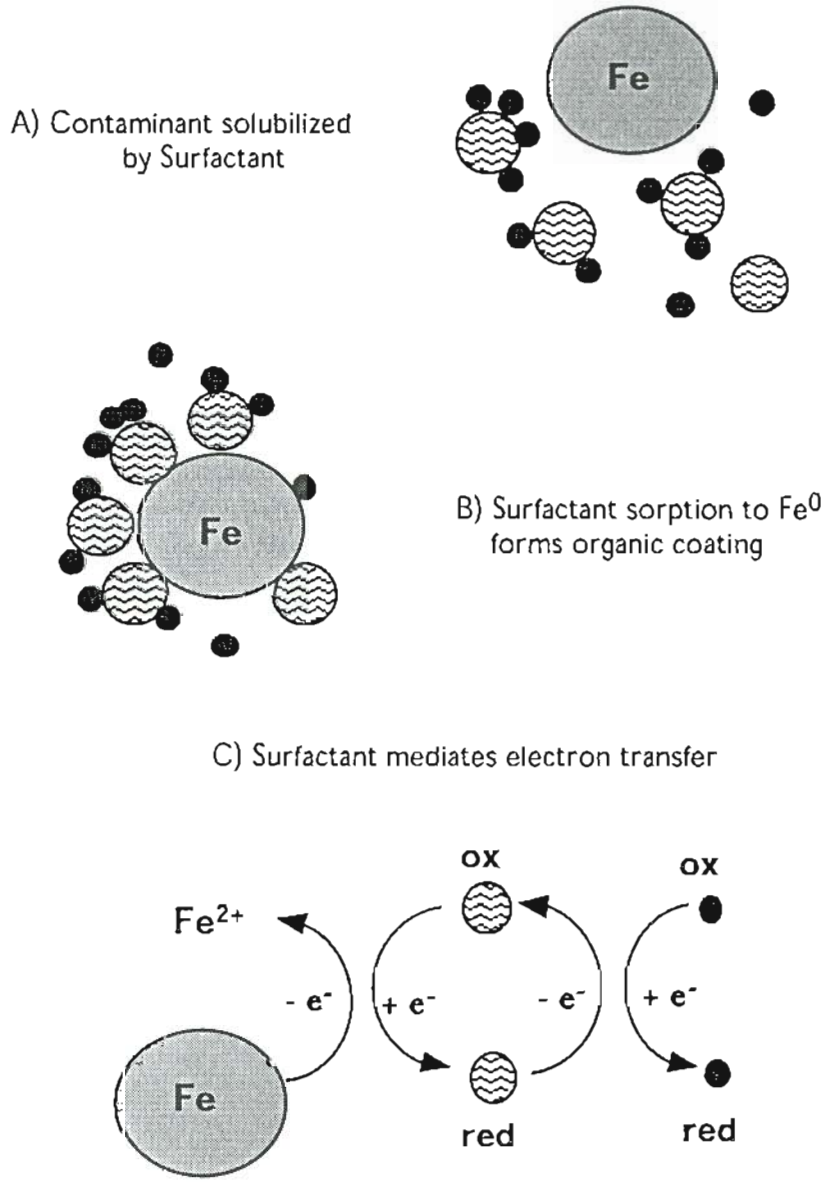

Figure 6.1 Scheme showing three possible effects of NOM on the reduction of contaminants by Fe^0. Small solid circles are dissolved HOC molecules and hatched circles are surface active molecules.

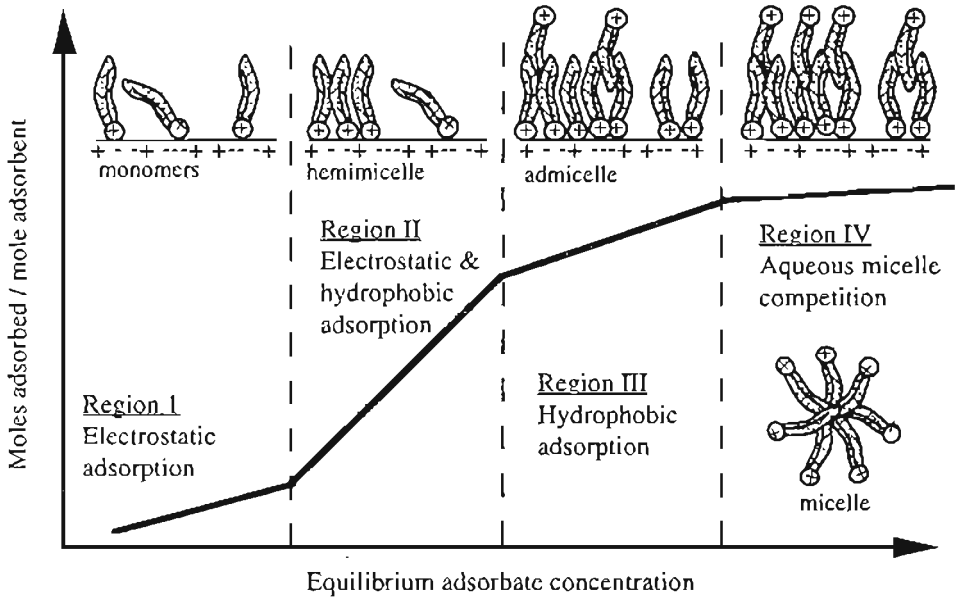

Figure 6.2 Relationship between growth of surfactant aggregates and surfactant adsorption isotherm. Schematic drawn for sorption of a cationic surfactant on a polar surface. (Adapted from (15, 33))

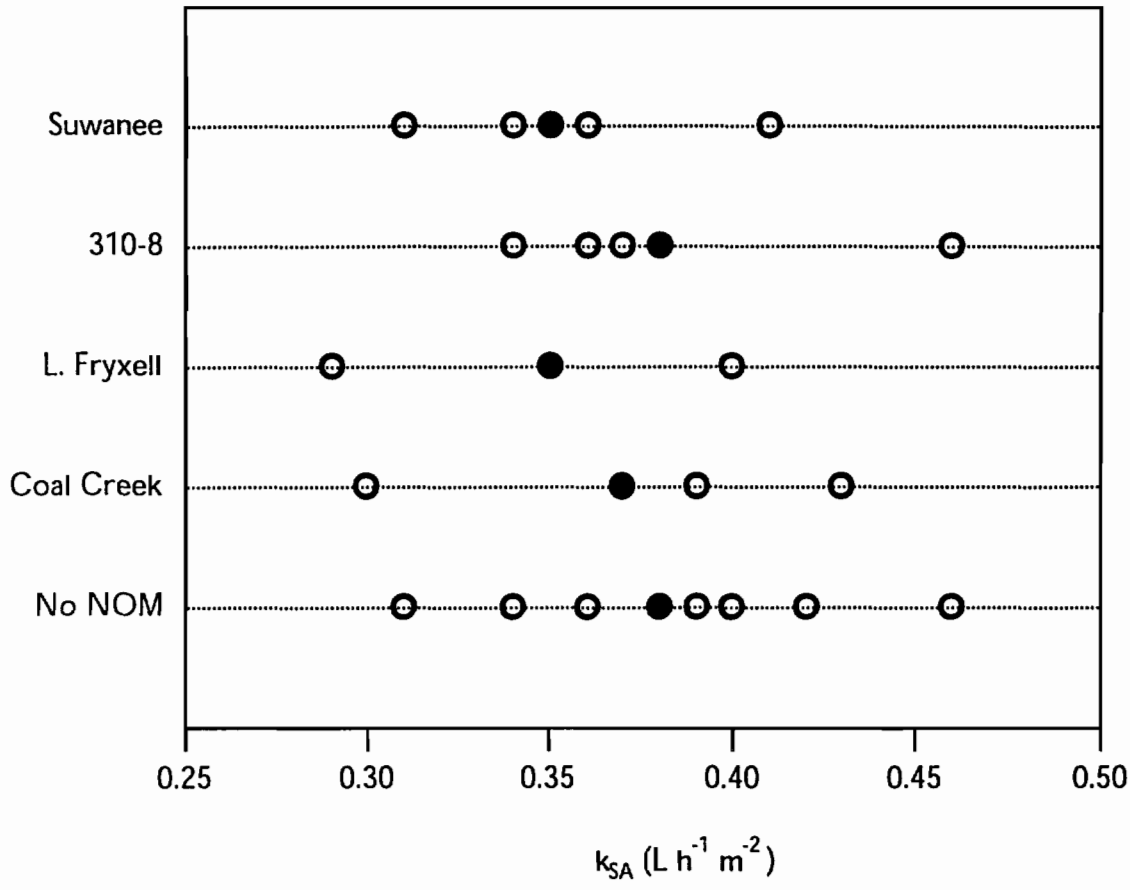

Figure 6.3 Distribution of k_{SA} values for the reduction of CCl_4 by Fe^0 in the presence of four fulvic acids. FA concentration is 5 mg L^{-1}. Open circles are single values of k_{obs} normalized to ρ_a and closed circles are the average of the individual data points. Experimental conditions are pH 5.8 carbonate buffer using untreated Fluka iron (1 g in 12 mL; ρ_a = 1.6 m^2 L^{-1}) rotating at 36 rpm in the dark.

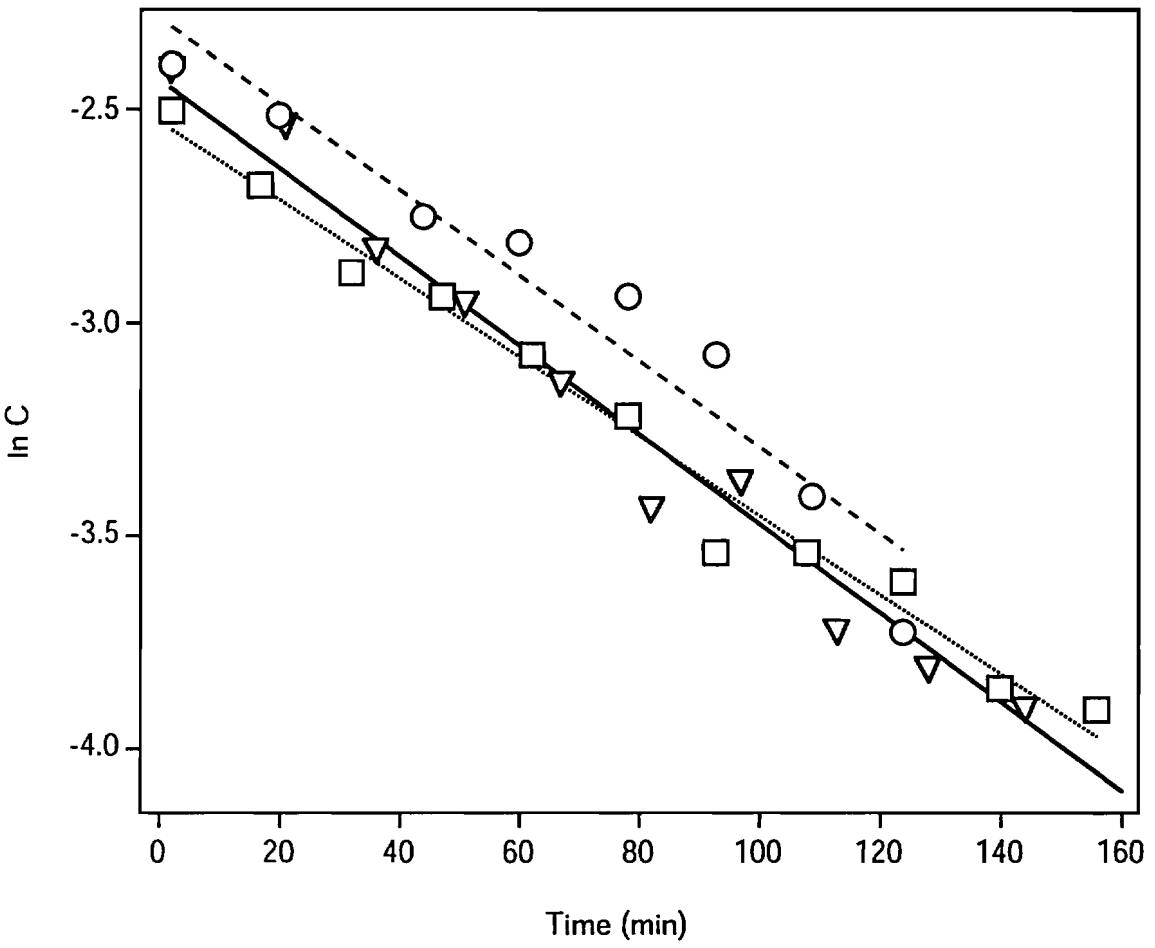

Figure 6.4 Effect of concentration of Coal Creek FA on reduction of CCl_4 by Fe^0. Circles represent a FA concentration of 5 mg L^{-1} (dashed line, $k_{SA} = 0.40 \pm 0.02$ L hr^{-1} m^{-2}), squares represent a FA concentration of 10 mg L^{-1} (dotted line, $k_{SA} = 0.35 \pm 0.02$ L hr^{-1} m^{-2}), and triangles represent a FA concentration of 15 mg L^{-1} (solid line, $k_{SA} = 0.38 \pm 0.04$ L hr^{-1} m^{-2}). Experimental conditions are the same as those described in Figure 6.3.

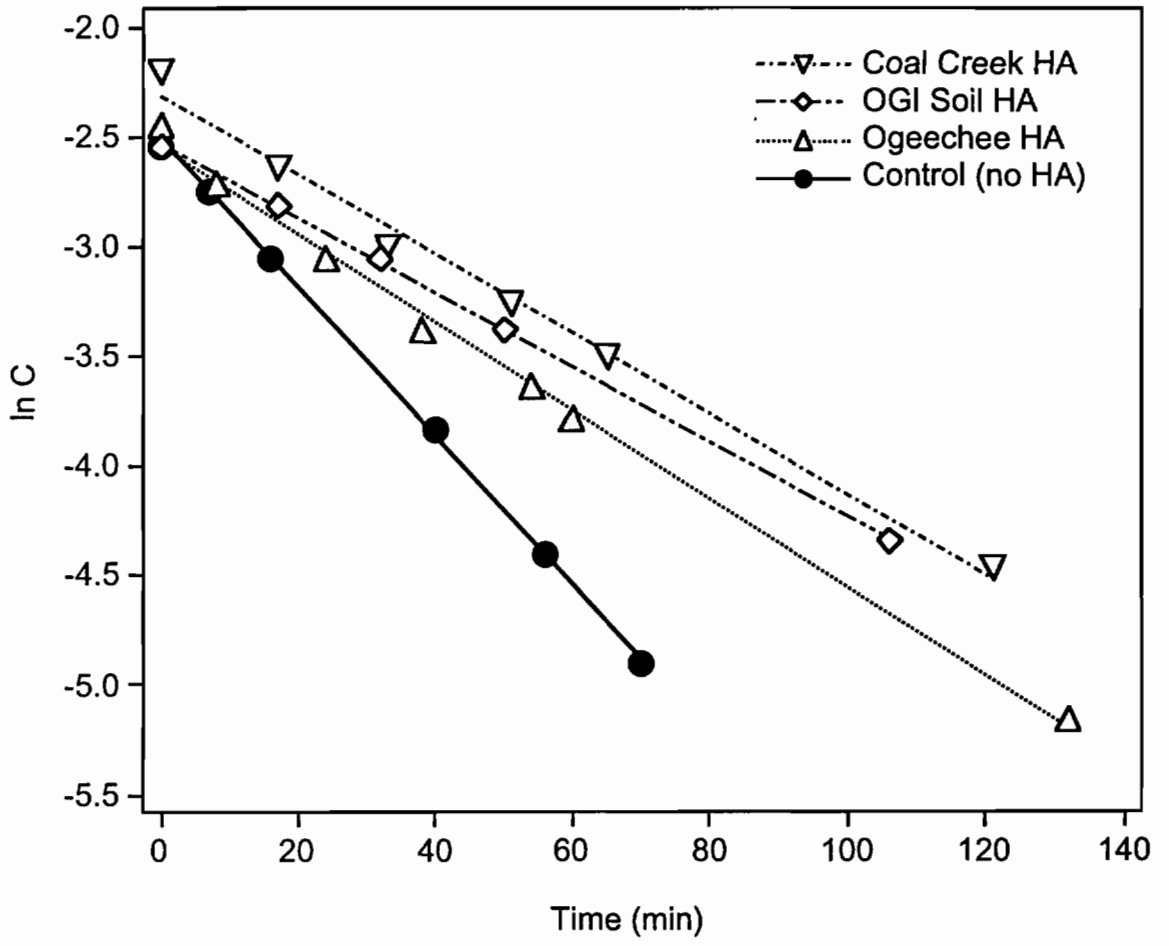

Figure 6.5 Effect of three humic acids on the reduction of CCl_4 by Fe^0. HA concentration is 5 mg L^{-1}. Control with no HA (k_{SA} = 1.28 ± 0.01 L hr^{-1} m^{-2}), Coal Creek HA (k_{SA} = 0.69 ± 0.03 L hr^{-1} m^{-2}), Ogeechee HA (k_{SA} = 0.76 ± 0.02 L hr^{-1} m^{-2}), OGI Soil HA (k_{SA} = 0.64 ± 0.01 L hr^{-1} m^{-2}). Experimental conditions are pH 5.6 carbonate buffer using untreated Fluka iron (ρ_a = 1.6 m^2 L^{-1}) rotating at 36 rpm in the dark.

Biographical Sketch

I was born on March 3, 1967 in Brooklyn, New York. I attended the University of Virginia from 1985-1989 and received a Bachelor of Science degree in Systems Engineering. Upon completing my undergraduate degree, I moved to Alexandria, Virginia where I worked for American Management Systems, Inc. as an environmental analyst for the U.S. Environmental Protection Agency's (EPA) Office of Underground Storage Tanks. I then continued my education at the University of Connecticut where I received a Master of Science Degree in Civil and Environmental Engineering. My publications include:

(1) Scherer, M. M.; Balko, B. A.; Tratnyek, P. G. The role of oxides in reduction reactions at the metal-water interface. In *Kinetics and Mechanisms of Reactions at the Mineral-Water Interface*; Sparks, D.; Grundl, T., Eds; American Chemical Society: Washington, DC, 1998.

(2) Tratnyek, P. G.; Scherer, M. M. Kinetic controls on the performance of remediation technologies based on zero-valent iron; Proceedings of the 1998 National Environmental Engineering Conference: Water Resources in the Urban Environment, Chicago, IL, American Society of Civil Engineers, pp. 110-115.

(3) Scherer, M. M., J. C. Westall, M. Ziomek-Moroz, and P. G. Tratnyek. 1997. Kinetics of carbon tetrachloride reduction at an oxide-free iron electrode. Environ. Sci. Technol., 31(8): 2385-2391.

(4) Tratnyek, P. G., T. L. Johnson, M. M. Scherer, and G. R. Eykholt. 1997. Remediating groundwater with zero-valent metals: Kinetic considerations in barrier design. Ground Water Monitor. Remed., Fall: 108-114.

(5) Johnson, T. L., M. M. Scherer, and P. G. Tratnyek. 1996. Kinetics of halogenated organic compound degradation by iron metal. Environ. Sci. Technol., 30(8): 2634-2640.

(6) Nikolaidis, N. P., G. A. Robbins, M. M. Scherer, B. McAninch, G. Binkhorst, J. Asikainen, and S. L. Suib. 1994. Vertical distribution and partitioning of chromium in a glaciofluvial aquifer. Ground Water Monitor. Remed., Summer: 150-159.